METEONORM Version 6.0

Handbook part II: Theory

METEOTEST

6   Radiation

In this chapter, the theoretical basis of *METEONORM* is presented. To keep the length of the text within reasonable limits, some of the material (i.e. longer explanations) has been omitted. A more detailed discussion of the basic issues is contained in the technical documentation to the 1995 edition (version 2) (SFOE, 1995). Reference is also made to the contribution in Solar Energy concerning interpolation and generation of radiation data (Remund et al., 1998) and the technical publication on data interpolation presented at the 14th Solar Energy PV Conference in Barcelona (Remund and Kunz, 1997).

6.1   Reference time in *METEONORM*

Hourly values are designated by the **end time** of the interval. Thus the value for 14.00 hours refers to the average value of the interval from 13.00 to 14.00 hours. The central value of this interval is 13.30 hours. The computer program contains an internal time reference in minutes, which defines the position of the center of the interval in relation to the end time. In the example given here it is -30 minutes.

The reference time can be changed in the program. Alterations are, however, only necessary in two cases:

1. When hourly values whose central value does not correspond to the half-hour are imported.
2. When hourly values whose central value does not correspond to the half-hour are to be generated.

Example of 1: Measured values are assumed to be available. The measurement interval extended from one half-hour to the next (e.g. 00:30 to 01:30). The hourly average was calculated based on this interval and stored at the end time (e.g. 01:30). As, however, *METEONORM* only allows integer hourly values (h) from 1 to 24, it is only possible to use the full hour (e.g. 1) as end time for the interval. The computer program must be in a position to determine by how much the **given** end time (e.g. 1) differs from the **effective** center value (e.g. 01:00). As the measurement interval (e.g. 01:00) corresponds in this example to the given end time (e.g. 1), the reference time required by *METEONORM* (IZRM = difference between the **effective** center of the interval and the **given** end time in minutes) is **0**.

Example of 2: Hourly values are to be generated using the reference time for measured data of the Swiss Meteorological Office (SMA). The measurement interval of the SMA extends from 10 minutes before the full hour to 20 minutes before the next full hour (e.g. 00:50 to 01:40), e.g. the 10-minute values are averaged and stored at the end time (e.g. 01:40). The center of the interval is 10 minutes after the full hour (e.g. 01:10). The end time output in the *METEONORM* computer program corresponds to the full hour (e.g. 1). The **effective** center of the interval (e.g. 01:10) differs in this case by 10 minutes from the **given** end time (e.g. 1). *METEONORM* thus requires **10** as reference time.

For countries with time zones with half-hours, such as India (-7.5 h), the following procedure must be adopted in operating the program. The zone time to be rounded down to the next full hour (India: -8 h) and the internal reference time set to 0.

6.2 Worldwide interpolation of meteorological data

For the simulation of solar energy systems, meteorological data from all parts of the world is needed. For many regions, measured data may only be applied within a radius of 50 km from weather stations. This makes it necessary to interpolate parameters between stations. The method given below enables the data to be interpolated and monthly values to be obtained for almost all points of the globe.

6.2.1 Methods

To calculate meteorological data for any desired location in the world, an interpolation procedure must be applied. For global radiation, this is done with a 3-D inverse distance model (Shepard's gravity interpolation), based on the introduction by Zelenka et al. (1992) (IEA Task 9), with additional North-South distance penalty (Wald and Lefèvre, 2001), where:

$$G_h(x) = \sum w_i \cdot [G_h(x_i) + (z_i - z_x) \cdot g_v]$$

$$w_i = [(1 - \delta_i)/\delta_i^2] / \sum w_k \text{ with}$$

$$\delta_i = d_i/R \text{ for } d_i < R$$

$$w_i = 0 \text{ otherwise}$$

$$d_i^2 = f_{NS}^2 \cdot \{s^2 + [v \cdot (z_i - z_x)]^2\}$$

$$f_{NS} = 1 + 0.3 \cdot |\Phi_i - \Phi_x| \cdot [1 + (\sin \Phi_i + \sin \Phi_x)/2]$$

(6.2.1)

w_i :	weight i	w_k :	sum of over all weights
R :	search radius (max. 2000 km)	v :	vertical scale factor
s :	horizontal (geodetic) distance [m]	z_x, z_i :	altitudes of the sites [m]
i:	Number of sites (maximum 6)	Φ_i, Φ_x:	latitudes of the points
g_v:	vertical gradient		

The vertical scale factor v and the vertical gradient g_v are depending on the parameter (Tab. 6.2.1).

Tab. 6.2.1: Monthly vertical scale factors v and gradients g_v for interpolation

Parameter	v	g_v
Gh	150	0.0
Ta	400	0.001
Td	400	0.002
FF	300	0.0
RR	200	0.0
Rd	300	0.0
Sd	400	0.002

The special model used in versions 2 - 5 for Switzerland is not used any more.

The other parameters (temperature, wind, humidity and rain) can be interpolated using similar procedures. The vertical factor v in Eqn. 6.2.1 is adjusted to get the smallest deviations. For interpolating temperature and wind data, further information on local effects is needed. The influence of the sea shore is considered in the following way: increased wind speed (1 m/s) for all months, increased temperature in winter, and lower temperature in summer (not applied to tropical regions) (Tab 6.2.2).

Maps of monthly average global radiation and temperature are included on the CD-ROM.

Tab. 6.2.2: Monthly correction factors for temperature for local features in °C (slightly modified sia model)

Feature	Zone	Jan	Feb	Mar	April	May	June	July	Aug	Sep	Oct	Nov	Dec
level ground	A	0.0	0.0	0.0	0.0	0.0	0.0	0.0	0.0	0.0	0.0	0.0	0.0
depression	A	-1.6	-0.7	-0.5	-0.4	-0.4	-0.3	-0.3	-0.2	-0.2	-0.4	-0.7	-1.2
cold hollow	A	-3.9	-2.8	-1.7	-0.4	-0.4	-0.3	-0.3	-0.2	-0.2	-1.0	-2.2	-3.8
lake	A	1.2	0.8	0.0	-0.5	-0.7	-0.7	-0.4	-0.1	0.4	0.6	0.7	1.1
city	A	1.1	1.0	0.8	0.8	0.8	0.8	0.8	0.9	0.9	0.9	1.1	1.2
S-facing incline	N	1.8	1.2	1.0	0.8	0.8	0.6	0.8	0.8	1.1	1.4	1.7	1.7
S-facing incline	S	3.4	2.9	1.9	1.3	1.3	1.3	1.5	1.7	1.8	2.1	2.8	3.7
W/E-facing incline	N	0.9	1.8	0.6	0.5	0.4	0.4	0.3	0.4	0.4	0.6	0.7	0.9
W/E-facing incline	S	1.7	1.5	1.0	0.7	0.7	0.7	0.8	0.9	0.9	1.1	1.4	1.9
valley	N	0.3	0.3	0.2	0.2	0.2	0.2	0.1	0.1	0.1	0.2	0.2	0.2
valley	S	1.8	1.6	1.1	1.0	1.0	0.7	0.9	1.0	1.0	1.2	1.6	2.1

*S-facing incline. For southern hemisphere: N-facing incline!
Zone: **N**: Regions north of 45°N or south of 45°S   **A**: General   **S**: Regions south of 45°N and north of 45°S

Feature: **Depression**: Small and medium depressions with formation of cold hollows, particularly in winter, or strongly shaded. Mainly confined to mountainous regions.
Cold hollow: Includes the extensive cold hollows of central Alpine valleys such as in upper Engadine in Switzerland.
Lake: Vicinity of sea or larger lakes (> 100 km^2). Site not more than 1 km from the shore.
City: Applicable to centers of larger cities with over 100,000 inhabitants.
(See also Fig. 2.2.1 and Tab. 2.2.1)

Tab. 6.2.3: Monthly correction factors for wind speed in m/s depending on terrain. Simplified WASP model (Risoe National Laboratory, 1990).

Terrain	Correction factor [m/s] (applicable to all months of year)
Sheltered terrain (cities)	-1.0
Level ground	0.0
Sea shore	1.0
Hills and ridges	3.0

6.2.2   Quality of the interpolation on monthly means

Following interpolation, the accuracy of the results was found to be as follows: Interpolation of global radiation: mean biased error (mbe): 0 W/m^2 (0 %); root mean square error (rmse): 15 W/m^2 (9%) (Tab. 6.2.4). For temperature interpolation, the mbe was 0.0 °C and the rmse 1.5 °C. Had the "nearest neighbour" method been adopted, the rmse for global radiation would have been 14%, and that for temperature 3.4 °C.

The rmse of *yearly* mean global radiation comes to 17 W/m^2 (10%), and that of *yearly* mean temperature to 1.2 °C (Td: 1.3°C, FF: 1.1 m/s, RR: 31 mm / 35%, Rd: 2.1 days, Sd: 10%).

Tab. 6.2.4:   Quality of the interpolated monthly values (n designates number of stations).

	Gh [%]	Ta [°C]	Td [°C]	FF [m/s]	RR [%]	Rd [d]	Sd [%]
Time period	All	96-05	96-05	96-05	61-90	61-90	61-90
Europe	8.0	1.1	1.1	1.3	24	2.2	14
Germany	5.9	0.8	0.6	0.7	18	2.0	9
France	5.2	1.0	0.6	1.3	17	2.7	8
Asia	8.6	1.5	1.8	1.0	45	2.4	11
Africa	10.0	1.8	2.5	1.1	51	4.1	11
North America	7.1	1.2	1.2	0.9	26	1.7	12
South/Cen. Amer.	10.4	2.0	2.0	1.3	67	2.8	10
Australia/Ocean.	10.6	1.5	1.6	1.5	64	4.2	14
World	**8.9**	**1.4**	**1.5**	**1.1**	**40**	**2.7**	**12**

6.2.3   Conclusions

With the *METEONORM* Version 6.1 database, it is possible to simulate solar energy systems in all parts of the world on a consistent basis. The interpolation errors are within the variations of climate from one year to the next.

The quality of the interpolation of all parameters was improved with the additional stations of version 6.0. For radiation, further improvements were made using ground and satellite data (Chapter 3.1.2).

6.3   Solar trajectory

In solar energy applications, the knowledge of the geometrical parameters of the solar trajectory is necessary. In version 5.0 a new set of algorithms based on the European Solar Radiation Atlas ESRA (2000) was introduced. In the following formulae, angles are given in radians [rad] when not otherwise stated.

Viewed from a fixed point on the earth's surface, the solar position is defined by two angles (Figs. 6.3.1 and 6.3.2):

1. **Solar altitude hs**: Angle between horizontal plane and line joining the centers of the earth and the sun (solar elevation).

2. **Solar azimuth γ_s**: Angle between the projection of the straight line joining the centers of the earth and the sun on the horizontal plane and due south. $\gamma_s > 0$ in positive solar direction, $\gamma_s < 0$ in negative solar direction.
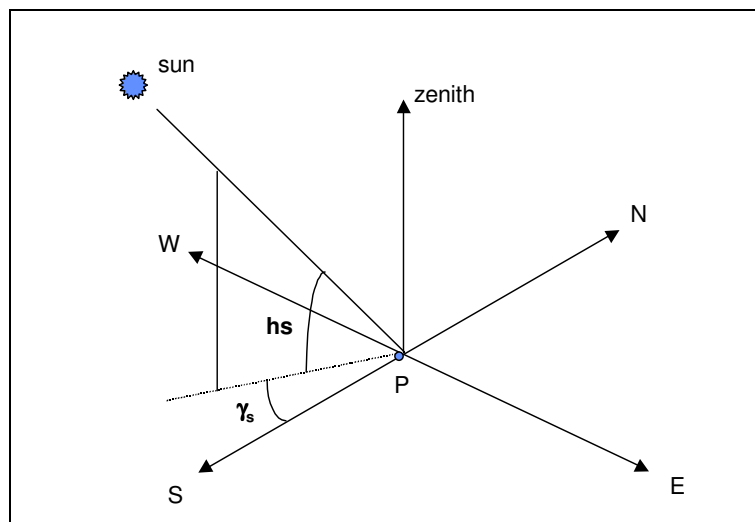

Fig. 6.3.1:   Solar position viewed from a point P on the earth's surface
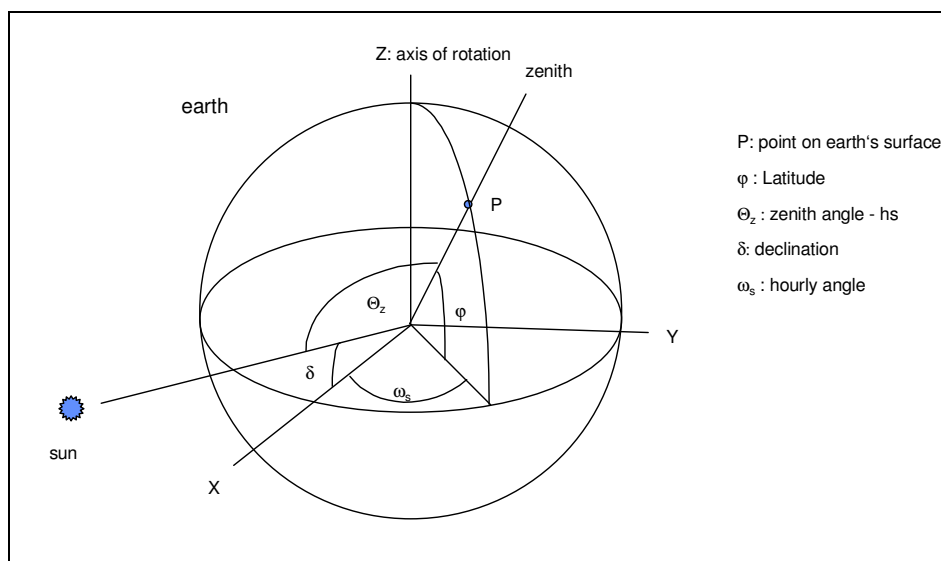

Fig. 6.3.2:   Solar position (declination, zenith angle and hourly angle)

The two angles may be expressed as a function of latitude (φ), solar declination (δ) and hourly angle (ω_s) (6.3.1 to 6.3.4).

$$hs = Arc\ \sin\left[\sin(\varphi)\cdot\sin(\delta)+\cos(\varphi)\cdot\cos(\delta)\cdot\cos(\omega_s)\right] \tag{6.3.1}$$

$$\gamma_s = Arc\ \sin\left[\frac{\cos(\delta)\cdot\sin(\omega_s)}{\cos(hs)}\right] \tag{6.3.2}$$

The declination (δ) is the angle between the equatorial plane and the straight line joining the centers of the earth and the sun. It is determined by the laws governing the solar trajectory, and can be expressed as given in Eqn. 6.3.3a and b (Bourges, 1985).

$$\delta = 0.0064979 + 0.405906\sin\omega_t + 0.0020054\sin 2\omega_t - 0.002988\sin 3\omega_t$$
$$- 0.0132296\cos\omega_t + 0.0063809\cos 2\omega_t + 0.0003508\cos 3\omega_t \tag{6.3.3a}$$

with

$$\omega_t = \omega_0(dy+t_1)$$
$$t_1 = -0.5 - \lambda/2\pi - n_0$$
$$\omega_0 = 2\pi/365.2422$$
$$n_0 = 78.8946 + 0.2422\cdot(y-1957) - INT\left[(y-1957)/4\right] \tag{6.3.3b}$$

δ :   declination [rad] dy :   day of year
y: year λ :   longitude
INT stands for integer part of the argument and y for year and dy for day number of the year.

For the equinox, the declination is zero, for the summer solstice +23.4° and for the winter solstice - 23.4°. It is this variation which is responsible for the seasons of the year.

The hourly angle (ω_s) is also known as solar time (ST) in radians (6.3.4).

$$\omega_s = \arccos\left[-\tan(\varphi)\cdot\tan(\delta)\right] \tag{6.3.4}$$

The astronomical day begins and ends when the center of the sun's disk is precisely on the (flat) horizon. The calculation of the angles of sunrise and sunset (ω_{ss}) is made using Eqn. 6.3.5, obtained by solving Eqn. 6.3.1 with hs = 0.

$$\omega_{ss} = Arc\ \cos\left[-\tan(\varphi)\cdot\tan(\delta)\right] \tag{6.3.5}$$

As a new feature in *METEONORM* Version 6.0 the radiation is also modeled for those hours, when the elevation is positive at the beginning or the end of the hourly time period, but not at the centre. Either the begin or the end (the one with positive elevation) is taken as solar elevation for those hours. For those hours the part of the time, when the sun is above the astronomic horizon is calculated. The generated radiation values are multiplied with this part. Generally the radiation parameters are very small for those hours.

Dimensionless quantities

For many chain links the clearness index is used. This index is defined by

Monthly

$$KT_m = \frac{Gh_m}{Gh_{0m}}$$

daily

$$KT_d = \frac{Gh_d}{G_{0d}} \tag{6.3.6}$$

hourly

$$KT_h = \frac{Gh}{G_0}$$

Optical air mass

In calculating the radiation on the earth's surface, the optical mass m is required. This is defined as the relative thickness of the air path traversed by a sun's ray when it reaches the earth's surface. For vertical impingement of the sunrays at sea level, m assumes the value 1. The value of the optical air mass declines with increasing altitude, and increases with declining solar altitude (Eqn. 6.3.7)

The solar altitude angle is first corrected for refraction.

$$m = \frac{p}{p_0} \Big/ \left[\sin\left(hs^{true}\right) + 0.50572 \cdot \left(57.29578 \cdot hs^{true} + 6.07995\right)^{-1.6364} \right]$$

$$\frac{p}{p_0} = \exp\left(-\frac{z}{8435.2}\right)$$

$$hs^{true} = hs + \Delta hs_{refr} \tag{6.3.7}$$

$$\Delta hs_{refr} = 0.061359 \frac{0.1594 + 1.1230 \cdot hs + 0.065656 \cdot hs^2}{1 + 28.9344 \cdot hs + 277.3971 \cdot hs^2}$$

z: Height above sea level [m]   hs: Solar altitude angle [rad]

6.4   Extraterrestrial solar radiation

Outside the earth's atmosphere, the solar radiation intensity is 1'367 W/m^2 (I_0) (6.4.1). A surface exposed to the sun can only receive this value if it is placed normal to the direction of radiation. Any deviation from this direction leads to a reduction of incident radiation. In the case of a surface lying outside the earth's atmosphere that is parallel to the horizontal plane, the radiation is described as extraterrestrial horizontal solar radiation (G_0). This radiation corresponds to the maximum possible radiation which would occur at the earth's surface if it were unhindered by the atmosphere and the horizon.

Fig. 6.4.1:   Extraterrestrial solar radiation (G_0) and maximum radiation for clear sky ($G_{h\,max}$).

Using the equation for radiation outside the earth's atmosphere and for the solar angle (hs) (6.3.1), the extraterrestrial horizontal solar radiation can be calculated (6.4.1) (Sfeir and Guarracino, 1981).

$$G_0 = I_0 \cdot \varepsilon \cdot \sin \gamma_s$$
$$I_0 = 1367 \text{ W/m}^2 \tag{6.4.1}$$
$$\varepsilon = 1 + 0.0334 \cdot \cos\left(dy \cdot \frac{2\pi}{365.25} - 0.048869 \right)$$

where ε is the correction to actual solar distance at any specific time in the year.

dy : day of year   hs : Solar altitude angle

6.5   Clear sky radiation

The maximum radiation is defined as the radiation occurring on days with a clear, cloudless sky. Not only the global but also the direct and diffuse radiation are of interest. For a cloudless sky, the global radiation takes maximum values. The maximum global radiation calculated here corresponds to the greatest possible value of global radiation per hour at the specified altitude. For a restricted period, the global radiation can attain very high values even with a cloudy sky. This occurs when sunlight, having penetrated through intensively reflecting clouds, impinges directly on the earth's surface. The maximum global radiation is strongly altitude dependent, and increases with increasing height above sea level. At the upper edge of the atmosphere, it takes the value of the extraterrestrial global radiation.

Since version 5.0 of *METEONORM,* a new set for clear sky radiation is used. The European Union FP5 framework project SoDa studies (Remund and Page, 2002) showed that the use of a slightly enhanced ESRA clear sky irradiance model (Rigollier et al., 2000) delivers best results. The following chapters are a direct result of these studies.

6.5.1   Underlying basic concepts in the SoDa/ESRA clear sky model

The clarity of the sky above any site has an important impact on the intensity of both the beam irradiance and the amount of scattered diffuse radiation under cloudless sky conditions. A capacity to address these issues is critical in achieving sound irradiation estimates.

Energy is lost from the solar beam by three routes:

   i)   molecular scattering by the gases in the atmosphere.

   ii)   spectral absorption, for example by gaseous water vapour, primarily located in the lower atmosphere, and by ozone, which is located primarily in the stratosphere, and also by the permanent atmospheric gases like carbon dioxide.

   iii)   scattering and absorption due to natural aerosols and man made aerosols in the atmosphere.

The elevation of the site above sea level reduces the effective atmospheric path length and has to be taken into account. The amount of aerosol present in the atmosphere and the amount of water vapour present typically decrease exponentially with increases in solar altitude. The modeling process has to allow for this.

The detailed assessment of these impacts is complex. There are advantages for practical users to be able to express the impacts of various factors, like variations atmospheric water vapour contents and aerosols, in a single easily comprehensible index. The ESRA/SoDa clear sky resource is based on the use of the concept of the Linke turbidity factor to achieve this simplicity. The guidance of Kasten (1996) was sought in the evolution of the precise formulation adopted.

The Linke turbidity factor at height z metres above sea level, $T_L(z)$, was objectively defined by Kasten (1983) as:

$$T_L(z) = 1 + \frac{\delta_D(z)}{\delta_R(z)} \qquad\qquad (6.5.1)$$

where $\delta_R(z)$ is the relative optical thickness relating to Rayleigh scattering by the gaseous molecules in the atmosphere and ozone absorption and $\delta_D(z)$ is the relative optical thickness associated with aerosol extinction and gaseous absorption other than ozone in the stratosphere.

Further elaboration may be found in Terzenbach (1995). Note: in some recent scientific studies the gaseous absorption by the permanent gases in the atmosphere has been incorporated within $\delta_R(z)$. This produces a different definition of the Linke turbidity factor.

The actual path length through the atmosphere is described quantitatively using the concept of the relative optical air mass. The relative optical air mass at sea level can be calculated with Eqn. 6.3.7, by setting p=p0.

$\delta_R(z)$ and $\delta_D(z)$ are both functions of air mass because we are dealing with broadband radiation (as opposed to monochromatic radiation).

The beam irradiance normal to the beam is given by:

$$B_n = I_0 \cdot \varepsilon \cdot \exp\left[-m \cdot T_L(z) \cdot \delta_R(z)\right] \ [W/m^2]$$

(6.5.2)

In recent years several scientists have widened the concept of Rayleigh optical thickness to include absorption by a range of absorbing gases that occur naturally in the clean dry atmosphere like carbon dioxide, oxygen, and certain oxides of nitrogen. This process increases the value of $\delta_R(z)$, the denominator in Eqn. 6.5.1, and so yields lower values of the calculated turbidity factor from irradiance observations.

The SoDa/ESRA policy in the face of these recent changes has been to retain a constant quantitative definition over historic time of the Linke turbidity factor. The compromise adopted takes advantage of recent improved knowledge about the effect of air mass on the Rayleigh optical thickness. The old Rayleigh optical thickness values are aligned with the new clear sky optical thickness values at air mass 2. This alignment is done by making a defined match at air mass 2 between the new algorithms and the old, which have been maintained as the reference for Linke turbidity factor inputs. This alignment yields an adjustment factor of 0.8662 needed to achieve this match which is included in Equation 6.5.3.

The beam irradiance normal to the beam is calculated using the standardized original Kasten air mass 2 Linke turbidity factor, as:

$$B_n = I_0 \cdot \varepsilon \cdot \exp\left[-m \cdot 0.8622 \cdot T_L \cdot \delta_R(m)\right] \ [W/m^2]$$

(6.5.3)

where T_L is the air mass 2 Linke turbidity factor as defined by Kasten's formulation and m is the relative optical air mass corrected for station pressure.

Kasten has provided the following guideline for typical values of T_L in Europe (Tab. 6.5.1).

Tab. 6.5.1:   Typical values of T_L in Europe.

Very clean cold air	$T_{LK} = 2$
Moist warm or stagnating air	$T_{LK} = 4$ to 6
Clean warm air	$T_{LK} = 3$
Polluted air	$T_{LK} > 6$

6.5.2 The estimation of clear sky radiation

For equations of global clear sky radiation we refer to the publication of Rigollier et al. (2000), chapter about irradiance model.

For diffuse clear sky radiation the following corrections are used:

The formulation of the horizontal surface diffuse radiation irradiance algorithm in ESRA (2000) and Rigollier et al. (2000) did not make any allowance for variations in the site atmospheric pressure though such a correction was made in the associated beam estimates. Further investigation has shown the desirability of including the pressure correction in the ESRA diffuse algorithm.

Setting $(T_L^*) = p/p_0 \, T_L$, the ESRA diffuse irradiance estimation equations were rewritten as follows:

$$D_c = I_0 \cdot \varepsilon \cdot F_d(\gamma_s) \cdot T_{rd}(T_L^*) \ [W/m^2]$$

(6.5.4)

$T_{rd}(T_L^*)$ is the diffuse transmittance function which represents the transmittance with the sun at the zenith, It is calculated using Eqn. 6.5.5.

$$T_{rd}\left(T_L^*\right) = -1.5843 \cdot 10^{-2} + 3.0543 \cdot 10^{-2} \cdot T_L^* + 3.797 \cdot 10^{-4} \cdot \left(T_L^*\right)^2$$

(6.5.5)

$F_d(\gamma_s)$ is the diffuse solar elevation function which adjusts the diffuse zenith transmittance $T_{rd}(T_L^*)$ to the actual solar elevation angle γ_s. It is calculated using Eqn. 6.5.6, where γ_s is in radians.

$$F_d\left(y_s\right) = A_0 + A_1 \cdot \sin \gamma_s + A_2 \cdot \sin \gamma_s^2$$

(6.5.6)

The coefficients A_0, A_1 and A_2 are calculated using Equations 6.5.7:

$$A_0 = 0.26463 - 0.061581 \cdot T_L^* + 0.0031408 \cdot \left(T_L^*\right)^2$$
$$A_1 = 2.04020 + 0.018945 \cdot T_L^* - 0.011161 \cdot \left(T_L^*\right)^2$$
$$A_2 = -1.33025 + 0.03231 \cdot T_L^* + 0.0085079 \cdot \left(T_L^*\right)^2$$

(6.5.7)

For regions below approximately 500 m, the changes due to the new formulation are small. In Switzerland the clear sky diffuse radiation at 1'000 m a.s.l. is lowered by 10 % and the global clear sky is lowered by about 2.5% by this change. At 2'500 m the clear sky diffuse is lowered by 30% and the global is lowered by about 3% (the diffuse part forms a smaller proportion of the clear sky global irradiation at higher site elevations).

The outcome of the validation in Rigollier et al. (2000) is therefore not touched by the change, as only stations below 500m were used in the validation.

6.5.3   Linke turbidity

Linke turbidity (TL) is used for input of the ESRA clear sky model. For version 6.0 a new turbidity climatology has been included. It's based on ground measurements of Aeronet (Holben et al. 2001) and satellite measurements of MISR and MODIS (NASA 2007) for the years 2000-2006.

During validation of downstream models, it was detected, that the obtained values of TL are too high and therefore the clear sky radiation too low. The reason for this was not examined in detail, but similar observations have been reported by Ineichen and Dürr (2007). The monthly mean Linke turbidity (TLm) is lowered with Eq. (6.5.8):

$$TL_m' = TL_m \cdot \left(1.133 - 0.0667 \cdot TL_m\right)$$

(6.5.8)

High turbidity values are reduced more than lower values. For mean conditions at mid latitudes and industrialized regions like Europe with Linke turbidity of about 5, the value is lowered by 20% to a value of 4.

Additionally it was detected, that with varied turbidity values the observed distribution of clear sky conditions could be matched better. Also models producing beam radiation gave better results, when using varied turbidities. By default the daily Linke turbidity (TLd) values are varied stochastically (optionally it can set constant) (Eq. 6.5.9).

$$TL_d\left(d\right) = \phi_1 \cdot TL_d\left(d-1\right) + r$$
$$\phi_1 = 0.7$$
$$\sigma\left(TL_m'\right) = 0.1 \cdot TL_m'$$
$$\sigma' = \sigma \cdot \left(1 - \phi_1^2\right)^{0.5}$$
$$r = N\left(0, \sigma'\right)$$
$$TL_m' \cdot 0.75 < TL_d < TL_m' \cdot 1.2$$

(6.5.9)

ϕ_1:   First order autocorrelation

$\sigma\left(TL_m\right)$: Standard deviation of y perturbations depending on monthly means of TL

σ´ : Standard deviation of the normally distributed random function

r : Normally distributed random variable with expected value 0 and standard deviation σ´ .

World digital maps of the Linke turbidity factor have been prepared on a 1" grid as a basic resource (Fig. 6.5.1).
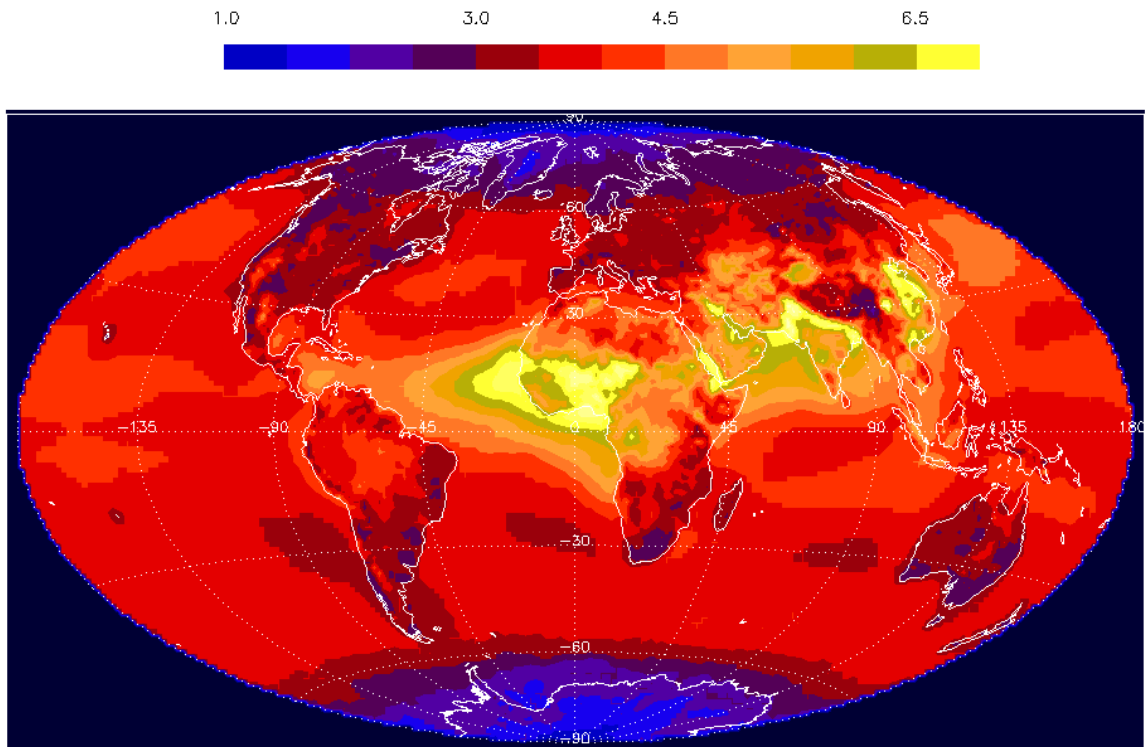

Fig. 6.5.1: Yearly long term mean of Linke turbidity factor (period 2000 – 2008).

In *METEONORM* version 6.1 these maps (12 – one per month) are accessed internally. They have been updated in patch version 6.1.0.17 (November 27th 2009). The update can result in slightly changed beam values. The new climatology will be described in the final report of IEA SHC Task 36.

The given TL values are coupled to the mean altitude of the pixels. In the software, the TL values are adopted to the real altitude of the sites with the following equation:

$$T_L(z_1) = T_L(z_2) \cdot \exp\left(\frac{(z_2 - z_1)}{6000} \right)$$

(6.5.10)

The original scale height of 8435.2 m has been changed in patch 6.1.0.17 to 6000 m according the results in IEA SHC Task 36.

6.6   Generation of global radiation

To meet present day needs, monthly average data is no longer sufficient, and many design codes call for hourly data. However, since the interpolation of hourly values at arbitrary locations is extremely time consuming (only feasible using satellite data), and necessitates extensive storage capacity, only interpolated monthly values at nodal points are stored.

In order to generate hourly values at any desired location, stochastic models are used. The stochastic models generate intermediate data having the same statistical properties as the measured data, i.e. average value, variance, and characteristic sequence (autocorrelation). The generated data approximates the natural characteristics as far as possible. Recent research shows that data generated in this way can be used satisfactorily in place of long-term measured data (Gansler et al., 1994).

The following generation procedure is adopted. Starting with the monthly global radiation values, first the daily values, then the hourly values are generated stochastically. Further characteristic values, e.g. temperature, humidity, wind, longwave radiation, are derived from these as required.

6.6.1   Stochastic generation of global radiation

6.6.1.1 Generation of daily values

For generation of daily values a new model was introduced in version 5.0 as an outcome of the SoDa project.

The model of Aguiar et al. (1988), used already in versions 2–5, provides the starting point for this methodology. It calculates daily values of G_d with monthly mean values of G_m as inputs. The following changes have been introduced:

The original model gives one single distribution of daily clearness index KT_d values for any one monthly mean value KT_m. The model does not take into account any local factors like site altitude above sea level (higher maximum irradiation values at higher altitude) or different turbidity situations. There are also problems with the coupling to the clear sky model of ESRA when this original model is used in the SoDa chain of algorithms. The estimated clear sky values, using Chain 1, can be much higher or much lower than the maximum values predicted by the unmodified Aguiar.

The whole system of the matrices was therefore changed from a clearness index basis to a clear sky clearness index basis. Formulated like this, the maximum value of $KT_{d,c}$ (=1) must correspond automatically to the clear sky model predictions used. $KT_{d,c}$ is calculated as the ratio $G_d/G_{c,d}$.

The basic SoDa mapped resource of monthly mean Linke turbidity factors is used to drive the clear sky model using algorithmic to obtain the required monthly mean daily values of $G_{c,d}$ needed to calculate $KT_{d,c}$ in any selected month for any point. This change required the daily Markov transition matrices tables to be completely revised to match the new formulation. The new Tables giving the revised distributions and their validation in application are discussed in the chapter Chapters 6.6.1.2 and 6.6.1.3.

Example: generation of a sequence for one month

This Section is based on the description of the methodology by Aguiar et al. (1988). It gives an example of how to use the Markov Transition Matrices (MTM) to calculate a daily sequence of clear sky daily clearness indices.

Suppose that, for each month of the year, the location X has the following values of monthly clear sky clearness indices $KT_{m,c}$:

	January	February	November	December
$KT_{m,c}$	0.424	0.522	0.475	0.389

In a first step the clear sky monthly mean $KT_{m,c}$ values have to be calculated from the monthly global radiation and monthly clear sky radiation.

A simulation for the month of January would proceed as follows.

1. The appropriate MTM is selected using the value of $KT_{m,c}$ for Jan.: since $0.40 < KT_{m,c} \leq 0.50$ the appropriate matrix is Table 6.6.4.
2. The daily $KT_{d,c}$ value corresponding to day 1 of the series to be generated is calculated by assuming that $KT_{m,c}$ (Month 0) i.e. $KT_{m,c}$(Dec.) = 0.389.
3. Note that $KT_{m,c}$(Month = 0) belongs to the interval 0.3–0.4, which is line 4 of the selected MTM.
4. Using a random number generator with a uniform distribution between 0 and 1, suppose a number R = 0.350 is found. This is used to determine the next state of $KT_{d,c}$ by summing the values of $P_{41}+P_{42}+...+P_{4j}$ (4th row, j[th] column of Table B5) until the sum is greater than R. This finds the state in which $KT_{d,c}$ will be in the next day. In this case, the result is $P_{41}+P_{42}+P_{43}+P_{44}$ = 0.020+0.111+0.175 +0.208 = 0.514.

The first and simplest way to calculate the new value of $KT_{d,c}(1)$ consists of giving it the value of the intervals corresponding to the new state column j = 4, in this case 0.40 (j = 1 would mean 0.1, j = 2 would mean 0.2, ...). Another slightly more complicated way, which is used here, depends on a linear interpolation within the interval. In this case, the procedure is best described in terms of the distribution function for state i:

$$F_i\left(KT_{d,c}\right) = \int_0^{KT_{d,c}} P\left(KT_{d,c}'\right) dKT_{d,c}' \qquad (6.6.1)$$

which in this (discrete) case has a graphical form like the on shown in Figure 6.6.1. This Figure also shows how $KT_{d,c}$ is found at the intersection of the horizontal line at R with the linear interpolation within the appropriate interval of $KT_{d,c}$. In the present example, the final result using this process is $KT_{d,c}(1) = 0.321$.

The second day of the sequence, $KT_{d,c}(2)$ is found by taking $KT_{d,c}(1)$ as the previous day's value and repeating steps (2) to (4). A series $KT_{d,c}$(dy) with 31 values is thus obtained for January. Daily global radiation is calculated by multiplying $KT_{d,c}$(dy) with the clear sky global radiation G_d(dy).

The average value of this sequence may not be equal to the monthly mean global radiation in the starting data. The synthetic data generation process is repeated until a sequence is obtained that lies within the desired limits of accuracy. This limit is set in the SoDa procedures to 1%.
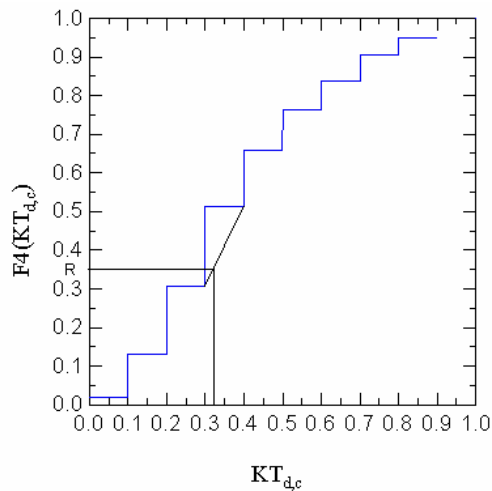
Fig. 6.6.1: Obtaining the daily clear sky clearness index using a random number R and interpolating in the accumulated probabilities of the transition supplied by the MTM library of the previous KTd,c(dy-1) value.

6.6.1.2 New Markov transition matrices (MTM)

The new Markov transition matrices (MTM) were calculated using a total of 121 stations, drawn from the USA (from San Juan PR to Barrow AK), Europe, North Africa and Saudi Arabia. These cover all major climate zones. The original Aguiar et al. version was made with data from 12 stations.

The result is a 9x10x10 matrix. Values of 0.05 and 1 were used as the minimum and maximum values of daily clear sky clearness index. The classes of the monthly $KT_{d,c}$ were set from 0.1–0.2, 0.2–0.3, ..., 0.9–1.0. No monthly values of $KT_{d,c}$ below 0.1 were found (this is the reason for the **9**x10x10 matrix). A second change was made in accepting only daily values smaller than 102% of the estimated clear sky value. This is especially important for high latitude sites during spring and autumn, where the day length changes very much during each month.

The issue, whether more parameters could enhance the quality of random generation, was explored. Different MTMs were calculated for continental and maritime climates, as well as for low solar and high solar elevations. As none of the additional parameters led to significantly better results, they were not used. The problem of too low daily clearness index was also examined and found not to be of great importance. Only an overall minimum $KT_{d,c}$ value of 0.05 was set. Tables 6.6.1 to 6.6.9 show the Markov transition matrices.

For version 6 MTM's for KT <= 0.20 have been changed in order to able to generate data for more diverse climates. As for the production of these tables not enough values have been available and therefore the distribution is not representative. The introduced values are grouped mainly around the diagonal line, which means, that the weather does not change much from day to day.

Tab. 6.6.1: Markov transition matrix for $0.10 < KT_{m,c} \leq 0.20$

	0.0-0.1	0.1-0.2	0.2-0.3	0.3-0.4	0.4-0.5	0.5-0.6	0.6-0.7	0.7-0.8	0.8-0.9	0.9-1.0
0.0-0.1	0.500	0.280	0.150	0.050	0.020	0.000	0.000	0.000	0.000	0.000
0.1-0.2	0.200	0.480	0.200	0.100	0.020	0.000	0.000	0.000	0.000	0.000
0.2-0.3	0.050	0.200	0.480	0.200	0.050	0.020	0.000	0.000	0.000	0.000
0.3-0.4	0.020	0.050	0.180	0.500	0.180	0.050	0.020	0.000	0.000	0.000
0.4-0.5	0.000	0.020	0.050	0.180	0.500	0.180	0.050	0.020	0.000	0.000
0.5-0.6	0.000	0.000	0.020	0.050	0.180	0.500	0.180	0.050	0.020	0.000
0.6-0.7	0.000	0.000	0.000	0.000	0.050	0.200	0.300	0.200	0.000	0.250
0.7-0.8	0.000	0.000	0.000	0.000	0.020	0.050	0.200	0.480	0.200	0.050
0.8-0.9	0.000	0.000	0.000	0.000	0.000	0.000	0.050	0.200	0.500	0.250
0.9-1.0	0.000	0.000	0.000	0.000	0.000	0.000	0.200	0.050	0.050	0.700

Tab. 6.6.2: Markov transition matrix for 0.20 < KTm,c ≤ 0.30

	0.0-0.1	0.1-0.2	0.2-0.3	0.3-0.4	0.4-0.5	0.5-0.6	0.6-0.7	0.7-0.8	0.8-0.9	0.9-1.0
0.0-0.1	0.500	0.280	0.150	0.050	0.020	0.000	0.000	0.000	0.000	0.000
0.1-0.2	0.200	0.480	0.200	0.100	0.020	0.000	0.000	0.000	0.000	0.000
0.2-0.3	0.100	0.650	0.200	0.050	0.000	0.000	0.000	0.000	0.000	0.000
0.3-0.4	0.000	0.250	0.000	0.050	0.300	0.050	0.000	0.000	0.050	0.300
0.4-0.5	0.000	0.400	0.050	0.100	0.400	0.050	0.000	0.000	0.000	0.000
0.5-0.6	0.000	0.000	0.000	0.000	0.250	0.500	0.250	0.000	0.000	0.000
0.6-0.7	0.000	0.000	0.000	0.000	0.000	0.250	0.500	0.250	0.000	0.000
0.7-0.8	0.000	0.000	0.000	0.000	0.000	0.000	0.250	0.500	0.250	0.000
0.8-0.9	0.000	0.000	0.000	0.000	0.000	0.000	0.000	0.250	0.500	0.250
0.9-1.0	0.000	0.000	0.000	0.000	0.000	0.700	0.050	0.000	0.000	0.250

Tab. 6.6.3: Markov transition matrix for 0.30 < KTm,c ≤ 0.40

	0.0-0.1	0.1-0.2	0.2-0.3	0.3-0.4	0.4-0.5	0.5-0.6	0.6-0.7	0.7-0.8	0.8-0.9	0.9-1.0
0.0-0.1	0.133	0.319	0.204	0.115	0.074	0.033	0.030	0.044	0.011	0.037
0.1-0.2	0.081	0.303	0.232	0.127	0.088	0.060	0.029	0.031	0.018	0.033
0.2-0.3	0.036	0.195	0.379	0.135	0.087	0.039	0.042	0.027	0.025	0.036
0.3-0.4	0.032	0.190	0.205	0.189	0.119	0.069	0.059	0.038	0.045	0.054
0.4-0.5	0.051	0.175	0.189	0.185	0.140	0.079	0.060	0.040	0.017	0.064
0.5-0.6	0.042	0.213	0.243	0.126	0.117	0.090	0.045	0.036	0.021	0.069
0.6-0.7	0.017	0.166	0.237	0.141	0.100	0.091	0.054	0.062	0.046	0.087
0.7-0.8	0.038	0.171	0.190	0.133	0.095	0.090	0.057	0.062	0.043	0.119
0.8-0.9	0.044	0.093	0.231	0.143	0.115	0.066	0.038	0.060	0.099	0.110
0.9-1.0	0.029	0.131	0.163	0.127	0.062	0.092	0.065	0.072	0.078	0.180

Tab. 6.6.4: Markov transition matrix for 0.40 < KTm,c ≤ 0.50

	0.0-0.1	0.1-0.2	0.2-0.3	0.3-0.4	0.4-0.5	0.5-0.6	0.6-0.7	0.7-0.8	0.8-0.9	0.9-1.0
0.0-0.1	0.116	0.223	0.196	0.129	0.093	0.077	0.054	0.044	0.032	0.037
0.1-0.2	0.051	0.228	0.199	0.143	0.101	0.083	0.065	0.052	0.035	0.043
0.2-0.3	0.028	0.146	0.244	0.156	0.120	0.092	0.069	0.053	0.040	0.052
0.3-0.4	0.020	0.111	0.175	0.208	0.146	0.104	0.074	0.067	0.044	0.052
0.4-0.5	0.017	0.115	0.161	0.177	0.155	0.102	0.085	0.067	0.054	0.068
0.5-0.6	0.018	0.114	0.147	0.156	0.142	0.123	0.088	0.075	0.060	0.077
0.6-0.7	0.019	0.116	0.152	0.153	0.133	0.100	0.090	0.078	0.061	0.098
0.7-0.8	0.022	0.105	0.145	0.134	0.112	0.109	0.103	0.085	0.077	0.108
0.8-0.9	0.016	0.100	0.119	0.120	0.100	0.105	0.099	0.096	0.120	0.126
0.9-1.0	0.012	0.081	0.109	0.115	0.101	0.082	0.075	0.091	0.107	0.226

Tab. 6.6.5: Markov transition matrix for 0.50 < KTm,c ≤ 0.60

	0.0-0.1	0.1-0.2	0.2-0.3	0.3-0.4	0.4-0.5	0.5-0.6	0.6-0.7	0.7-0.8	0.8-0.9	0.9-1.0
0.0-0.1	0.095	0.201	0.140	0.121	0.112	0.076	0.073	0.066	0.055	0.061
0.1-0.2	0.029	0.176	0.158	0.133	0.121	0.096	0.078	0.079	0.067	0.063
0.2-0.3	0.015	0.096	0.171	0.157	0.139	0.121	0.093	0.080	0.066	0.062
0.3-0.4	0.008	0.055	0.103	0.199	0.186	0.130	0.108	0.085	0.063	0.063
0.4-0.5	0.006	0.039	0.077	0.145	0.236	0.167	0.113	0.083	0.064	0.069
0.5-0.6	0.006	0.044	0.080	0.128	0.192	0.166	0.123	0.100	0.081	0.080
0.6-0.7	0.006	0.049	0.082	0.132	0.152	0.139	0.125	0.110	0.095	0.109
0.7-0.8	0.007	0.047	0.086	0.113	0.138	0.125	0.114	0.124	0.112	0.134
0.8-0.9	0.006	0.048	0.079	0.105	0.120	0.108	0.100	0.120	0.138	0.177
0.9-1.0	0.005	0.033	0.062	0.085	0.102	0.086	0.088	0.103	0.144	0.291

Tab. 6.6.6: Markov transition matrix for 0.60 < KTm,c ≤ 0.70

	0.0-0.1	0.1-0.2	0.2-0.3	0.3-0.4	0.4-0.5	0.5-0.6	0.6-0.7	0.7-0.8	0.8-0.9	0.9-1.0
0.0-0.1	0.061	0.169	0.146	0.095	0.106	0.094	0.108	0.085	0.067	0.070
0.1-0.2	0.023	0.113	0.130	0.114	0.107	0.111	0.102	0.108	0.100	0.092
0.2-0.3	0.007	0.062	0.105	0.132	0.151	0.126	0.113	0.106	0.097	0.100
0.3-0.4	0.004	0.026	0.063	0.150	0.189	0.147	0.118	0.108	0.097	0.099
0.4-0.5	0.002	0.017	0.040	0.098	0.230	0.164	0.130	0.111	0.103	0.106
0.5-0.6	0.002	0.016	0.040	0.084	0.162	0.179	0.149	0.129	0.119	0.120
0.6-0.7	0.003	0.018	0.040	0.079	0.142	0.143	0.153	0.140	0.139	0.144
0.7-0.8	0.002	0.017	0.041	0.079	0.126	0.120	0.135	0.151	0.162	0.167
0.8-0.9	0.002	0.017	0.034	0.069	0.108	0.106	0.114	0.144	0.191	0.215
0.9-1.0	0.001	0.012	0.023	0.050	0.083	0.079	0.088	0.118	0.185	0.362

Tab. 6.6.7:   Markov transition matrix for 0.70 < KTm,c ≤ 0.80

	0.0-0.1	0.1-0.2	0.2-0.3	0.3-0.4	0.4-0.5	0.5-0.6	0.6-0.7	0.7-0.8	0.8-0.9	0.9-1.0
0.0-0.1	0.049	0.091	0.112	0.070	0.098	0.077	0.105	0.119	0.112	0.168
0.1-0.2	0.019	0.070	0.090	0.105	0.119	0.113	0.103	0.134	0.121	0.125
0.2-0.3	0.005	0.028	0.074	0.114	0.130	0.123	0.113	0.118	0.145	0.151
0.3-0.4	0.001	0.011	0.039	0.102	0.169	0.135	0.123	0.126	0.136	0.156
0.4-0.5	0.001	0.007	0.021	0.062	0.175	0.143	0.132	0.137	0.157	0.167
0.5-0.6	0.001	0.007	0.020	0.049	0.117	0.146	0.150	0.157	0.172	0.182
0.6-0.7	0.000	0.005	0.015	0.047	0.097	0.122	0.151	0.169	0.197	0.197
0.7-0.8	0.001	0.006	0.016	0.040	0.084	0.098	0.130	0.179	0.224	0.223
0.8-0.9	0.001	0.005	0.011	0.034	0.067	0.079	0.107	0.161	0.262	0.275
0.9-1.0	0.000	0.003	0.007	0.022	0.045	0.055	0.074	0.112	0.222	0.459

Tab. 6.6.8:   Markov transition matrix for 0.80 < KTm,c ≤ 0.90

	0.0-0.1	0.1-0.2	0.2-0.3	0.3-0.4	0.4-0.5	0.5-0.6	0.6-0.7	0.7-0.8	0.8-0.9	0.9-1.0
0.0-0.1	0.000	0.000	0.077	0.077	0.154	0.077	0.154	0.154	0.077	0.231
0.1-0.2	0.000	0.043	0.061	0.070	0.061	0.087	0.087	0.217	0.148	0.226
0.2-0.3	0.000	0.017	0.042	0.073	0.095	0.112	0.120	0.137	0.212	0.193
0.3-0.4	0.001	0.003	0.015	0.055	0.106	0.091	0.120	0.139	0.219	0.250
0.4-0.5	0.000	0.002	0.009	0.035	0.097	0.113	0.123	0.155	0.209	0.258
0.5-0.6	0.000	0.002	0.007	0.028	0.063	0.089	0.123	0.157	0.235	0.295
0.6-0.7	0.000	0.002	0.005	0.020	0.054	0.069	0.114	0.170	0.260	0.307
0.7-0.8	0.000	0.001	0.004	0.015	0.043	0.058	0.097	0.174	0.288	0.320
0.8-0.9	0.000	0.001	0.002	0.011	0.027	0.039	0.071	0.139	0.319	0.390
0.9-1.0	0.000	0.001	0.001	0.005	0.015	0.024	0.043	0.086	0.225	0.600

Tab. 6.6.9:   Markov transition matrix for 0.90 < KTd,c ≤ 1.00

	0.0-0.1	0.1-0.2	0.2-0.3	0.3-0.4	0.4-0.5	0.5-0.6	0.6-0.7	0.7-0.8	0.8-0.9	0.9-1.0
0.0-0.1	0.500	0.250	0.200	0.050	0.000	0.000	0.000	0.000	0.000	0.000
0.1-0.2	0.200	0.500	0.200	0.050	0.050	0.000	0.000	0.000	0.000	0.000
0.2-0.3	0.000	0.000	0.250	0.000	0.000	0.000	0.250	0.250	0.000	0.250
0.3-0.4	0.000	0.000	0.000	0.000	0.048	0.000	0.143	0.095	0.190	0.524
0.4-0.5	0.000	0.000	0.014	0.000	0.027	0.041	0.041	0.233	0.192	0.452
0.5-0.6	0.000	0.000	0.000	0.008	0.039	0.031	0.078	0.093	0.326	0.425
0.6-0.7	0.000	0.000	0.000	0.006	0.019	0.019	0.067	0.102	0.254	0.533
0.7-0.8	0.000	0.000	0.000	0.005	0.012	0.024	0.041	0.106	0.252	0.560
0.8-0.9	0.000	0.000	0.000	0.001	0.006	0.012	0.031	0.078	0.283	0.589
0.9-1.0	0.000	0.000	0.000	0.001	0.002	0.004	0.012	0.029	0.134	0.818

6.6.1.3 Validation

The calculated mean values are adapted to the measured, so there is no difference at this level. The distribution has been tested at 5 stations of the Baseline Surface Radiation Network (BSRN) (WRCP 2001) (Table 2) with Kolmogorov-Smirnov (KS) test (Massey 1951).

The interval distance p is defined as

$$p = \frac{x_{\max} - x_{\min}}{m}, m = 100 \tag{6.6.5}$$

where xmin and xmax are the extreme values of the independent variable. Then, the distances between the cumulative distribution function are defined, for each interval, as

$$D_n = \max \left| F(x_i) - R(x_i) \right|, x_i \in \left[x_{\min} + (n+1)p, x_{\min} + np \right] \tag{6.6.6}$$

If at any of the intervals considered, this distance as given in equation (Eq. 5) is above a critical value V_c (which depends on the population size N) the null hypothesis that the sets are statistically the same must be rejected. The critical value is calculated for 99.9% level of confidence (Eq. 6)

$$V_c = \frac{1.63}{\sqrt{N}}, N \geq 35 \tag{6.6.7}$$

A special test (KSI over) (Espinar et al., 2007) was used to estimate the proportion of the distribution, where the critical value is overshot:

$$aux = \begin{cases} D_n - V_c & \text{if } D_n > V_c \\ 0 & \text{if } D_n \leq V_c \end{cases} \qquad (6.6.8)$$

The KSI over % parameters are then calculated as the trapezoidal integral of that auxiliary vector and its corresponding normalization to the critical area:

$$KSI \text{ over}\% = \frac{\int aux \ dx}{a_{critical}} \cdot 100 \qquad (6.6.9)$$

where $a_{critical}$ is calculated as

$$a_{critical} = V_c \cdot (x_{max} - x_{min}) \qquad (6.6.10)$$

Generally a good agreement is achieved. At 4 of the 5 sites the distributions are statistically the same (Table 6.6.10). Figure 6.6.2 shows a typical cumulative distribution function for Camborne (GBR).

Tab. 6.6.10:   Kolmogorov-Smirnov (KSI over %) test for daily global radiation.

Site	KSI over %
Payerne (CHE)	0.0%
Camborne (GBR)	0.0%
Boulder (CO, USA)	0.0%
Alice Springs (AUS)	0.0%
Ilorin (NGR)	8.5%
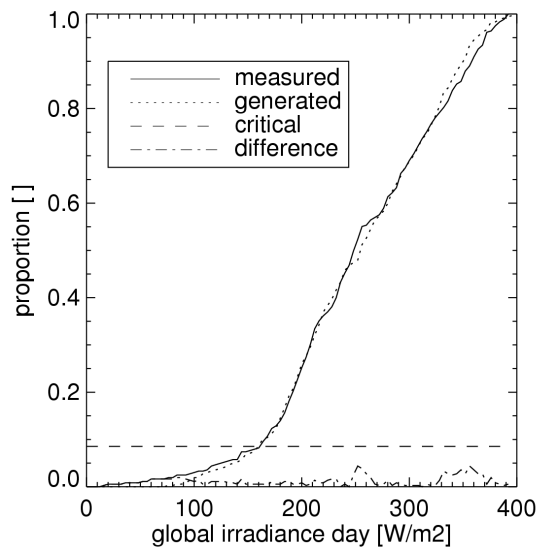
Fig. 6.6.2:   Cumulative distribution functions of daily values of global irradiance for Alice Springs (AUS).

6.6.1.4 Generation of hourly values from daily values

The generation of hourly values is based on the model of Aguiar and Collares-Pereira (1992) (TAG-model: **T**ime dependent, **A**utoregressive, **G**aussian model). This model consists of two parts: the first part calculates an average daily profile (Eqn. 6.6.2); the second part simulates the intermittent hourly variations by superimposing an autoregressive procedure of the first order (AR(1)-procedure) (Box et al., 1994) (Eqn. 6.6.3).

$$k_t(h) = k_{tM}(h) + y(h) \tag{6.6.11}$$

$k_t(h)$: hourly clearness index

$k_{tM}(h)$: hourly clearness index of the average daily profile

$y(h)$: first order autoregressive function

h: hour

Average daily profile

The proposed model is based on the clear sky daily profile:

$$Gh = Gh_d \cdot \frac{Gh_c}{Gh_{c,d}} \tag{6.6.12}$$

where Gh_d is the daily global horizontal irradiance, Gh_c the clear sky hourly global irradiance, $Gh_{c,d}$ the daily clear sky global irradiance. Other authors like Grüter et al. (1986) have used this approach as well. Clearness index k_{tM} is calculated with Eqn 6.3.6. Fig. 6.6.3 shows typical forms of the profiles.
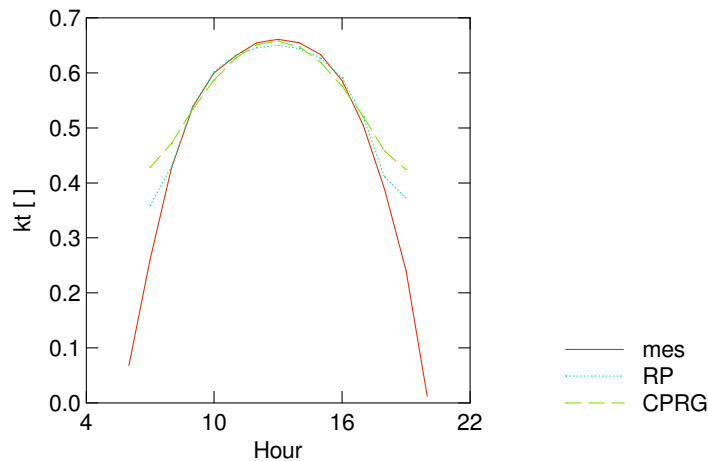
Fig. 6.6.3:   Mean daily profiles of KT_h for daily KT_d values of 0.6 at San Juan PR.

At noon all lines are very close. At low solar altitude the measured values are lower than the modeled ones; the new model is in between the measurements and the values of the model used in ESRA. Further, significantly higher KT_h values are measured and calculated for very low solar altitudes. The model quite often yields – as do the measured values – higher KT_h values for the first and the last hour of the day. This is due to the one dimensional concept of the clearness index, where, as in nature, the radiation – particularly at low solar elevation – is influenced by the three dimensional form of the atmosphere. To avoid unreasonable values, the KT_h values are limited to values of 0.8 for solar elevation below 10°.

Hourly variations

The amplitude of the daily profile and the standard deviation of the perturbations are dependent on the daily K_t value and the solar altitude. The first order autocorrelation depends on the K_t value, i.e. it is smaller for high and low values of K_t than for central values. The standard deviation of two adjacent hourly values is far greater for central K_t values than for extreme values (Eqn. 6.6.4). Owing to this, the daily profiles at small daily average radiation are comparatively flat, for central values highly intermittent, and for large values flat again.

The model is site independent. Model definition and validation were performed using data from Belgium, Germany, Switzerland, United Kingdom, Australia and USA. The autoregressive function y(h) is determined as follows:

$$y(h) = \phi_1 \cdot y(h-1) + r$$

$$\phi_1 = 0.148 + 2.356 \cdot K_t - 5.195 \cdot K_t^2 + 3.758 \cdot K_t^3$$

$$\sigma(K_t) = 0.32 \cdot \exp\left[-50 \cdot (K_t - 0.4)^2\right] + 0.002 \qquad (6.6.13)$$

$$\sigma' = \sigma \cdot \left(1 - \phi_1^2\right)^{0.5}$$

$$r = N(0, \sigma')$$

ϕ_1 :　　　　First order autocorrelation

$\sigma(K_t)$:　　Standard deviation of y perturbations

σ' :　　　Standard deviation of the normally distributed random function

r :　　　　Normally distributed random variable with expected value 0 and standard deviation s'

Limiting KT_h values are set for clear sky radiation, where an overshoot of 10% is allowed. There is also the condition that only positive values can occur. The application of limiting values does, however, alter the AR(1) procedure, since the hourly average values of the perturbations are then no longer normally distributed. The result is a reduction of the first order auto-correlation, i.e. the generated data do not display the auto-correlation values defined by the model. This became apparent during validation of the TAG model. A decision was made to modify the auto-correlation function.

In Version 6.0 new limiting conditions have been introduced in order to lower this effect. Instead of capping the values outside the limits, the y values have been stretched to the allowed minimum and maximum values.

It is essential that the auto-correlation and the standard deviation be both correctly modelled. When using the Perez (1991) model to calculate diffuse radiation from the (generated) global radiation, the model uses a time series of G_h (3 successive hourly values). The problem of the non-Gaussian distribution of the intermittent hourly values was accounted for in Graham and Holland's (1990) model using a function that maps the Gaussian distribution to a beta distribution. A simpler procedure was chosen in the present model. The distortion of the first order correlation is corrected using a multiplication factor, k (Eqn. 6.6.14). In this procedure, the value of the standard deviation, which is well reproduced by the model, is retained. Thus, in calculating the standard deviation, the uncorrected first order auto-correlation value must be used. The effect of including the factor k would be to increase the standard deviation. Since, however, ϕ_1 is reduced again during data generation. The standard deviation defined by the model can be used.

$$y(h) = k \cdot \phi_1 \cdot y(h-1) + r$$

$$\text{correction factor}: k = 2.0 \qquad (6.6.14)$$

The autocorrelation function has been adopted to 5 BSRN sites in the USA (Fig. 6.6.4). This subset was chosen, as it showed the best results (for all test sites). The standard deviation model has been modeled by hand. Adopted models showed less good results.
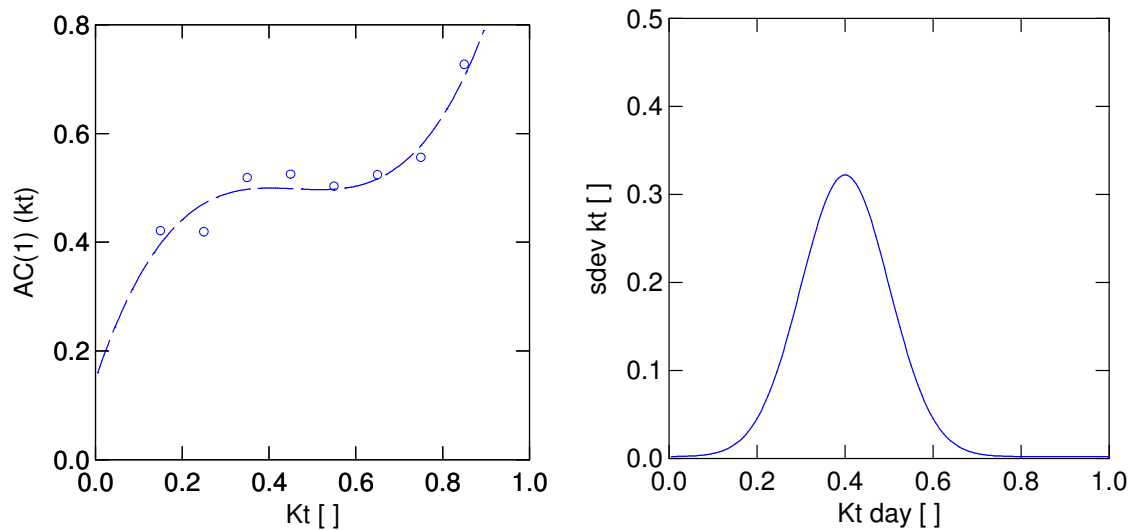
Fig. 6.6.4:   Left: First order autocorrelation as a function of daily K_t value adopted for five BSRN stations in the USA. Right: Modeled standard deviation function.

The TAG model permits small discrepancies between the daily and monthly average value of the generated values and the given values. The generated values are modified accordingly to ensure that the average values are always equal (as would be expected). If the daily or the monthly average of the generated data differs from the original value by less than 5%, the generated data are multiplied by a normalisation factor, otherwise the hourly values are regenerated using a new run. The procedure causes no appreciable distortion of the data distribution.

During validation it became clear, that the generation process is clearly linked to the diffuse generation process. Changing this model, also the diffuse generation is changed.

Validation

The calculated mean values are adapted to the measured, so there is no difference at this level. The distribution has been tested at 5 BSRN sites (Tab. 6.6.12) with Kolmogorov-Smirnov (KS) test: Generally a good agreement is achieved. Nevertheless at all sites there are areas, where the critical value is overshot (Tab. 6.6.11). Most of the sites show biggest differences at 50-300 W/m^2. Figure 6.6.5 shows a typical cumulative distribution function for Camborne (GBR). Figure 6.6.6 shows the histograms of the same site.

Tab. 6.6.11:   Kolmogorov-Smirnov test (KSI over %) for hourly global radiation.

Site	KSI over %
Payerne (CHE)	0.9%
Camborne (GBR)	12.5%
Boulder (CO, USA)	12.6%
Alice Springs (AUS)	17.5%
Ilorin (NGR)	11.8%
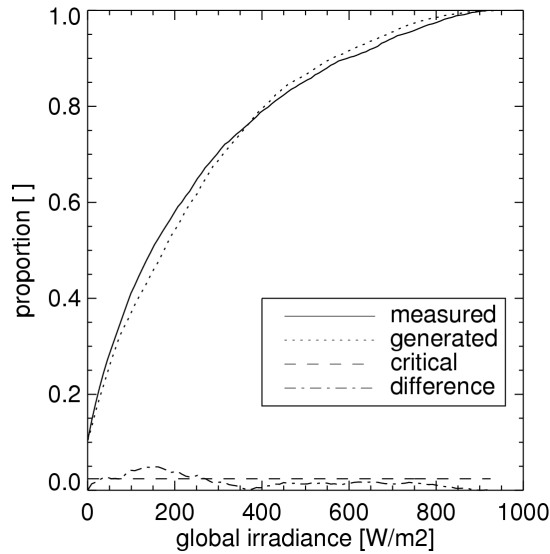
Fig. 6.6.5:   Cumulative distribution functions of hourly values of global irradiance for Camborne (GBR).
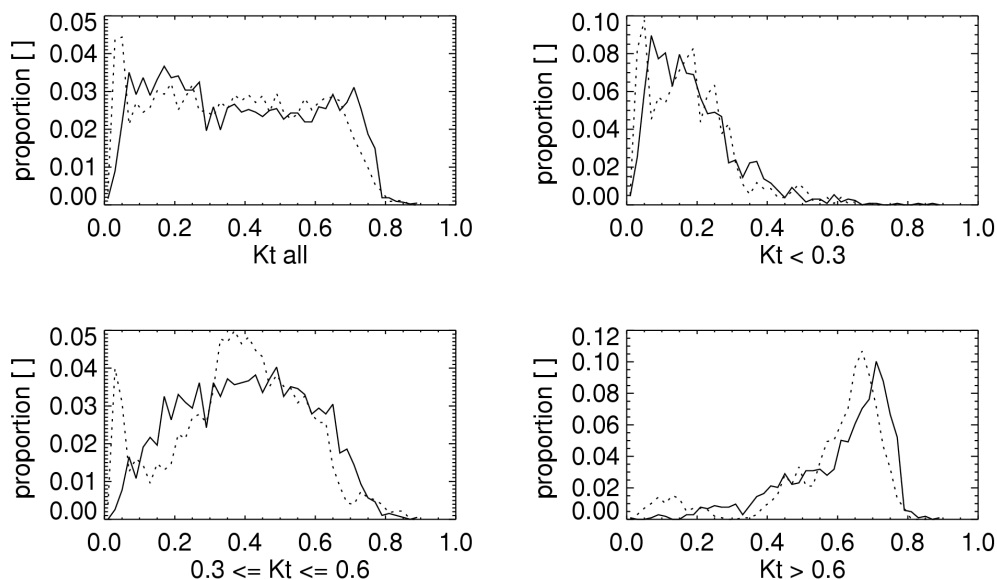
Fig. 6.6.6.   Histograms of hourly global irradiance for Camborne (GBR) depending on the daily clearness index (Kt). Measured values: full line, generated: dotted line

The autocorrelation was examined for 17 sites (Tab. 6.6.12). The first autocorrelation value (ac(1) – which is the measured equivalent to $\phi 1$ in Eqn. 6.6.13) and the standard deviation (sd – which is the measured equivalent of σ in Eqn. 6.6.13) depending on the daily clearness index (Kt) were compared graphically (Fig. 6.6.7). The autocorrelation ac(1) is underestimated on average by 14%, the standard deviation (sd) is underestimated on average by 23% (Tab. 6.6.13). Tests with enhanced values showed better results in this test, but did lead to much less accurate beam and diffuse separation. This was the reason to leave the values at this level.
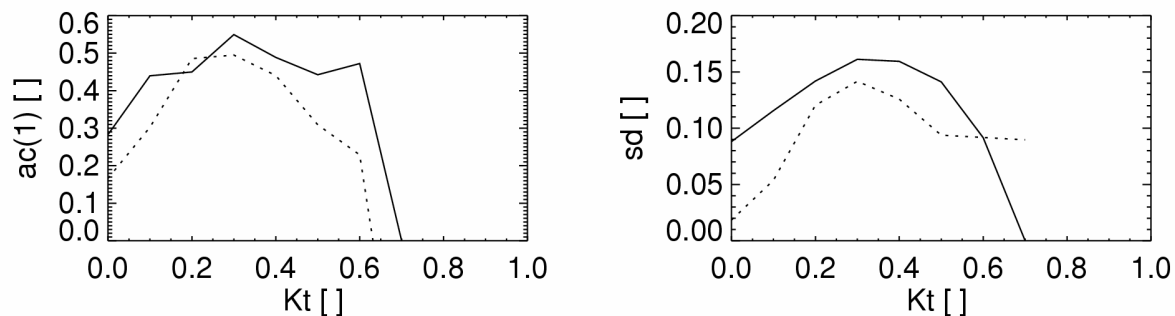
Fig. 6.6.7:   Comparison of measured values (full line) and generated (dotted line) autocorrelation (ac(1)) and standard deviation sd at Cambourne (GBR).

Table 6.6.12:   Measured autocorrelation (AC(1)) and standard deviation and factors of the generated values.

Site	AC(1) mes. [ ]	AC(1) gen factor [%]	Std dev. mes. [ ]	Std dev. mes. factor [%]
Uccle	0.428	58.1	0.100	43.3
Trier	0.474	103.5	0.109	84.0
Dresden	0.476	127.7	0.111	67.8
Hamburg	0.449	99.8	0.101	74.0
Braunschweig	0.461	113.1	0.107	71.2
Würzburg	0.475	55.2	0.110	34.6
Weihenstephan	0.445	127.4	0.116	77.8
Payerne	0.436	72.7	0.119	66.7
Alice Springs	0.335	70.8	0.124	102.5
Camborne	0.454	97.1	0.111	81.4
Bonville	0.370	70.2	0.116	90.8
Goodwin Creek	0.452	83.9	0.115	90.7
Penn State Univ.	0.433	88.5	0.113	87.8
Desert Rock	0.317	56.8	0.136	87.6
Sioux Falls	0.453	82.5	0.141	84.8
Table Mountain	0.436	87.7	0.157	94.8
Fort Peck	0.391	69.3	0.142	83.8
Mean value		86.1		77.7

6.7   Radiation on inclined surfaces

Radiation data on horizontal surfaces is seldom needed. A collector, the wall of a building, or a roof, for example, regards the sun from another "viewpoint". Thus methods are required by means of which the hourly values can be obtained by transforming given (generated) radiation data to an arbitrarily orientated surface.

The calculation of radiation on an inclined surface using (generated) hourly values of global horizontal radiation is done in two steps: First the average hourly global horizontal radiation values are resolved into direct and diffuse components. This is done using the model of Perez et al. (1991). In a second step, the radiation on an inclined surface is calculated with the help of these components. For this, another model of Perez (1986) is used. The second model also includes the effect of raised skyline.

6.7.1   Calculation of radiation components with given global horizontal radiation

The dynamic model of Perez et al. (1991), which transforms global hourly horizontal radiation values into hourly values of direct normal radiation (direct radiation on a surface normal to the radiation) is based on parameters defining sky conditions. The model requires input in the form of time series of global radiation values. The model can also be extended to include the dew point temperature.

The model, in fact, is based on a variable selection of input parameters. The greater the number of available parameters, the better the approximation of direct normal radiation. The following input is required:

- Global horizontal radiation, or alternatively, normalized clearness index k_t', whereby for k_t' a formula independent of the zenith angle is used (Perez et al. 1990b).

- Zenith angle of the sun.

- When time series of global radiation are available, a stability index $\Delta k_t'$ can be calculated giving the dynamics of the time series. $\Delta k_t' = 0.5 \cdot \left(\left| k_t'_i - k_t'_{i+1} \right| + \left| k_t'_i - k_t'_{i-1} \right| \right)$ where points i and i + 1 refer to the present, previous and subsequent hour.

- When the dew point temperature is available, it can be used to provide an accurate estimate of water content (humidity) in the atmosphere which in turn influences the absorption and the production of aerosols. The humidity is estimated on the basis of dew point temperature by the method of Wright et al. (1989).

The present model was derived empirically from a large series of data for a range of climatic regions in Europe and America. Depending on the form of the input data, it utilizes two to four parameters. It consists in the main of look-up tables together with a simple mathematical section.

Further information on the models and their mode of operation may be found in the conference proceedings of the International Solar Energy Society (Perez et al., 1991).

6.7.1.1 Validation

Diffuse radiation is tested in two steps. First the model was tested alone with measured hourly values of global radiation as input, and secondly within the combined model using generated hourly values.

<u>Test using measured hourly values:</u>

The tests were carried out for three weather stations in Payerne (BSRN, CH), Vaulx-en-Velin (IDMP, F) and Melbourne (IDMP, AUS). The average mbe error was 4 W/m^2 (over all hours) (generated values slightly too high) and the rmse standard deviation 39 W/m^2 ($G_h > 0$).

<u>Test using generated hourly values:</u>

The model performance has been tested at 17 sites by looking at the yearly means of generated diffuse and beam irradiances (Tab. 6.7.1). The calculated yearly means of beam radiation have a mean bias error (mbe) of 1.1 and a root mean squared error (rmse) (definition e.g. in Argiriou, 1999) of 11.3 W/m^2 (7.4%). For diffuse radiation a mbe of 0.8 and a rmse of 4.7 (7.1%) was estimated. The estimation of monthly values of diffuse irradiance has an rmse of 10.7 W/m^2. The accuracy could be enhanced significantly compared to older versions by introducing changes in the standard deviation and the autocorrelation function of the stochastic generation (Eqn. 6.6.13) and the new turbidity climatology with daily variations.

On a global scale, the error in calculated diffuse radiation does not show regional patterns. The error distribution shows a sligth yearly pattern. In winter the rmse's are registered somewhat bigger.

Tab. 6.7.1:   Comparison between yearly means of measured and generated diffuse and beam values.

Station	Years	Diffuse mes. [W/m^2]	Diffuse gen. [W/m^2]	Diffuse difference [W/m^2]	Beam mes. [W/m^2]	Beam gen. [W/m^2]	Beam difference [W/m^2]
Uccle (BEL)	1981-90	65.9	64.2	-1.7	81.6	88.5	6.9
Trier (DEU)	1981-90	67.1	63.7	-3.4	92.9	106.7	13.8
Dresden (DEU)	1981-90	61	65.3	4.3	100.3	96.8	-3.5
Hamburg (DEU)	1981-90	61.5	60.7	-0.8	84.5	91.9	7.4
Braunschweig (DEU)	1981-90	67.5	64.3	-3.2	85.3	97.7	12.4
Würzburg (DEU)	1981-90	69.2	63.3	-5.9	96	115.7	19.7
Weihenstephan (DEU)	1981-90	65.6	65.8	0.2	98.5	105.7	7.2
Payerne (CHE)	2005	63.7	66.3	2.6	154.5	148.1	-6.4
Alice Springs (AUS)	2005	56.5	69	12.5	315.4	295.2	-20.2
Camborne (GBR)	2005	69.3	68.4	-0.9	105.7	109.6	3.9
Bonville (USA)	2005	73.5	78.7	5.2	174.8	173.4	-1.4
Goodwin Creek (USA)	2005	75.1	83.8	8.7	189.3	165.9	-23.4
Penn State Univ. (USA)	2005	74.9	74.3	-0.6	135.4	144.2	8.8
Desert Rock (USA)	2005	51.4	53.3	1.9	290.5	295.2	4.7
Sioux Falls (USA)	2005	69.5	69	-0.5	183.7	182.3	-1.4
Table Mountain (USA)	2003	66.4	68.8	2.4	229.8	222.1	-7.7
Fort Peck (USA)	2005	66.1	62.5	-3.6	187.6	189.8	2.2
Mean value (USA)	2005	66.1		1.0	153.3		1.4
RMSE			4.7 (7.1 %)			11.3 (7.4 %)	

The distributions of generated and measured diffuse radiation are similar, but do differ statistically. In Table 6.7.2 the KSI over% test at 5 sites for hourly beam radiation are listed. Figure 6.7.1 shows the distributions at Boulder (CO, USA).

Tab. 6.7.2:   Kolmogorov-Smirnov test (KSI over %) for hourly beam radiation.

Site	KSI over %
Payerne (CHE)	22.8%
Camborne (GBR)	81.6%
Boulder (CO, USA)	59.9%
Alice Springs (AUS)	106%
Ilorin (NGR)	159%
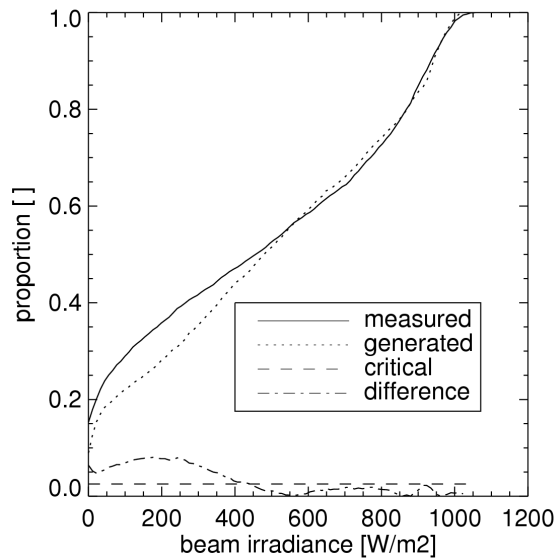
Fig. 6.7.1:   Cumulative distribution functions of hourly beam irradiance for Boulder (CO, USA).

Beam is slightly underestimated mainly for lower Linke turbdity values (Fig. 6.7.2).
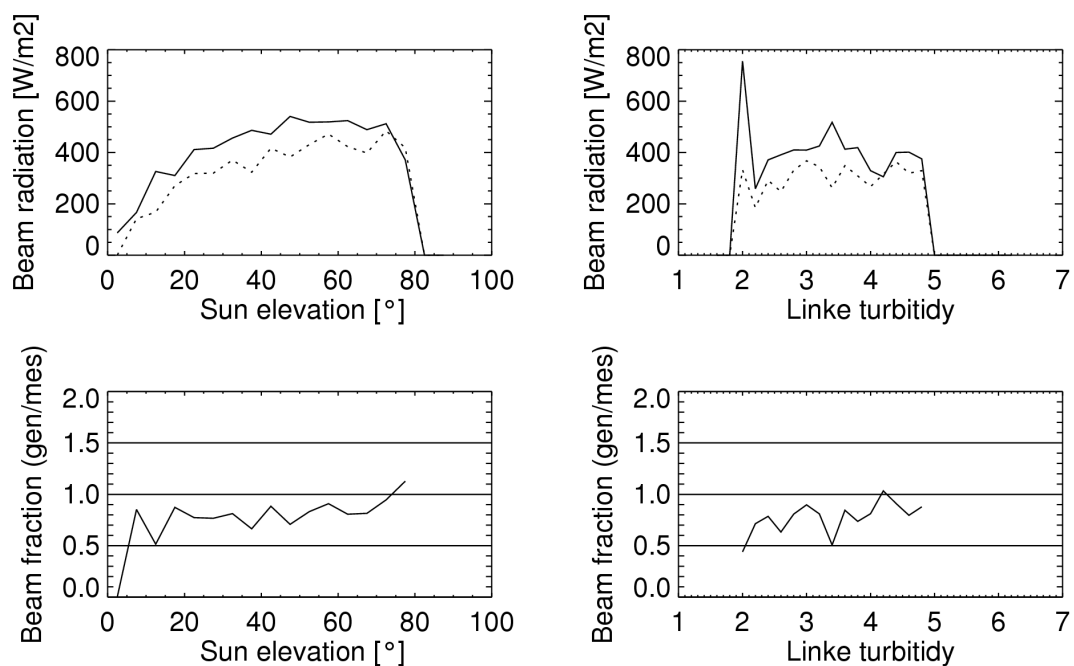
Fig. 6.7.3:   Analyses of the hourly values of beam for Goodwin Creek (MS, USA). Measured values for the years 2005 (full line) and generated data (dots).

6.7.2 Calculation of global and diffuse radiation on inclined surfaces

In Meteonorm Version 6.0 four models for calculation of radiation on inclined planes are included. The Perez model (Perez et al. 1986) is still the default model. All models enable global and diffuse radiation to be calculated on an inclined surface using the two input values of global horizontal and diffuse horizontal radiation. In version 6.0 the following three hourly models and a new model based on minute time resolution have been added:

- Hay's model (1979)

- Skartveit and Olset model (1986)

- Gueymard's model (1987)

- minute time resolution model (Skartveit and Olseth, 1986)

Perez model

In this handbook only the default model of Perez is described in some details. For the three other models we refer to publications. By means of Eqn. 6.7.1, the diffuse radiation on an inclined surface is calculated from the two components diffuse celestial irradiance (B_k and D_k^c) and diffuse reflected irradiance (G_k^r).

$$G_k = B_k + D_k^{\ c} + D_k^{\ r} \tag{6.7.1}$$

The diffuse reflected irradiance (D_k^r) is calculated with the following model:

$$D_k^{\ r} = \underbrace{\frac{1-\cos(\beta)}{2}}_{r_R} \cdot (\rho \cdot G_h) \tag{6.7.2}$$

where β is the surface inclination, r_R the isotropic reflected view factor and ρ the surface albedo (see Chapter 6.7.2.1).

The diffuse celestial radiation on an hourly basis may not be assumed to be isotropic. It is therefore further divided into the components circumsolar, isotropic and horizontal ribbon. The model governing the equation for diffuse celestial irradiance is (Eqn. 6.7.3):

$$D_k^{\ c} = \underbrace{D_h \cdot (1 - F_1)\underbrace{\frac{1 + \cos \beta}{2}}_{r_D}}_{\text{isotropic}} + \underbrace{D_h \cdot F_1 \cdot a/b}_{\text{circumsolar}} + \underbrace{D_h \cdot F_2 \cdot \sin \beta}_{\text{horizontal ribbon}} \tag{6.7.3}$$

where F1 and F2 are coefficients expressing the degree of circumsolar anisotropy and anisotropy at the horizon/zenith respectively, and a and b are as given below

$$a = \max(0, \cos\Theta) \text{ and } b = \max(0.087, \cos Z) \tag{6.7.4}$$

where Θ is the incidence angle of the sun on the inclined surface and r_D the isotropic diffuse view factor. r_D and r_R are related by the expression

$$r_R = 1 - r_D \tag{6.7.5}$$

The three components are calculated separately and then summed to provide the diffuse celestial irradiance. A detailed description of the Perez model for different values of F_1 and F_2 may be found in Perez et al. (1986, 1987 and 1990a).

6.7.2.1 Albedo

The albedo is calculated with a model that gives albedo as a function of temperature. The model was introduced for version 5. Data of GEBA (Goose, Fredericton, Jokmok, Toronto, Hamburg, Payerne) and WRC Davos (ASRB network Davos and Weissfluhjoch) have been used for adopting and testing the model.

For areas with great amount of snow :

$$\rho = 0.618 - 0.044 \cdot Ta \quad , 0.2 \leq \rho \leq 0.8$$

For the rest of the world :

(6.7.6)

$$\rho = 0.423 - 0.042 \cdot Ta \quad , 0.2 \leq \rho \leq 0.8$$

The r^2 values for both models are 0.92, resp. 0.93. A distinct separation for areas with a great amount of snow and areas with less snow was found. A great amount of snow enhances the possibility of fresh snow and therefore higher albedoes and prolongates the time of snow cover in spring. For temperatures below -10 °C and above 10 °C there is no difference between the models. The separation into the 2 groups is not easy. As a first approximation the following rule is used for areas with a great amount of snow:

- Sum of precipitation for 3 winter months > 150 mm

- Mean temperature for 3 winter months < -3 °C

The new model gives very similar results to the model used in versions 3 and 4 in the range of 0.2–0.5 (Fig. 6.7.4). The big difference is for values greater than 0.5, which did not exist with the old model – but has been found in the data.
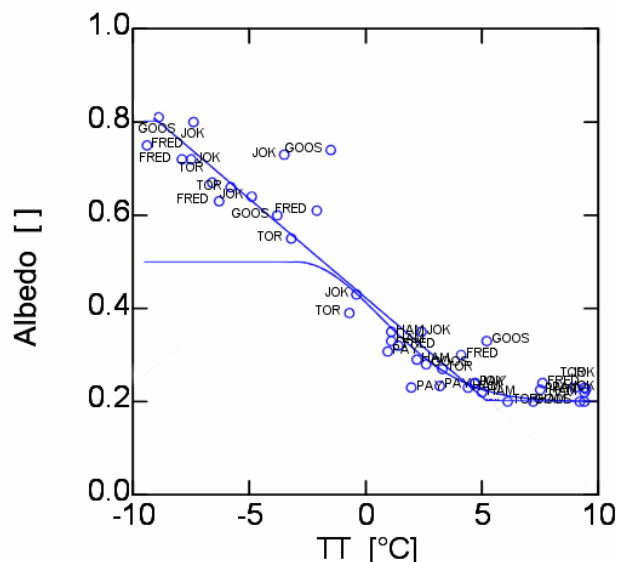
Fig. 6.7.4:   Albedo vs. temperature (TT). Model used in version 3 and 4 (with max. at 0.5) and new model (max. at 0.8).

In various tests the following temperatures have been evaluated to use for albedo calculation: With hourly generated data the mean of the last 2 weeks is used. If only monthly temperature values are available the interpolated daily value of the day 5 days before is used.

6.7.2.2 Validation of the slope irradiance model

The generated diffuse radiation on inclined planes is calculated in two stages. The two Perez models were first tested alone with measured hourly values of global radiation as inputs. Secondly they were tested within the combined model, using generated hourly radiation values.

Validation with measured hourly radiation was carried out for 2 sites in Switzerland for inclinations of 33–45° with a more or less South orientation (typical for solar energy applications) and also for a West facing facade in Bavaria (typical exposure for overheating studies).

Validation with generated hourly radiation was made at 18 sites throughout the world.

Tests using measured hourly values:

Inclined surfaces:

The tests were carried out for 2 sites in Switzerland with data of 1993 (Berne-Marzili, 46.95°N, 7.45°E, 520 m, inclination 35°, azimuth: 37°E; Locarno-Magadino: 46.18°N, 8.85°E, 197 m, inclination: 35°S, azimuth: 15°W). The average mbe error in the hourly values was 5 W/m^2 (over all hours) (generated values slightly too high) and the rmse standard deviation 33 W/m^2 ($G_h > 0$). For monthly average values, the mbe was 3 W/m^2 (5%) and the rmse 5 W/m^2.

Facades:

The test was carried out at Holzkirchen (Bavaria; 11.71°E, 47.87°N, 680 m) for a West facade. The average mbe error in the hourly values was 3 W/m^2 (over all hours) (generated values slightly too high) and the rmse standard deviation 51 W/m^2 ($G_h > 0$). For monthly average values, the mbe was 3 W/m^2 (0%) and the rmse 8 W/m^2 (13%).

Tests using generated hourly values:

The monthly and yearly means are examined. The tests were carried out for 14 sites in many different climate zones and different inclinations (18° to 90°) (PVPS 2007) (Tab. 6.7.3). Only measurements with pyranometers (for horizontal as well as inclined planes) have been used.

Tab. 6.7.3:   Test sites for global radiation on inclined plane models

Site	country	Source	Altitude	Latitude	Longitude	Azimuth	Inclination
			[m]	[°]	[°]	[°]	[°]
Locarno-Magadino	Switzerland	PVPS	222	46.18	8.86	195	45
Kobe	Japan	PVPS	100	34.70	135.10	180	20
Mexicali	Mexico	PVPS	3	32.66	-115.46	180	18
Cloppenburg	Germany	PVPS	40	52.85	8.03	180	32
Akakuma	Japan	PVPS	200	35.05	135.48	158	27
Kanan	Japan	PVPS	0	38.40	141.30	140	27
Burgdorf	Switzerland	HTI	530	47.02	7.62	170	28
Huvudsta	Sweden	PVPS	50	59.20	18.00	162	**80**
Bern-Marzili	Switzerland	PVPS	540	46.95	7.44	143	35
Mt. Soleil	Switzerland	PVPS	1270	47.15	7.00	153	50
Liestal	Switzerland	PVPS	327	47.29	7.44	180	30
Gontenschwil	Switzerland	PVPS	352	47.28	8.12	212	30
Toyooka	Japan	PVPS	163	35.50	134.80	180	20
Holzkirchen	Germany	HOKI	680	47.87	11.71	270	**90**

The 4 different models did show similar results (Tab. 6.7.4). Due to uncertainties based on the measurements the differences are too small to rank the models seriously. Nevertheless for monthly values Perez model showed the best results, followed by Gueymard's, Hay's and Skartveit's model. The average mbe error of Perez' model was 0 W/m^2 and the rmse standard deviation 8 W/m^2.

Tab. 6.7.4:   Accuracy of monthly and yearly values of radiation on tilted planes

	Perez	**Hay**	**Gueymard**	**Skartveit**
Monthly mbe [W/m^2]	0.4	-2.7	-1.7	-3.4
Monthly rmse [W/m^2]	8.0	9.9	8.8	8.6
Yearly mbe [W/m^2]	-0.9	-5.2	-3.8	-6.2
Yearly rmse [W/m^2]	5.5	7.2	6.5	7.6
Yearly rmse [%]	4.0	5.3	4.7	5.5
Yearly rmse 0-50° [W/m^2]	5.0	7.7	6.7	8.1
Yearly rmse > 50° [W/m^2]	8.2	3.1	5.0	3.2

At some sites the differences have a distinct yearly pattern with an overestimation in winter (e.g. Switzerland). In other regions these effects are not visible.

For yearly average values, the mbe of Perez model was -1 W/m2 and the rmse 6 W/m^2 (4%). For inclination above 50° the calculation is partly better. For facades Hay's and Skartveit's model are the best, followed by Gueymard's and Perez' model.

6.7.3   Modification of radiation due to horizon

The aim of the modification method described here is to calculate the radiation at sites with raised (distant) horizons. A number of assumptions which were used in the raised (local) skyline model are not valid in this case. In the following chapter, the modification procedure for the different radiation components is described.

6.7.3.1 Modification of direct radiation by skyline profile

It is clear that direct radiation is affected by a raised (i.e. non-horizontal) horizon in such a way that when the sun is occluded by the horizon, no direct radiation can impinge on the inclined surface. In other words, the surface in question receives less direct radiation than it would with a horizontal skyline. In calculating hourly values, a check has therefore to be made whether the sun is above or below the skyline. If occluded by the skyline, the direct radiation on the inclined surface is zero.

The hourly direct radiation on an inclined surface (B_k) is set to zero under the following conditions:

- When the sun has not yet risen or has already set (hs<0).

- When the sun is behind the surface (cos(Θ)<0 ; where Θ = incident angle of radiation on inclined surface; Eqn. 6.7.5).

- When the sun is behind the skyline (hs < skyline altitude). Thus a check has to made each hour based on azimuth and solar altitude to establish whether the skyline altitude is greater or smaller than the solar altitude.

6.7.3.2 Modification of diffuse radiation by skyline profile

The diffuse radiation components are processed as follows:

- Circumsolar component: this is treated in the same way as direct radiation.

- The horizontal ribbon: this part of the diffuse radiation remains unchanged, i.e. it retains its original value independently of skyline profile. This is assumed for the reason that the sky immediately above the horizon is often brighter than the rest of the sky. This applies not only in regions with

practically level horizons but also in mountainous regions. In mountainous regions in summer, this is often caused by the bright convective clouds that tend to form above ridges and peaks.

- Diffuse isotropic and reflected irradiance (D_k^r) are calculated as follows:
  If the skyline is not horizontal, a larger proportion of ground and smaller proportion of sky is visible to the surface. This implies that the view factors (r_D, r_R) must be modified when a raised skyline is present. The skyline profile is normally given as a closed polygon whose points are specified in terms of azimuth and altitude. The proportion of the sky which, despite the existence of a skyline profile is still seen by the inclined surface, may be calculated by numerical integration. From the isotropic diffuse view factor calculated in this way, the isotropic reflected view factor may be calculated as given in Eqn. 6.7.5. The diffuse radiation with skyline effect can be calculated using the new values of r_R and r_D in Eqn. 6.7.2 or 6.7.5. In Eqn. 6.7.2, the global horizontal radiation (G_h) must also be changed. This is done by calculating horizontal radiation with raised horizon (G_h^{hor}) for a horizontal surface.
  In case of far horizons (typically from mountains) the circumsolar part is kept (Eqn. 6.7.7):

$$\cos(\Theta) > 0, \text{hs} > \text{skyline altitude}, \; G_h{}^{hor} = \frac{B_n + D_h \cdot \left[(1 - F_1) \cdot r_D{}^{hor} + F_1 \cdot a/b\right]}{1 - \rho \cdot r_R{}^{hor}}$$

$$0 < \text{hs} < \text{skyline altitude}, \; G_h{}^{hor} = \frac{D_h \cdot \left[(1 - F_1) \cdot r_D{}^{hor}\right]}{1 - \rho \cdot r_R{}^{hor}}$$

$$(6.7.7)$$

6.7.4   Conclusions

The validation procedure for the complete model shows that coupling the various models to provide hourly values produces satisfactory results. Thus the basic procedure for generating hourly values of meteorological data at any desired location has proved to be a valid approach. On average, the model overestimates yearly average global radiation values by 0 W/m^2 by the default model. The rmse comes to 6 W/m^2 (4%).

The distributions of daily global irradiance values are similar to the measured at all test sites. For hourly values the discrepancies are bigger and for beam irradiance the distributions don't pass the nullhypothesis of KS test. Nevertheless the distributions are similar at most sites for the biggest part of possible values (especially for higher values above 500 W/m^2).

Although most of the models were checked independently, not all of them could be validated in depth. For example, those for removing and superimposing raised horizons could not be checked owing to a lack of data.

6.8 Minute time resolution radiation data

6.8.1 Minute to minute generation model

6.8.1.1 Data

The following sites (alle BSRN stations) have been used to adapt the model (Tab. 6.8.1)

Tab. 6.8.1: Sites used to adapt the model (all BSRN sites)

Name	Country	Period / time resolution
Payerne	Switzerland	1.1.2005 – 31.12.2005, 1 Minute
Camborne	UK	1.1.2005 – 31.12.2005, 1 Minute
Fort Peck	USA	1.1.2005 – 31.12.2005, 3 Minute
Penn State Univ.	USA	1.1.2005 – 31.12.2005, 3 Minute
Table Mountain	USA	1.1.2005 – 31.12.2005, 3 Minute
Bondville	USA	1.1.2005 – 31.12.2005, 3 Minute

6.8.1.2 Model

A new model was used, which is based on the TAG model of Aguiar and Collares-Pereira (1992), which is also used for stochastic generation of hourly values (chapter 6.1.1.4).

$$k_t(\min) = k_{tM}(\min) + y(\min) \tag{6.8.1}$$

$k_t(\min)$: Minute clearness index

$k_{tM}(\min)$: minute clearness index: linear interpolation between each hourly values

$y(\min)$: first order autoregressive function

$\min$: minute

$$y(\min) = \phi_1 \cdot y(\min-1) + r$$
$$\sigma' = \sigma \cdot \left(1 - \phi_1^2\right)^{0.5}$$
$$r = N(0, \sigma') \tag{6.8.2}$$
$$k_{t\min}(\min) \leq k_t(\min) \leq k_{t\max}(\min)$$

Instead of modelled values of ϕ, σ, $k_{t\,min}$ und $k_{t\,max}$, lookup tables values are used for minute values. These tables have been made with help of measurements. Some values of ϕ have been adopted by hand to enhance the results.

Tab. 6.8.2: ϕ, σ, $k_{t\,min}$ und $k_{t\,max}$ in dependency of $k_{t\,day}$ und $k_{t\,hour}$

ϕ	Kt_{day}	Kt_{day}	Kt_{day}	Kt_{day}	Kt_{day}	Kt_{day}	Kt_{day}	Kt_{day}
kt_{hour}	0.05-0.15	0.15-0.25	0.25-0.35	0.35-0.45	0.45-0.55	0.55-0.65	0.65-0.75	0.75-0.85
0.05 - 0.15	0.980	0.963	0.960	0.917	0.925	0.890	0.880	0.904
0.15 - 0.25	0.980	0.998	0.983	0.975	0.961	0.950	0.932	0.906
0.25 - 0.35	0.980	0.997	0.989	0.983	0.980	0.979	0.964	0.920
0.35 - 0.45	0.968	0.983	0.971	0.965	0.970	0.982	0.980	0.968
0.45 - 0.55	0.980	0.856	0.947	0.936	0.936	0.956	0.977	0.980
0.55 - 0.65	0.500	0.727	0.910	0.899	0.890	0.910	0.952	0.980
0.65 - 0.75	0.500	0.625	0.920	0.893	0.851	0.847	0.909	0.980
0.75 - 0.85	0.500	0.966	0.980	0.941	0.785	0.778	0.787	0.980
kt_{hour}	0.05-0.15	0.15-0.25	0.25-0.35	0.35-0.45	0.45-0.55	0.55-0.65	0.65-0.75	0.75-0.85
0.05 - 0.15	0.010	0.030	0.080	0.100	0.150	0.150	0.150	0.200
0.15 - 0.25	0.040	0.050	0.100	0.125	0.150	0.150	0.200	0.200
0.25 - 0.35	0.080	0.100	0.150	0.150	0.200	0.200	0.250	0.250
0.35 - 0.45	0.125	0.150	0.250	0.250	0.350	0.350	0.300	0.250
0.45 - 0.55	0.100	0.150	0.200	0.250	0.250	0.200	0.250	0.200
0.55 - 0.65	0.080	0.150	0.175	0.175	0.175	0.150	0.150	0.050
0.65 - 0.75	0.040	0.080	0.125	0.100	0.100	0.100	0.050	0.010
0.75 - 0.85	0.010	0.050	0.075	0.075	0.050	0.050	0.005	0.002
k_{tmin}	0.05-0.15	0.15-0.25	0.25-0.35	0.35-0.45	0.45-0.55	0.55-0.65	0.65-0.75	0.75-0.85
0.05 - 0.15	0.014	0.013	0.012	0.019	0.013	0.037	0.038	0.089
0.15 - 0.25	0.018	0.042	0.036	0.032	0.034	0.043	0.078	0.132
0.25 - 0.35	0.118	0.078	0.057	0.048	0.051	0.061	0.103	0.173
0.35 - 0.45	0.180	0.123	0.084	0.075	0.070	0.078	0.118	0.199
0.45 - 0.55	0.250	0.142	0.123	0.099	0.092	0.099	0.132	0.185
0.55 - 0.65	0.020	0.159	0.175	0.155	0.120	0.115	0.130	0.170
0.65 - 0.75	0.020	0.192	0.274	0.238	0.183	0.146	0.146	0.133
0.75 - 0.85	0.020	0.383	0.414	0.436	0.229	0.181	0.144	0.192
k_{tmax}	0.05-0.15	0.15-0.25	0.25-0.35	0.35-0.45	0.45-0.55	0.55-0.65	0.65-0.75	0.75-0.85
0.05 - 0.15	0.718	0.813	0.812	0.893	0.838	0.938	0.966	0.931
0.15 - 0.25	0.932	0.803	0.854	0.898	0.922	0.918	0.928	0.961
0.25 - 0.35	0.683	0.856	0.896	0.943	0.954	0.936	0.932	0.933
0.35 - 0.45	0.899	0.874	0.943	0.975	0.975	0.962	0.953	0.952
0.45 - 0.55	0.708	0.816	0.965	0.982	0.988	0.982	0.972	0.976
0.55 - 0.65	0.400	0.709	0.958	0.978	0.989	0.989	0.982	0.951
0.65 - 0.75	0.400	0.601	0.923	0.951	0.981	0.989	0.981	0.975
0.75 - 0.85	0.400	0.855	0.787	0.927	0.995	0.968	0.998	0.979

6.8.1.3 Validation

In Table 6.8.3 measured and generated values (ϕ, σ, mo/af = factor between morning and afternoon) are compared.

Tab. 6.8.3: Comparison between measured and generated values (minute time resolution). Mo/af: factor between radiation before and after noon.

Site	measured			generated			Factor		
	σ	ϕ	Mo/af	σ	ϕ	Mo/af	σ	ϕ	Mo/af
Boulder	0.199	0.915	1.126	0.284	0.693	1.061	1.427	0.757	0.942
Payerne	0.173	0.901	0.961	0.257	0.687	1.071	1.486	0.762	1.114
Camborne	0.141	0.803	0.966	0.221	0.694	1.015	1.567	0.864	1.051
Alice springs	0.243	0.929	1.031	0.337	0.686	1.038	1.387	0.738	1.007
Florianopolis	0.293	0.969	0.985	0.262	0.696	1.029	0.894	0.718	1.045
Ilorin	0.144	0.850	0.947	0.266	0.690	1.043	1.819	0.819	1.087
Mean	0.199	0.895	1.003	0.272	0.691	1.043	1.369	0.773	1.040

On average the sigma is overestimated by 37%, phi is underestimated by 23% and the mo/af factor is overestimated by 4%. That means, that variation is too high, the connection from minute to minute is tool low and the morning radiation is somewhat overestimated. Sigma isn't overestimated at every place, whereas phi is underestimated everywhere.

The distribution has been tested at 5 BSRN sites (Tab. 6.8.4) with Kolmogorov-Smirnov (KS) test:.

The distributions of generated and measured diffuse radiation are similar, but do differ statistically. In Table 6.8.4 the KSI over% test at 5 sites for hourly beam radiation are listed. Figure 6.8.1 shows the distributions at Payerne (CHE).

Tab. 6.8.4: Kolmogorov-Smirnov (KSI over %) test for minute global radiation.

Site	KSI over %
Payerne (CHE)	509%
Camborne (GBR)	635%
Boulder (CO, USA)	604%
Alice Springs (AUS)	471%
Ilorin (NGR)	750%
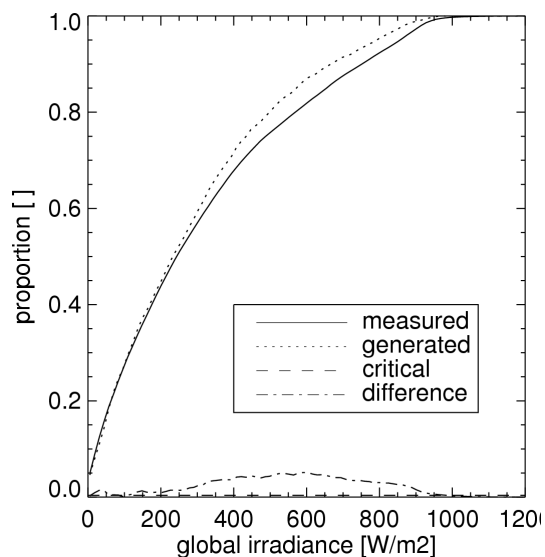
Fig. 6.8.1: Cumulative distribution of minute global radiation (Payerne CHE)

The two peaks of the distribution of clearness index can be reproduced, but are not that pronounced as in reality.
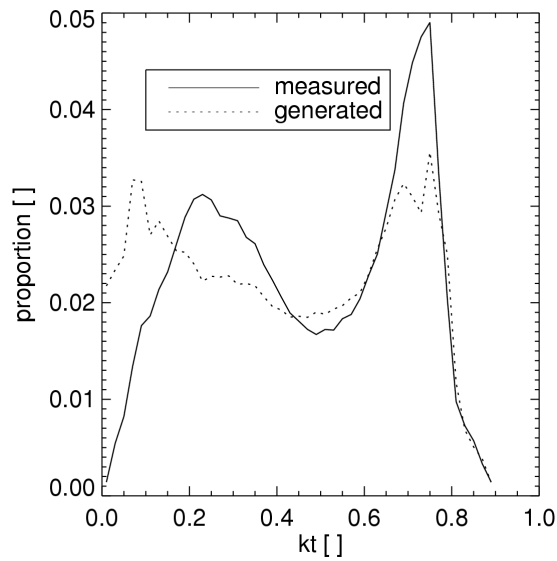
Fig. 6.8.2:   Distribution of minute clearness index (Payerne CHE)

Fig. 6.8.3 shows a time series of minute global and diffuse radiation at Florianopolis (BRA). All 3 types of days are shown realistic (low radiation and high radiation levels with low variations as well as mid radiation level with high variations).
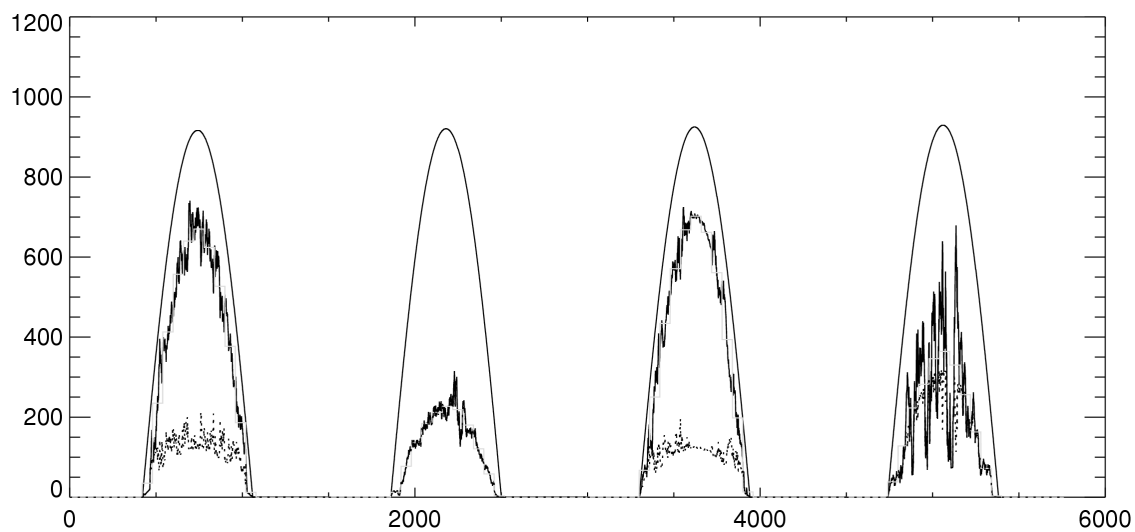
Fig. 6.8.3:   Time series of generated minute global radiation (Florianopolis BRA). Clear sky radiation (top solid line), global radiation (solid line) and diffuse radiation (dotted line) are shown.

6.8.1.4 Conclusions

The generated time series look reasonable. The distributions differ statistically, but are similar to measured ones. The generation process is able to produce distributions with two maxima. Nevertheless the generated distribution peaks are not that concise as the measured.

6.8.2   Minute to minute diffuse radiation

For radiation splitting the model of Perez et al. is (1991) used (the same model as used for hourly values). Some short tests with Erbs model (1982) have been made. Erbs model did give significant worse distribution results, allthough the mean values were also produced well.

Within the Perez model a factor for the variation parameter Δkt have been tested. We tested factors of 0.5, 0.75, 1.0 (no change), 1.25 and 1.5 to adopt to different variation levels of hourly and minute data. A short validation at 4 BSRN sites showed, that the factor 1 did give the best results. Therefore the original model is used.

Tab. 6.8.5:   Validation at 4 BSRN sites (yearly values).

	Beam Meas. [W/m^2]	Beam Gener. [W/m^2]	Difference Meas. – gen. [W/m^2]	Difference Meas. – gen. [%]
Camborne GBR	105	110	5	5
Payerne CHE	151	156	5	3
Alice Springs AUS	317	300	-17	-5
Boulder USA	224	229	5	2
Mean			1	0
Standard dev.			9	4

The distribution has been tested at 5 BSRN sites (Tab. 6.8.6) with Kolmogorov-Smirnov (KS) test:.

The distributions of generated and measured diffuse radiation are similar, but do differ statistically. In Table 6.8.6 the KSI over% test at 5 sites for hourly beam radiation are listed. Figure 6.8.1 shows the distributions at Payerne (CHE).

Tab. 6.8.6:   Kolmogorov-Smirnov (KSI over %) test for minute beam radiation.

Site	KSI over %
Payerne (CHE)	452%
Camborne (GBR)	622%
Boulder (CO, USA)	924%
Alice Springs (AUS)	1090%
Ilorin (NGR)	515%
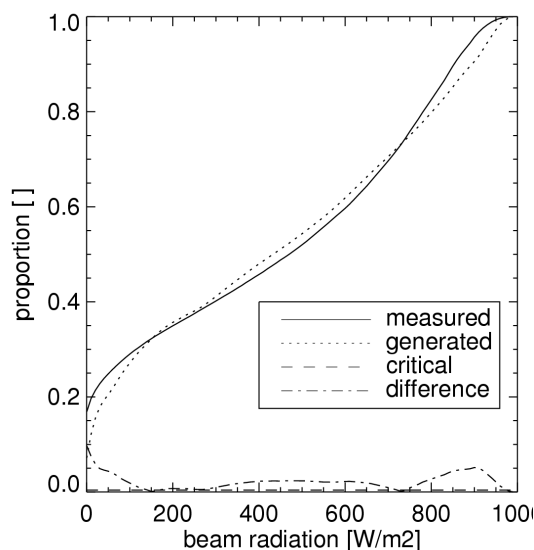
Fig. 6.8.4: Cumulative distribution of measured and generated beam irradiance at 1 minute time resolution in Payerne (Switzerland).

6.8.3 Minute to minute global radiation on inclined planes

For radiation on inclined planes the model of Skartveit and Olseth (1986) has been used.

The following errors have been estimated at 17 sites throughout the world (Tab. 6.7.3). Most error values are smaller for the minute time resolution model than for default hourly model.

Tab. 6.8.3: Validation of model for minute global radiation on inclined planes. Comparison with Perez' model used with hourly values.

	Perez diffuse Perez inclined pl. hourly values	Perez diffuse Skartveit inclined pl. minute values
Monthly values mbe W/m^2	3.8	0.2
Monthly values rmse W/m^2	9.9	9.5
20-50° inclination rmse %	5.7	5.5
80-90° inclination rmse %	9.8	9.1

7   Temperature and additional parameters

7.1   Temperature generation

7.1.1   Introduction

Any temperature values provided must conjoin with the global radiation time series, as daily temperature variations and solar radiation are inter-linked. For example, temperature is an important factor for simulation of solar energy systems (PV or thermal). The combination of solar radiation and temperature is critical in assessment of heating and cooling loads in buildings. The production of stochastically generated radiation data sets in isolation is not enough to help in such applications.

From the interpolation and radiation generation procedure described above, hourly values of global radiation and monthly temperature required for temperature generation are now available at all points. Using these, hourly temperature values may be calculated as follows.

In *METEONORM* Versions 2–4 a model based on Scartezzini (1992) was used. In version 5.0 a completely new model was introduced. This model was developed in the framework of the EU IST project SoDa.

In Version 6 the model was only slightly changed. The lowering of the temperature during the second half of the night time has been lowered to give more realistic values. Additionally a very similar generation process is introduced which results in more extreme distributions instead of mean distributions.

The idea underlying the model is still based on the assumption that the amplitude of the temperature variation during daytime is approximately proportional to the amplitude of the daily global radiation profile. Thus the temperature profile is calculated by transforming the radiation profile.

The model consists mainly of three parts:

1. The stochastic generation of daily values, based on monthly temperature and daily radiation values and measured temperature distributions.

2. The calculation of daily minimum and maximum temperatures, based on daily temperature values and daily and monthly radiation values.

3. The generation of hourly values, based on daily minimum and maximum temperature values and hourly radiation values.

7.1.2   Estimation of daily mean air temperatures

The daily temperature prediction problem faced was addressed by creating a new worldwide database describing the statistical patterns of observed temperature data across the world in different months of the year. The detailed description of this temperature database and its development is provided in Chapter 7.1.2.3. It is described how this statistical temperature data resource accessible to the generation process was created for approximately 8'000 stations using the Globalsod data prepared by the US National Climatic Data Centre (NCDC) covering the period 1996–2005.

A new and very fast generation process has been developed which draws on this database. It is described in Chapter 7.1.2.1.

7.1.2.1 Stochastic generation

First, a auto-regressive AR(1) process is run with almost no boundary settings. Then the distribution is mapped to the measured or interpolated distribution (according to the input), drawing on the statistical temperature data base resource.

Auto-regressive process

The auto-regressive process for daily temperature is executed in the following way:

$$Ta_d(dy) = Ta_d(dy-1) + \delta T$$
$$\delta T = dT' + r \cdot dT'_{sd}$$
$$r = N(0,1) \qquad\qquad (7.1.1)$$
$$dT' = \frac{dT(dy-1) + dT(dy)}{2}$$
$$dT'_{sd} = \frac{dT_{sd}(dy-1) + dT_{sd}(dy)}{2}$$

where, dT is the mean day to day difference, dT_{sd} is the standard deviation of the day to day difference, dy is the day number in the month and r is a normally distributed random variable with expected value 0 and standard deviation 1.

The temperature database is accessed to gain temperature data at the selected site using the nearest site interpolation procedure. This provides the statistical data needed to estimate dT' and dT'_{sd} which are needed to carry out the auto-regressive operation described by Equation 7.1.1. The stochastically generated time series of hourly global solar radiation is of course produced first as it is the temperature driving agent in this procedure. Both difference values are varied according to the calculated daily insolation. If this is above 50% of the clear sky value, the measured "mostly clear sky" value is used, otherwise the "mostly overcast" value is used. In order to get a more realistic daily difference, the mean of the current and the previous day is taken for both values.

This process is first run without any limitations on the minimum, maximum or mean values. After the generation of each month, a check is made whether the difference between the month's last daily value and the mean of the current and the following month is more than 4°C. If so, a correction term is introduced in order to keep the above difference below 4°C. The monthly mean of December is taken as the first value.

Mapping the distribution

After the generation and the application of the end of month correction, the daily values are mapped to the measured mean distribution, which is interpolated between the 7 stored quantiles (see "Input variables extracted …" below). This produces mean distributions and not extreme distributions. This means a statistically normal year is generated. Additionally, the yearly one day minimum is adopted as the January minimum in the northern hemisphere, or as the July minimum in the southern hemisphere and the yearly one day maximum is adopted as the summer (July/January) maximum in order to include mean one year extremes and not only monthly extremes.

The 4 days minimum temperature is calculated for January (in the northern hemisphere) or for July (in the southern hemisphere). This value is introduced in order to reproduce minimum design temperatures, which are normally defined using a period of several days.

If the generated 4-day minimum is more than 0.25°C higher than the measured value, the 4 days with the lowest minimum temperature are corrected to the measured value. If the difference is below 1°C, no changes to other days are made. If it is above 1°C the following 4 days or the 4 days before (dependent on the day of month) are raised in order not to change the monthly mean.

Input database

The Globalsod dataset was used. It contains approximately 8'000 stations worldwide with daily values and is accessible by internet. The data was collected by the National Climatic Data Center (NCDC), USA from national weather services.

Gathering data from each national meteorological service separately would have been both impractical and unaffordable to the SoDa and *METEONORM* project and could be not have been finished in the short time needed.

As for quality control, the data did undergo extensive automated control (by USAF, over 400 algorithms) to correctly 'decode' as much of the synoptic data as possible, and to eliminate many of the random errors found in the original data. Then, these data were controlled further as the summary daily data were derived. However, a very small percentage of errors still remain in the summaries of daily data.

The data of the 10 years 1996–2005 are used. Table 7.1.1 shows the number of stations in different continents. The worldwide total is 4'951 stations (not all of the 8'000 stations could be used), all with monthly data available. One drawback is that a 8 year period is climatologically rather short. But at least the data give a hint about the recent temperature distribution of a location and include any warming in the last decade of the century. The recent warming, widely interpreted as due to man induced climate change, will most probably continue.

Tab. 7.1.1:   Distribution of stations with temperature of the Globalsod database.

Region	Number
Europe without Russia	1'212
Asia with Russia	1'463
Africa	204
North America	1'375
South America	240
Australia and New Zealand	457
World	4'951

The data of the nearest stations is used to get interpolated values. The station network is not very dense in Africa, but fortunately, yearly temperature variations are smaller near the equator and therefore the spatial variations are not big compared with higher latitudes.

Input variables extracted for the assessment of temperature distributions

The monthly mean temperature and the hourly radiation values (all days and clear sky) are needed as inputs.

The following temperature parameters are used as statistical values:

- Monthly distribution of the daily temperature. Here 7 points of the monthly distribution are stored (1/31, 3/31, 6/31, 15/31, 25/31, 28/31, 30/31 quantiles).

- Monthly mean temperature

- Monthly mean of daily minimum and maximum hourly temperatures

- Mean monthly minimum and maximum hourly temperatures

- Mean standard deviation and difference of day to day variation, separated for days below and above the average daily difference between maximum and minimum temperatures. This

approximately corresponds to a separation into clear and overcast days or days with high and low radiation.

- Mean minimum daily temperature per year

- Mean 4 day minimum temperature per year

- Mean maximum daily temperature per year

- As a new parameter in version 6 the minimum and maximum hourly value per month of all 10 years is introduced. This enables the user to generate time series including 10 year extreme hourly values.

These values have to be estimated from the measurements at the available sites. The extreme values are estimated in the winter and summer period of each station. This procedure also works for interpolated monthly means. Here the statistical values of the nearest stations were used. The statistical values are adjusted by the difference of mean monthly temperatures between the actual site and temperature reference sites.

7.1.2.2 **Daily minimum and maximum temperatures**

The daily minimum and maximum temperatures are also calculated with help of the input data.

First, the monthly factor dX is calculated with measured monthly input values:

$$dX = \frac{\overline{Ta_{d,\max}} - \overline{Ta_{d,\min}}}{Gh_m}$$

(7.1.2)

with $\overline{Ta_{d,\max}}$ and $\overline{Ta_{d,\min}}$ as the monthly mean daily minimum and maximum hourly temperatures and G_m the monthly mean global radiation. This gives the general factor for conversion from radiation to temperature.

Then the daily difference between the maximum and minimum temperature is calculated using the daily radiation value Gh_d:

$$\Delta Ta_d = Gh_d \cdot dX$$

(7.1.3)

The daily minimum and maximum temperatures are calculated using this daily difference, a step based on the assumption that the mean value is the mean of the extreme daily values.

$$Ta_{d,\min} = Ta_d - \Delta Ta_d / 2$$
$$Ta_{d,\max} = Ta_d + \Delta Ta_d / 2$$

(7.1.4)

A check is made to ensure that the daily extremes are within the limits set by the monthly extreme hourly values. If the monthly extremes are not equal (a difference of 0.5°C is allowed), the calculated maximum and minimum values are set to the monthly extremes.

7.1.2.3 Deriving the temperature profile from the irradiance profile

This model was derived in SoDa by Dumortier (2002).

First, a term showing the response of the air temperature to the solar radiation input is introduced. This ratio is called the ground to extraterrestrial irradiation ratio: **kx**. This is the ratio of the amount of solar radiation received on the ground since sunrise, to the amount of solar radiation that a surface perpendicular to the sunrays would have received during the same period:

$$kx(t) = \frac{\int_{sunrise}^{t} Gh(t)dt}{\int_{sunrise}^{t} G_0 dt} \tag{7.1.5}$$

Gh is the global horizontal irradiance
G_0 is the solar constant: 1367 W /m^2

It was shown that the variations of the temperature follow the variations of kx. The temperature increases when kx increases. The temperature reaches its maximum value at the same time as kx reaches its maximum (kx_{max}). When kx decreases, the temperature decreases.

It was concluded that during daylight hours the temperature varies linearly with the kx coefficient. The slope of this linear relationship seems to depend on the sky conditions. It also seems to be different before the maximum value of kx has been reached and afterwards. Finally, it is certainly influenced by incoming air masses.

These conclusions lead to the following Equation (7.1.6) for the slope:

$$slp_{before\,kx_{max}} = \frac{Ta_{d,max} - Ta_{d,min}}{kx_{max}}$$

$$slp_{after\,kx_{max}} = 1.7 \cdot slp_{before_{max}} \tag{7.1.6}$$

This slope is used to calculate the hourly temperature values during daytime:

$$t_{sunrise} < t \le t_{kx_{max}} :$$
$$Ta(t) = Ta(t_{sunrise}) + slp_{before_{max}} \cdot kx(t)$$

$$t_{kx_{max}} < t \le t_{sunset} :$$
$$Ta(t) = Ta(t_{max}) - slp_{after_{max}} \cdot (kx_{max} - kx(t)) \tag{7.1.7}$$

where Ta(t_{max}) = daily maximum temperature (< t_{kxmax}).
During night the temperature variation is mainly influenced by the amount of clouds.

To characterize the sky conditions, we used the Perraudeau nebulosity index: IN (Perraudeau, 1986). IN is based on the diffuse fraction and normalizes the value by taking the clear sky as a reference (Eqn. 7.1.8).

In order to define the night time nebulosity, the values between the last value of the day and the first value of the following day are interpolated linearly. As last and first value a limit of solar elevation of 5° was set.

The night time cooling rate (NCR) was set to:

$$NCR = 0.231 + 0.458 \cdot IN \quad [°C/hour] \tag{7.1.8}$$

This cooling rate is only used for the first day of the generation, because the daily minimum and maximum values define the cooling rates:

For day 1, before sunrise :

$$Ta(t) = Ta(1) - NCR(1) \cdot t$$

For day 1, after sunset and any other day :   (7.1.9)

$$NCR(j) = \frac{Ta_{sunset}(j) - Ta_{d,min}(j+1)}{t_{sunset}(j) - t_{sunrise}(j+1)}$$

$$Ta(t) = Ta(t_{sunset}) - NCR(j) \cdot (t - t_{sunset})$$

As a new feature in version 6.0 the NCR is lowered in the second half of the night (hours from midnight till sunrise). During the first 2/3 of this time the NCR is lowered by 50%, during the last 1/3 by 67%.

These algorithms are defined for middle latitudes. For polar regions, special cases have to be defined (e.g. a virtual maximum daylength of 19 hours).

7.1.3   Validation

The model introduced in version 5.0 was only sligtly corrected. The tests were carried out at 6 stations in the USA and Switzerland (Miami FL, Denver CO, Portland ME, Seattle WA, Bern CHE, Locarno-Magadino CHE). In general, validation of the model produced satisfactory results. Generated daily temperature profiles are, however, somewhat too flat and lie too near the monthly average. The minima and maxima in winter are well reproduced, the summer maxima are sometimes somewhat lower than the observed maxima. The average values are automatically corrected. The generator produces good distributions (Fig. 7.1.4). The mean extreme values are calculated well (Fig. 7.1.5).
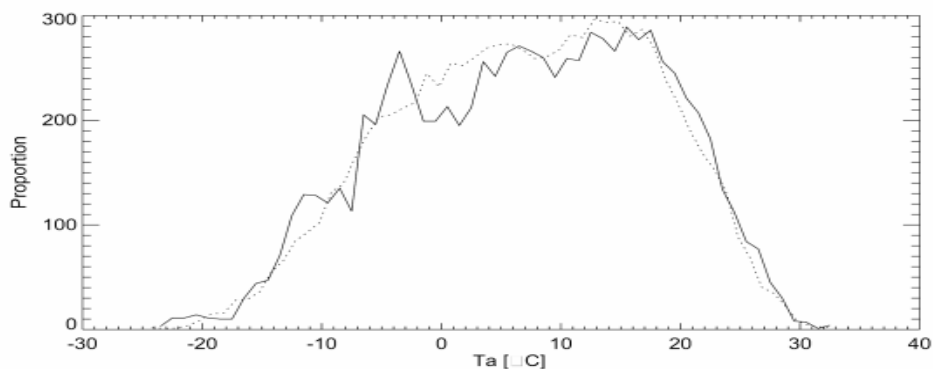
Fig. 7.1.4:   Distribution of hourly values of 3 generated (broken line) and 10 measured years (1981–90) (line). Temperature for **Portland** MN, USA.
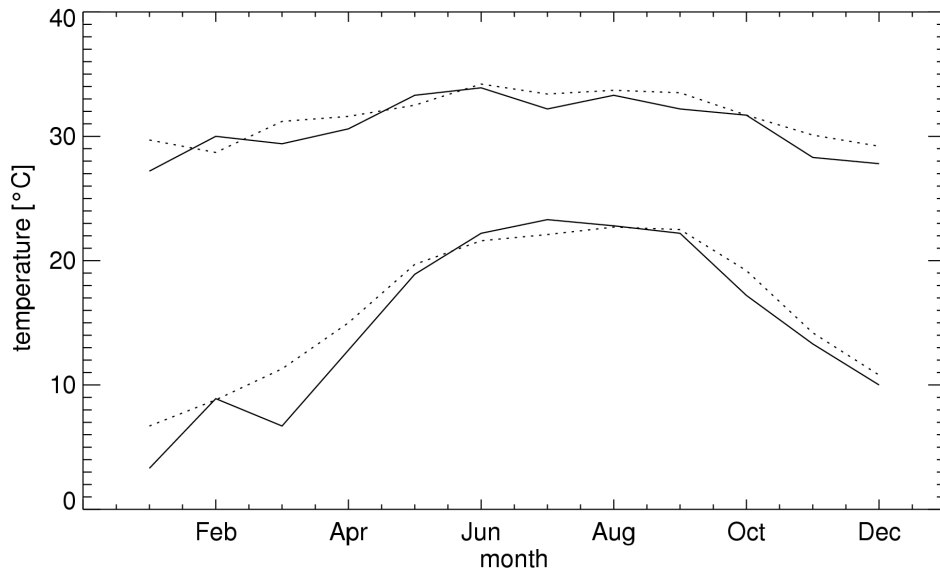
Fig. 7.1.5:   Minimum and maximum hourly temperature values per month for **Miami**, FL, USA.
                 Comparison between one generation run (dotted line) and the measured data for the
                 years 1981–90 (full line).

Owing to the fact that the radiation generator produces symmetrical values with respect to solar
altitude, the temperature generator also produces symmetrical daily profiles. Particularly for high solar
altitudes, this leads to discrepancies between the calculated and measured standard daily profiles.
Nevertheless, for most regions the mean temperatures per hour are calculated well (Fig. 7.1.6). The
standard deviation of the midnight temperature differences (Figs. 7.1.7 and 7.1.8) is well reproduced.
The distribution of the daily values and their variation are well reproduced despite the fact that these
are not generated in an intermediate step.
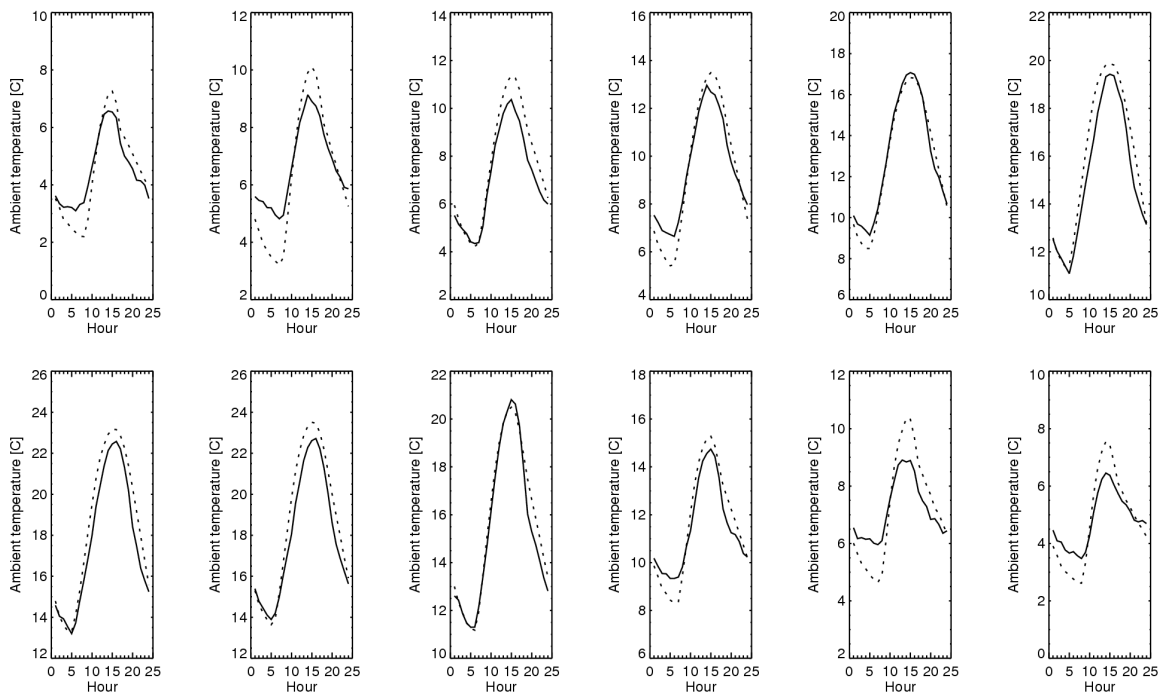
Fig. 7.1.6:   Comparison of measured and generated mean temperatures per hour and month in
                 Seattle (WA, USA) (January–December). Full lines: measured (1981-90), broken
                 lines: generated.
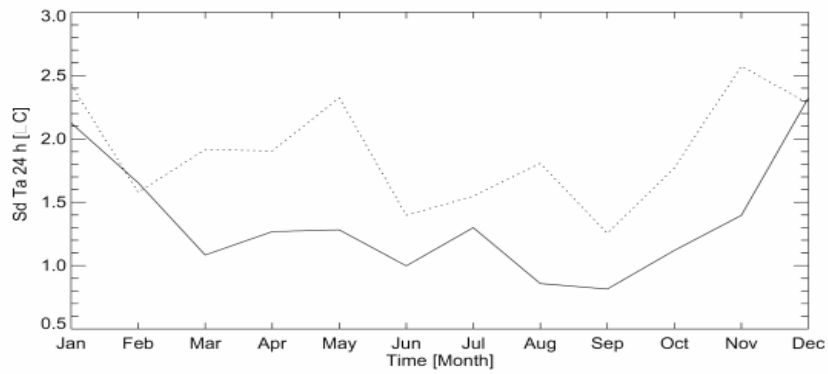
Fig. 7.1.7:   Monthly standard deviations of midnight temperature differences for **Seattle** (WA, USA). Full lines: 3 generated runs, broken lines: measured (1981–90).
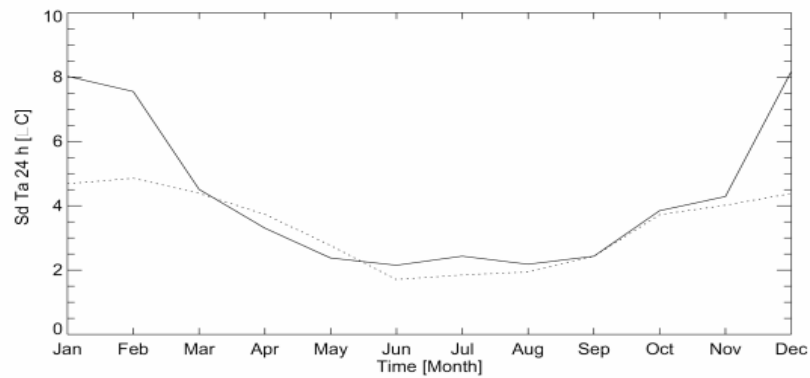
Fig. 7.1.8:   Monthly standard deviations of midnight temperature differences for **Fairbanks** (AK, USA). Full lines: 3 generated runs, broken lines: measured (1995–98).

7.2 Generation of supplementary parameters

METEONORM endeavours to provide suitable interfaces for most design programs in common use in photovoltaics, solar thermal applications and building simulation. For this, a range of output formats is provided. Several of these programs require further meteorological parameters in addition to global radiation and temperature. To provide these formats, simple formulae are presented below for estimating the required parameters. The additional parameters are referred to as supplementary parameters to distinguish them from the main parameters, i.e. radiation and temperature, described in the previous chapters. For a number of supplementary parameters, monthly values can only be obtained by first calculating hourly values. For certain parameters, calculation of hourly average values is not necessary if a meteorological or DRY station is chosen.

The principal problem in simulating further parameters is to ensure their compatibility with the previously obtained parameters. The approximate formulae and methods are described below. The supplementary parameters are not of the same quality as the main parameters (global radiation and temperature) and were not validated in an equally comprehensive way. Most adaptations were made using data from 15 weather stations in the USA and Switzerland.

The following supplementary parameters are calculated in *METEONORM*: Dew point temperature, relative humidity, mixing ratio, wet-bulb temperature, cloud cover, global and diffuse brightness, longwave radiation (incoming, vertical plane, outgoing), wind speed, wind direction, precipitation, driving rain, atmospheric pressure and UV radiation (UVA, UVB, erythemal, global and diffuse). The computational algorithms for the supplementary parameters are described below.

7.2.1 Dewpoint temperature and relative humidity

Dew point temperature (Td) and relative humidity (RH) are related. Using Eqn. 7.2.1, the dew point temperature can be calculated from the relative humidity (Iribarne and Godson, 1981) and the relative humidity from the dew point temperature using Eqn. 7.2.2 (DWD, 1979).

$$Td = \left[\frac{1}{Ta + 273.15} - \left(1.85 \cdot 10^{-4} \right) \cdot \log \left(\frac{RH}{100} \right) \right]^{-1} - 273.15 \qquad (7.2.1)$$

Ta: Air temperature [°C]   Td: Dew point temperature [°C]
RH: Relative humidity [%]

$$RH = 100 \cdot \left(\frac{e_s}{e} \right)$$

$$e(Ta) = 6.11 \cdot \exp \left(\frac{17.1 \cdot Ta}{234.2 + Ta} \right) \qquad (7.2.2)$$

$$e_s(Td) = 6.11 \cdot \exp \left(\frac{17.1 \cdot Td}{234.2 + Td} \right)$$

e: Saturated vapour pressure at Ta [hPa] e_s: Saturated vapour pressure at Td [hPa]

While endeavouring to find a simple definition, it was discovered that the relative humidity at sunrise hours is a linear function of average humidity (Eqn. 7.2.3).

$$RH_{m,06}(m) = 23 + 0.79 \cdot RH(m) \quad , \quad 30 < RH_{06}(m) < 95 \tag{7.2.3}$$

The monthly values are adopted with a new system to daily values, which constists of three parts:

1. Adoption to cloudiness during night:
   If night is cloudy (mean cloudiness > 5 octas): $RH_{m,06}(m) = RH_{m,06}(m) - 5$

   If night is not cloudy (mean cloudiness ≤ 5 octas): $RH_{m,06}(m) = RH_{m,06}(m) + 5$

2. Adoption to rain amount of last 3 days:

If $RR_d(d) > 5$ and $RR_d(d-1) = 0$, $RH_{m,0.6} = RH_{m,06} + 6$

If $RR_d(d) > 5$ and $RR(d-1) = 5$, $RH_{m,0.6} = RH_{m,06} + 12$

If $RR_d(d) = 0$ and $RR(d-1) = 0$, $RH_{m,0.6} = RH_{m,06} - 4$

3. Stochastic part: White Noise generation with N(0,12) [mm]

With these 3 adoptions the natural range of possible humidities can be reached better than with the model of version 5.

The dewpoint temperature at sunrise hours (here written as 6.00) is then calculated using Eqn. 7.2.1. The dewpoint temperature for each hour is calculated by linear interpolation between the sunrise values. Additionally (as a new feature in version 5) two different sinus functions were added depending on the amount of monthly radiation. If radiation is higher than 100 W/m^2 (a threshold for low radiation means) the following function is used:

1. Daily variations : $dTd(h) = -0.2 \cdot (Ta(h) - Ta(sunrise))$

2. Stochastic part :
   $$z = 0.3 \cdot N(0,1)$$
   $$x(h) = 0.9 * x(h-1) + z$$

   Both functions are added to the "flat" dewpoint temperature.

3. Precipitation:
   If $RR(h) > 0$ and $RR(h) < 1$, $RH(h) = RH(h) + 5$

   If $RR(h) \geq 1$ and $RR(h) \leq 5$, $RH(h) = RH(h) + 10$

   If $RR(h) > 5$, $RH(h) = RH(h) + 15$

These Equations were adapted to different measurements in the USA and Switzerland and reflect typical profiles.

The relative humidity for each hour is calculated using Eqn. 7.2.2.

Following this, the monthly values of generated data are fitted to the measured monthly average values first by lowering or increasing RHm,06 and secondly (if this does not help enough) by increasing the generated hourly values by the difference between generated and measured monthly average values. The corrections were mainly added at lower values of humidity, in order to avoid too many values with 100 % relative humidity. The differences are usually small (in the region of a few percent).

7.2.1.1 Validation

A short validation based on visual comparisons has been made at 6 stations (Tab. 7.2.1):

Tab. 7.2.1:   Model sites. Climate zones according Troll and Paffgen (1981).

Name	Lon [°]	Lat [°]	Alt [m]	Year	Climate zone
Miami FL USA	80.27	25.80	2	TMY (61-90)	V, 1
Seattle WA USA	-122.30	47.45	122	TMY (61-90)	III, 2
Portland ME USA	-70.32	43.65	19	TMY (61-90)	III, 8
Boulder CO USA	-105.25	40.02	1634	TMY (61-90)	III, 4
Bern-Liebefeld CHE	7.43	46.95	565	1999-2005	III, 3
Locarno-Magadino CHE	8.88	46.17	197	1999-2005	III, 3

The distributions and the mean daily profiles per month were compared (Fig. 7.2.1 to 7.2.2). The mean daily profiles (Fig. 7.2.3 to 7.2.4) as well as a plot of the mean hourly temperature vs. humidity (Fig. 7.2.5 and 7.2.6) were examined.

For both dry and wet climates the generated humidity values compare well with measured data. The differences between the climates can be distinguished clearly. Nevertheless we advise the user to check the outcomes of the humidity generation before using it for delicate simulation processes (like cooling).
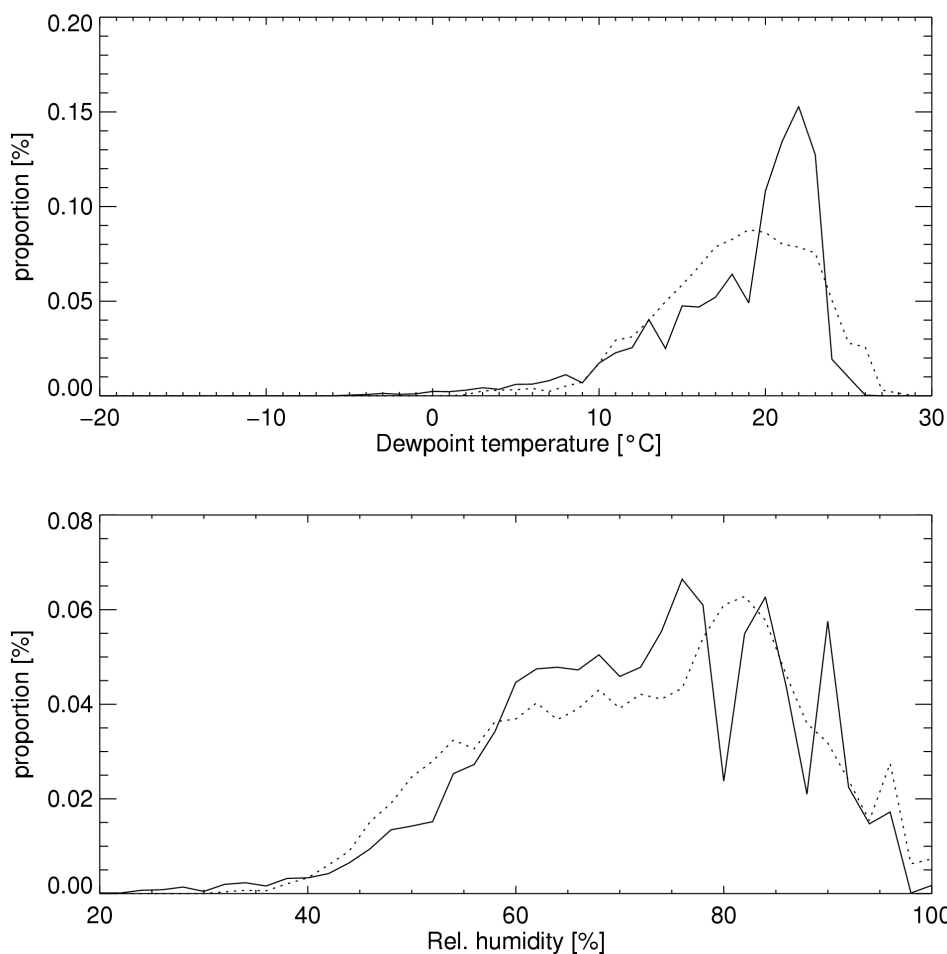
Fig. 7.2.1:   Distribution of dewpoint temperature and relative humidity at **Miami** FL USA. Solid line = measured, dotted line = generated values.
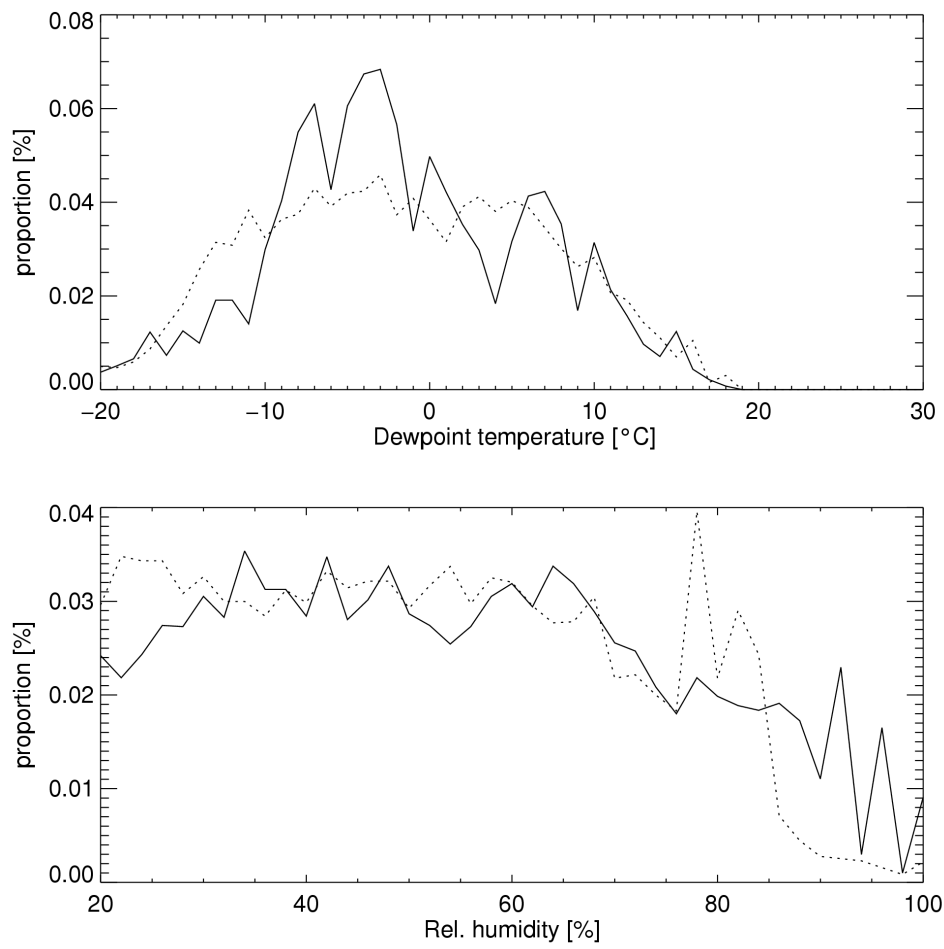
Fig. 7.2.2:   Distribution of dewpoint temperature and relative humidity at **Denver** CO USA. Solid line = measured, broken line = generated values.
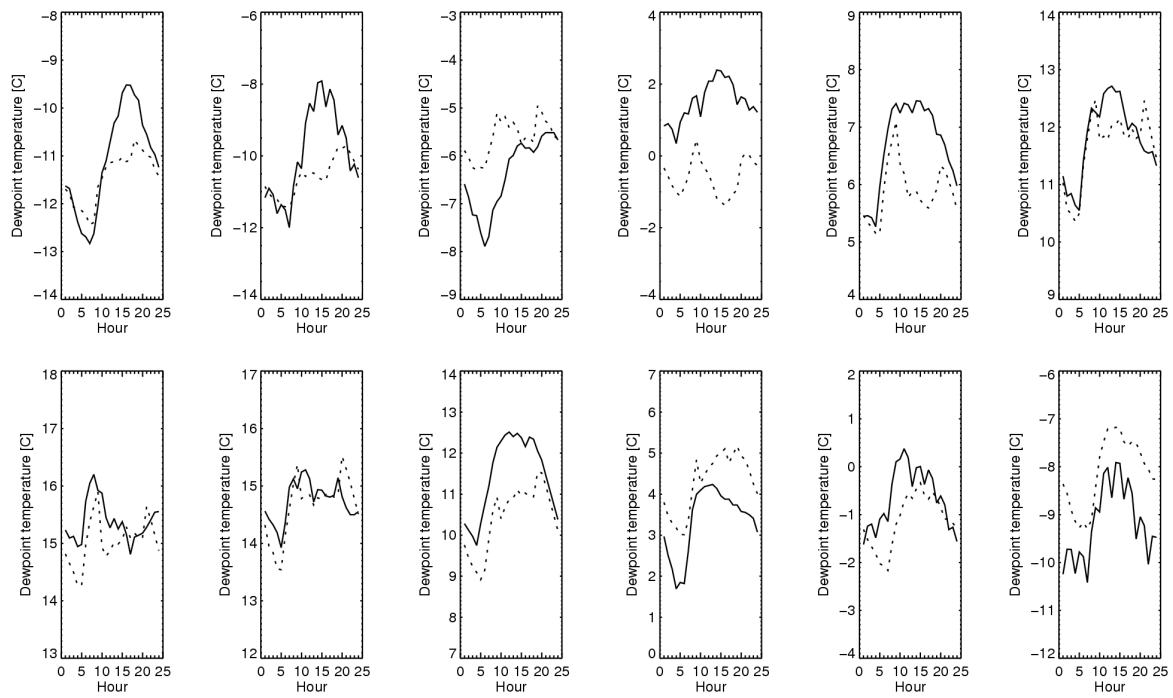
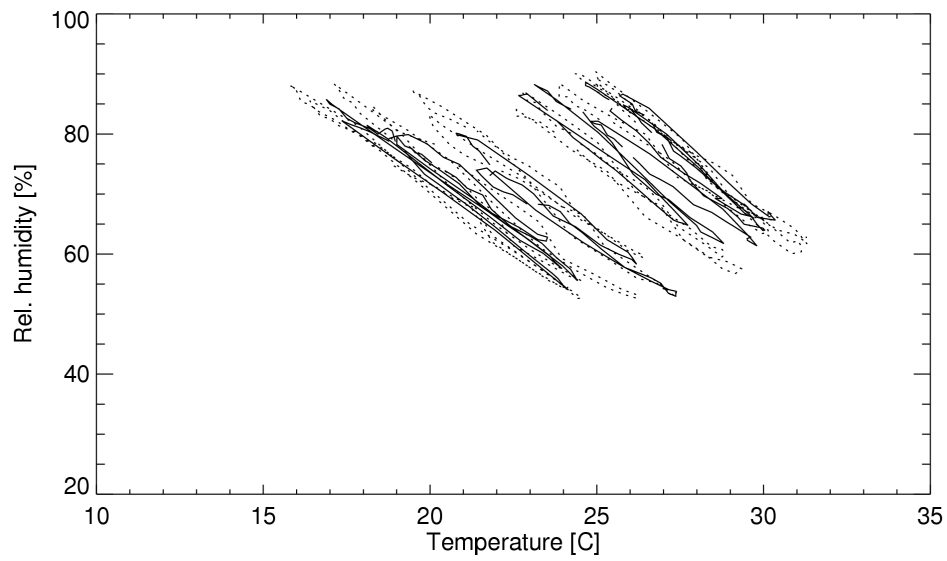Fig. 7.2.3:   Mean daily profile of dewpoint temperature at Portland ME USA. Solid line = measured, broken line = generated values. The second minimum after noon can be both seen at generated as well as at measured values.
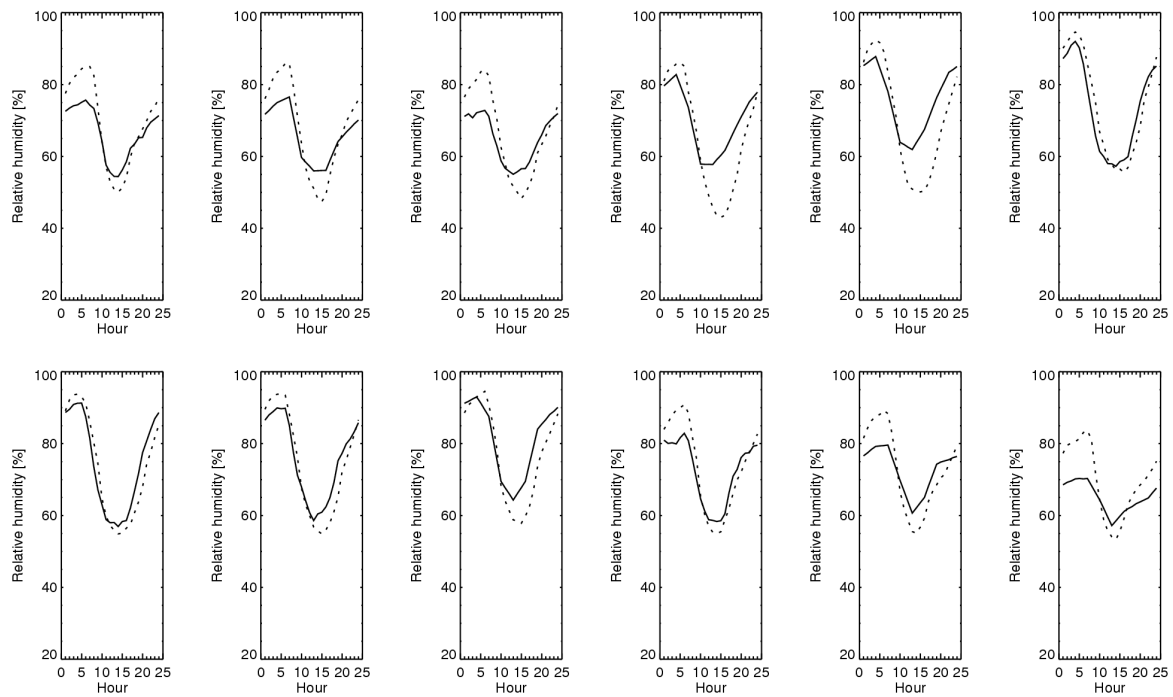
Fig. 7.2.4:   Mean daily profile of relative humidty at Portland ME USA. Solid line = measured, broken line = generated values.

Fig. 7.2.5:   Mean hourly humidity vs. temperature per month at **Miami.** E. Solid line = measured, broken line = generated values.
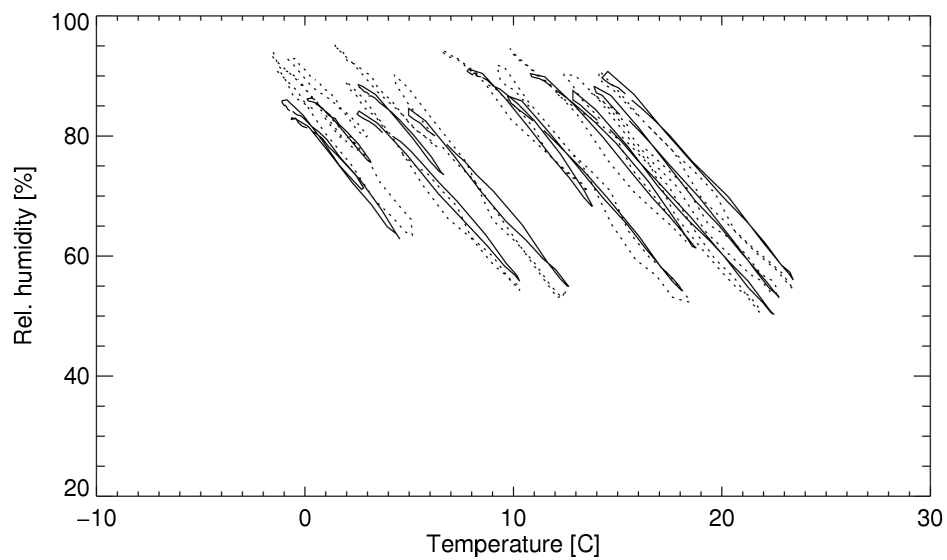
Fig. 7.2.6:   Mean hourly humidity vs. temperature per month at **Bern-Liebefeld** CH. Solid line = measured, broken line = generated values.

7.2.2   Wet bulb temperature and mixing ratio

The moisture content (**mixing ratio:** mass of water vapor to mass of dry air) is calculated with Eqn. 7.2.7:

$$r_s = 0.622 \cdot \frac{e_s}{p\text{-}e_s} \quad [g/g]$$

$$r_d = 0.622 \cdot \frac{e}{p\text{-}e} \quad [g/g]$$

(7.2.7)

r_s:	saturated mixing ratio [g/g]	p:	atmosphere pressure at station altitude [hPa]
e_s:	saturated vapor pressure [hPa]	e:	vapor pressure [hPa]
r_d:	mixing ratio [g/g]		

In version 6.013 (October 4th 2007) the approximation of wet bulb temperature according with Normand's law (Stull, 1995) was replaced with a numerical approximation. This gives the more precise results. With Normand's law the values have been partly too low.

Wet bulb temperature (Tp) is varied until the following rule is approximated:

$$e_s = e_p - p \cdot (Ta - Tp) \cdot 0.00066 \cdot (1 + 0.00115 \cdot Tp)$$

(7.2.8)

e_p = vapour pressure of Tp [hPa] according Eqn. 7.2.2

The Figures below show two comparisons of generated and measured mixing ratio distributions at Bern-Liebefeld CHE (Fig. 7.2.7) and Miami FL USA (Fig. 7.2.8). Both site have been generated with the new option including 10 year extreme hourly values.
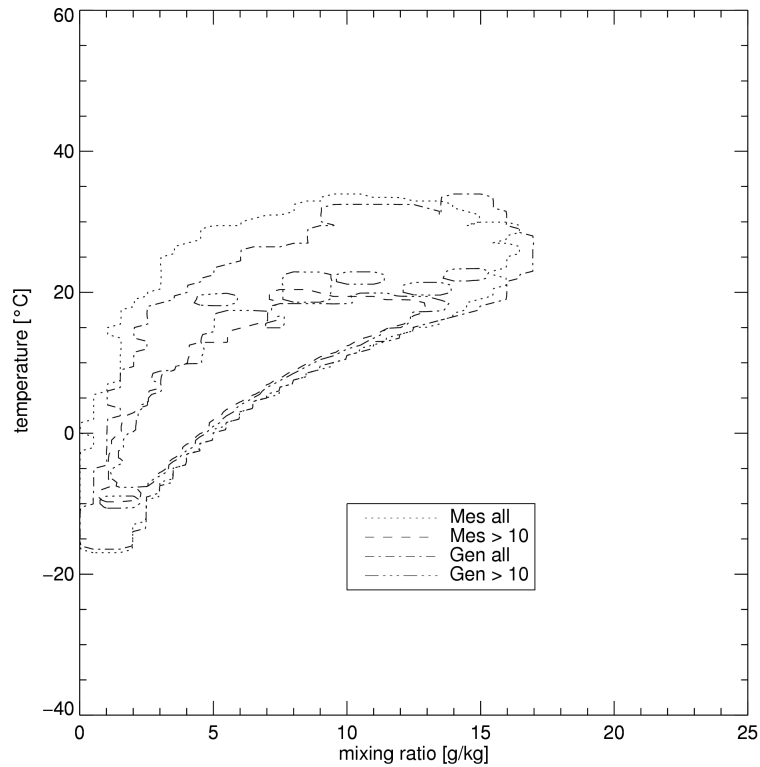
Fig. 7.2.7:   Distribution of mixing ratio at **Bern-Liebefeld CH**. Generated including 10 year extremes.
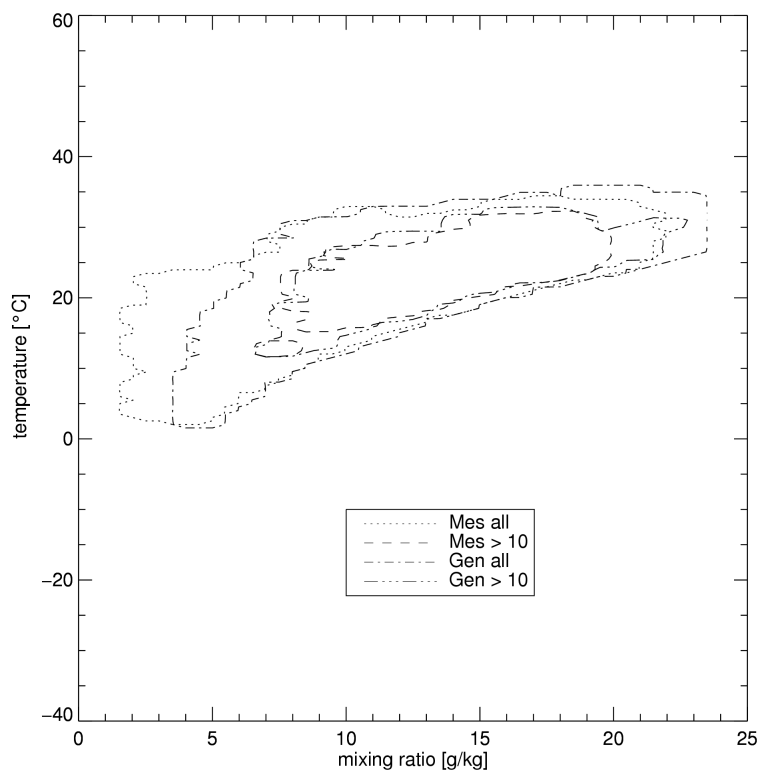

Fig. 7.2.8:   Distribution of mixing ratio at **Miami** FL USA. Generated including 10 year extremes.

As a new feature in version 6.0 the values for the above mixing ratio vs. temperature diagrams can be saved (output format humidity).

7.2.3 Cloud cover

Here too, a new model is used in version 5.0. The knowledge of the cloud cover index is essential for estimating the long wave radiation emitted by the atmosphere and for temperature modelling during night. The Equation of Kasten and Czeplak (1979) was used for calculating global radiation from clear sky radiation and the cloud cover index in two recent publications (Badescu, 1997; Gul et al., 1998). Initial checks with this model showed that it could be used for Europe and other temperate zones, but changes were needed for other regions. Additionally, when the Kasten and Czeplak algorithm was used in reverse to estimate cloud cover, it generally produced results biased towards cloud cover values that were too high.

Therefore, another model was investigated based on the Perraudeau's nebulosity index. This index is also needed in the chain of algorithm for temperature generation and is defined as:

$$I_P = \frac{1 - D_h/G_h}{1 - D_c/G_c} \tag{7.2.13}$$

The cloud cover index relationship was looked into at Anchorage AK, Seattle WA, Salt Lake City UT, Raleigh NC and San Juan PR (Table 7.2.2) and a new formulation has been developed for all sites (Fig. 7.2.9):

If $0.07 < I_P < 1$

$$N = INT\left(8 \cdot \sqrt{\frac{1 - I_P}{0.825}} + 0.5\right)$$

if $I_P \geq 1$

$N = 0$ $\tag{7.2.11}$

if $I_P \leq 0.07$

$N = 8$

The denominator in the square route term in Equation 7.2.11, a = 0.825, is a mean value. Its value varies slightly with site location Different models for specific sites have been constructed by varying the value of a. Because the differences were very small (Anchorage: a = 0.802, San Juan: a = 0.794), the use of one standard model is suggested.

Tab. 7.2.2:   Model sites. Climate zones according Troll and Paffgen (1981).

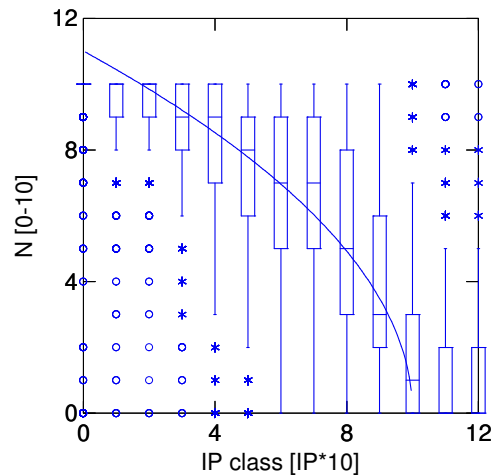| Name	Lon [°]	Lat [°]	Alt [m]	Year	CLIMATE ZONE
Anchorage USA	150.02 W	61.17 N	35	1990	II, 1
Seattle USA	122.30 W	47.45 N	122	1990	III, 2
Raleigh USA	78.78 W	35.87 N	134	1990	III, 8
Salt Lake City USA	111.96 W	40.77 N	1'288	1990	III, 10
San Juan PR	66.00 W	18.43 N	19	1990	V, 1

Fig. 7.2.9: Box plot of measured cloud cover (tenths) and model. Data of Anchorage, Seattle, Salt Lake City, Raleigh and San Juan 1990.

With stochastically generated data the distribution of Perraudeau's index is significantly different. The generated IP values are lower than the measured ones. Therefore, this distribution has to be adapted to get accurate and bias free cloud cover information. A simple factor of 1.15 introduced to correct the generated I_{Pc}:

If $0.06 < I_P < 0.869$

$$N = INT\left(8 \cdot \sqrt{\frac{1 - 1.15 \cdot I_{P.c}}{0.825}} + 0.5\right)$$

if $I_P \geq 0.869$

$N = 0$

if $I_P \leq 0.06$

$N = 8$

(7.2.12)

The factor was found by iteration at the 5 test stations (Table 7.2.2).

The factor is calculated with the Index for elevation of the sun above 5°. For night hours the cloud cover is interpolated linearly between sunrise and sunset.

Validation with measured radiation data

The validation at the same stations gave the following results:

Tab. 7.2.3:   Validation of cloud cover models:

Model	mbe	rmse
Perraudeau	-0.1	1.8
Kasten-Czeplak	0.4	2.2

The accuracy was significantly enhanced with the new model at the five sites. Additionally, the model is very simple and fast for computation and therefore very appropriate for use in *METEONORM*.

Validation with generated radiation data

The distribution and the mean values of all 5 sites together are better reproduced with the new method. The mean values are both 4.7 octas for generated and measured values. The histograms are given in Fig. 7.2.10. Generally, too many intermediate values are generated compared with the observed cloud cover.
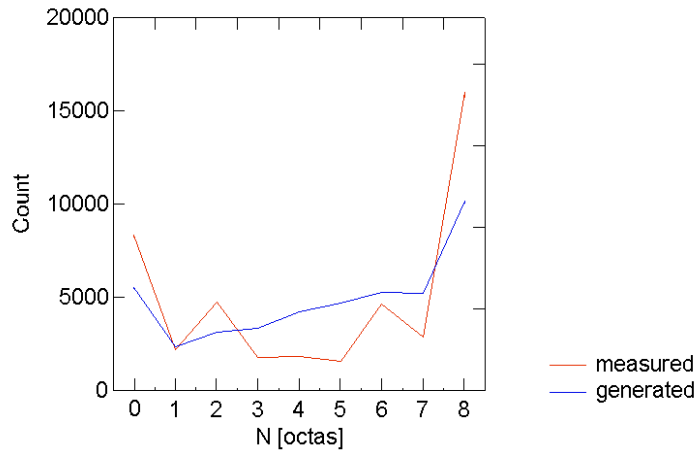

Fig. 7.2.10: Histogram of measured and generated cloud cover. Data of Anchorage, Seattle, Salt Lake City, Raleigh and San Juan 1990 and generated values with mean radiation values of 1961–90.

7.2.4   Longwave radiation

The longwave radiation (wavelength > 3 µm) is divided into two components:

1. Longwave horizontal radiation , **incoming** (L_{in}); radiation from the sky (upper hemisphere) on the horizontal plane (longwave incoming);

2. Longwave horizontal radiation, **upwards** (L_{up}); radiation from the earth's surface transmitted upwards (longwave outgoing).

The longwave radiation on a vertical surface (L_v) is derived from these two components. The radiation balance (R) may be determined from the two components (L_{in} and L_{up}) together with short wave radiation (global radiation) and albedo.

The new suggested model, as well as the above two existing models, have been validated using observed long wave data from 3 of the Baseline Surface Radiation Network (BSRN) stations, Payerne Switzerland, Boulder CO USA and Florianopolis Brazil. BSRN measurements are viewed as the world-leading source of high quality long wave radiation measurements.

7.2.4.1 Longwave radiation emitted from level ground

The outgoing longwave radiation from the ground is dependent on the temperature of the surface.

$$L_{up} = \varepsilon_g \cdot \sigma \cdot T_s^{\,4}$$
$$\sigma = 5.67 \cdot 10^{-8}$$
$$\varepsilon_g = 1.0$$

(7.2.13)

A preliminary investigation showed poor coincidence of existing models with BSRN data for hourly values. Therefore, a new model based on Swiss stations was developed. First a comparison between ground temperature estimated with Eqn. 7.2.13 and L_{up} at Payerne showed:

- that over grass the 5 cm temperature is the temperature of emission of the level ground and

- the emittance of natural ground ε_g is best set to 1.

Wind speed (measured at 10 m above ground) has been identified as an important factor. High wind speeds considerably lower the temperature differences between 2 m and 5 cm. If no wind speed data are available mean values of 3 m/s for the day and 1 m/s for the night can be used in sheltered regions.

During daylight hours, with G_h over 5 W/m^2, the following formula has been established, yielding a r^2 value of 0.867 at all 5 Swiss SMI sites (hourly values).

$$T_s = T_a + [0.015 \cdot (1 - \rho) \cdot G_h - 0.7] \cdot \exp(-0.09 \cdot FF) \tag{7.2.14}$$

A new model for night time hours was introduced. This model was constructed using the data of Payerne. A maximum deviation of 4.7 °C was found. Wind speed is even more important at night than during the day because of the higher stability of the planetary boundary layer. Very cold ground temperatures can only be reached when wind speed is very low.

$$T_s = T_a + [0.0006 \cdot N^3 - 0.037 \cdot N^2 + 0.376 \cdot N - 4.7] \cdot \exp(-0.218 \cdot FF) \tag{7.2.15}$$

For $Ta_m < -3$ °C, $\max(T_s) = 0$ °C (correction for snow coverage).

7.2.4.2 Longwave radiation emitted by the atmosphere

The model of Aubinet (1994) is recommended after comparison with models of Dogniaux and Lemoine (1984), EMPA (1985) and Gabathuler and Marti (2000). Dogniaux and Lemoine was used in ESRA, EMPA models in *METEONORM*. Not only did the results speak for Aubinet, but the input parameters (T_d, G_h and G_c) are also easily available.

$$L_{in} = \sigma \cdot [94 + 12.6 \log(100 \cdot e_s) - 13 \cdot KT_d + 0.341 \cdot (Ta + 273.15)]^4 \tag{7.2.16}$$

In addition to the horizontal information incoming longwave radiation for vertical planes (facades) is provided. Here the formulation used in ESRA based on Cole (1979), which addresses the anisotropy, is used:

$$L_v = L_{in} \cdot 0.5 + 0.0.031 \cdot [1 - N \cdot (0.7067 + 0.00822 \cdot Ta)] \cdot \sigma \cdot (Ta + 273.15)^4 + L_{up} \cdot 0.5 \tag{7.2.17}$$

7.2.4.3 Radiation balance

The radiation balance for horizontal surfaces can be calculated using shortwave and longwave parameters as well as albedo (ρ).

$$R = L_{up} - L_{in} + G_h \cdot (1 - \rho) \tag{7.2.18}$$

7.2.4.4 Conclusions on longwave radiation modelling

Although based on simple approximation of cloud cover and humidity, the long wave models show good results at the BSRN stations Payerne, Boulder and Florianopolis (Tab. 7.2.4).

The combination of the new models leads to a significantly higher accuracy for radiation balance than with any other tested combination.

Tab. 7.2.4:   Error of estimation of hourly values of long wave radiation and ground surface tempera-
              tures. mbe means is the error, rmse root mean square error. The dewpoint temperature
              and wind speed used were generated stochastically.

Station	R		Ldn		Lup		Ts	
(all BSRN)	mbe	rmse	mbe	rmse	mbe	rmse	mbe	rmse
Payerne	0.3	20.8	-0.6	21.3	-0.6	10.4	-0.2	2.0
Boulder	2.3	48.0	18.3	29.1	4.4	13.1	-	-
Florianopolis	-	-	-4.3	23.5	-	-	-	-

7.2.5   Illuminance

Global and diffuse illuminance is calculated using generated global radiation with the Perez et al.
(1990) model. A short comparison with TMY2 data at 7 stations throughout the USA (from Puerto Rico
to Fairbanks) showed the following discrepancies (METEONORM – TMY2): Global illuminance: mbe:
+0.17 klux, rmse: 0.55 klux; diffuse illuminance: mbe: +0.51 klux, rmse: 0.52 klux.

7.2.6   Wind

The provision of wind speed and wind direction in *METEONORM* is intended as an extension of its
output for design programs requiring wind data as input. The wind itself is not usually of great
importance for solar and building (energy) application, and the model presented here is not intended
to provide more than a rough approximation of monthly average and distributions (at 10 m above
ground). The present interpolation should not be used for designing wind power plants. The problem
of wind simulation for any desired location is practically insoluble, since wind speed is greatly
influenced by local features, and spatial variations are very large. The average monthly value is very
difficult to estimate without a detailed knowledge of local topography. Detailed information on wind
conditions throughout Europe may be found in the European Wind Atlas (Risoe National Laboratory,
1990).

7.2.6.1 Wind speed

Despite the difficulties described above, hourly wind speed values were nevertheless generated. The
model was adapted to 30 stations in the USA (Tab. 3.3.1) and 20 stations in Switzerland. It consists of
a daily model based on average daily global radiation, and on an independent stochastic model:

$$FF'(h) = F_m(h, Kt) + F_t(h) \tag{7.2.19}$$

where FF'(h) is the normal distribution of hourly wind speed, F_m is the daily model and F_t the stochastic
model. The stochastic model is defined as a first order autoregressive process AR(1):

$$
\begin{aligned}
F_t(h) &= x_m \cdot F_t(h-1) + Z \\
Z &= m_w + s_w \cdot \mathrm{r}(h) \\
m_w &= (1 - x_m) \cdot FFi(month) \\
s_w &= \left(1 - x_m{}^2\right)^{1/2} \cdot sdi(month)
\end{aligned}
\tag{7.2.20}
$$

where r(h) is a normally distributed random variable N(0.1). x_m is calculated for the relevant climatic
zone and continent:

Climatic zone 303 :

$$x_m = 1 - \left[-9.1 + 7.1 \cdot FFi(month)\right]^{-1}, \quad 0.75 < x_m < 0.99,$$
elsewhere :

$$x_m = 1 - \left[10.285 \cdot FFi(month)\right]^{-1}, \quad 0.75 < x_m < 0.99$$

(7.2.21)

The daily model F_m is calculated under local and climatic conditions with daily K_t and G_h values. The following categories were adopted:

Tab. 7.2.5:   Categories adopted in the daily model

No.	Climatic zone	Local terrain
1	Europe, III, 3 (e.g. central Europe)	open
2	III, 3 (Switzerland alone)	lake
3	Alpine zones II - IV	mountain valley
4	Alpine zones II - IV	summit
5	I, 1 – 4, II, 1 – 3, III, 1 – 2 (cold and very cold regions)	general
6	IV, 1 –7, V, 1 – 5 (tropics, subtropics)	lake, sea
7	III, 4 – 12 (e.g. continental regions of the USA)	general

In the daily model, the average values of the daily distribution of wind speed on clear days ($K_t > 0.45$, $G_h > 100$ W/m^2) are stored for each terrain (Tab. 7.2.6). If the radiation values lie below the limiting values, no daily model is included.

Tab. 7.2.6:   Daily model of average daily distribution (F_m) for clear days in each category. The values are normalized to 0.

Hour/climatic zone	1	2	3	4	5	6	7
1	-0.4	-0.1	-0.8	0.5	-0.3	-1.1	-0.7
2	-0.5	-0.2	-0.8	0.3	-0.4	-1.2	-0.7
3	-0.5	-0.2	-0.9	0.2	-0.4	-1.4	-0.8
4	-0.6	-0.2	-0.9	0.2	-0.5	-1.5	-0.9
5	-0.6	-0.1	-0.9	0.1	-0.6	-1.5	-0.9
6	-0.6	-0.3	-1.0	0.1	-0.6	-1.5	-0.9
7	-0.6	-0.4	-0.9	0.0	-0.6	-1.5	-0.9
8	-0.5	-0.4	-0.9	-0.2	-0.5	-1.4	-0.7
9	-0.2	-0.3	-0.7	-0.3	-0.3	-1.0	-0.4
10	0.0	-0.1	-0.3	-0.5	-0.1	-0.4	0.1
11	0.3	0.1	0.1	-0.5	0.0	0.3	0.5
12	0.5	0.2	0.7	-0.5	0.2	0.9	0.8
13	0.6	0.2	1.1	-0.5	0.4	1.4	1.0
14	0.7	0.2	1.6	-0.5	0.5	1.8	1.1
15	0.8	0.3	1.8	-0.4	0.7	2.1	1.2
16	0.8	0.2	1.9	-0.4	0.8	2.2	1.2
17	0.7	0.1	1.6	-0.3	0.8	2.1	1.2
18	0.6	0.1	1.2	-0.1	0.8	1.8	1.0
19	0.3	0.1	0.6	0.1	0.6	1.3	0.6
20	0.0	0.3	0.0	0.4	0.3	0.7	0.2
21	-0.1	0.3	-0.4	0.6	0.0	0.2	-0.3
22	-0.2	0.2	-0.6	0.7	-0.1	-0.5	-0.5
23	-0.3	0.1	-0.7	0.6	-0.2	-0.8	-0.6
24	-0.3	0.1	-0.8	0.6	-0.3	-1.0	-0.6

The hourly values (FF'(h)) were calculated using Eqns. 7.2.19 to 7.2.21 and then transformed to correspond to the distribution of hourly values for the site. It is assumed that the form of the distribution (f) corresponds to a Weibull distribution (SFOE, 1990) (Eqn. 7.2.21). Following transformation, the final values of FF(h) are obtained.

$$f(FF) = \frac{k}{A} \cdot \left(\frac{FF}{A}\right)^{k-1} \cdot \exp\left[-\left(\frac{FF}{A}\right)^{k}\right]$$
(7.2.21)

The parameters A and k required in the Weibull distribution, as well as the standard deviation sdi, are estimated from wind speed (Eqns. 7.2.22 to 7.2.29). To determine the parameters k, similar local and climatic categories are used as for the daily model. The models were changed for version 4. In the current version, the parameter A and sdi are calculated mathematically.

1. Open or Sea/Lake:

    Climate zone III:

    $$k = 1.48 + 0.35 \cdot \log(FFi(month) - 2.07)$$
    (7.2.22)

    Climate zone IV, 1, latitude > 35°N or latitude < 35°S:

    $$k = 1.21 + 0.29 \cdot \log(FFi(month) - 1.59)$$
    (7.2.23)

    Climate zone IV, 2 – 7, latitude > 35°N or latitude < 35°S:

    $$k = 1.48 + 0.35 \cdot \log(FFi(month) - 2.07)$$
    (7.2.24)

    Climate zone IV, V, 35°S < latitude < 35°N

    $$k = 1.09 + 0.21 \cdot FFi(month)$$
    (7.2.25)

2. Summits:

    $$k = 1.37 + 0.243 \cdot \log(FFi(month) - 2.08)$$
    (7.2.26)

3. Valleys, cities and sites with obstacles around:

    $$k = 1.21 + 0.37 \cdot \log(FFi(month) - 1.22)$$
    (7.2.27)

Calculation of A and sdi:

A and sdi are dependent on k:

$$A = FFi(month) \cdot \left[\left(\frac{1}{k}\right)!\right]^{-1} = FFi(month) \cdot \left[\Gamma\left(1 + \frac{1}{k}\right)\right]^{-1}$$
(7.2.28)

$$sdi = A \cdot \sqrt{\Gamma\left(1 + \frac{2}{k}\right) - \Gamma^2\left(1 + \frac{1}{k}\right)}$$
(7.2.29)

Validation

The calculated hourly wind values were tested using data from 15 stations in the USA and Switzerland (Tab. 3.3.2). The validation was restricted to checking the distributions. The results showed good agreement between calculated and measured data (Fig. 7.2.11). The average monthly values of generated data come to the original (interpolated or station) values.
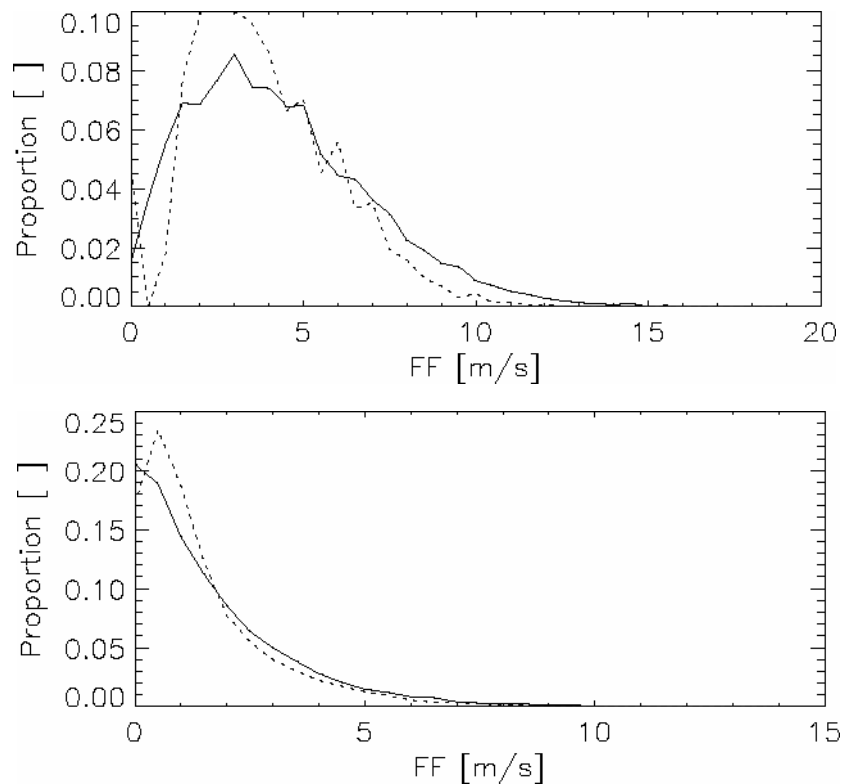
Fig. 7.2.11: Comparison between distributions of calculated (full line) and measured (broken lines)

wind speed, showing data from Portland (MN, USA) (above), and Bern-Liebefeld (CH) (below).

7.2.6.2 **Wind direction**

A totally new wind direction generation process is used for version 5.

The basis of the model are approximately 100 stations with stored wind direction distributions (45°) for the months of January and July. Mainly data from ISMCS (NCDC, 1995) are used.

The nearest site is chosen as representative. The monthly distributions are calculated as a weighted average of the July and the January distributions. If monthly mean values of wind direction are available, the distribution are turned in order that the maximum value of the distributions matches the mean direction value.

The generation process is based on 3 steps:

1. Stochastic generation of an hourly time series of wind direction

$$DD'(t) = 0.914 + DD'(t-1) + N(0,1) \qquad\qquad (7.2.30)$$

No relationship has been used between wind direction and other meteorological parameters.

2. Mapping of the generated values to the interpolated distribution (45° band with, 0 – 360°).

3. Overlying a second stochastic process in order to get finer resolution:

$$DD''(t) = 0.914 + DD''(t-1) + 8 \cdot N(0,1) \qquad\qquad (7.2.31)$$

4. The definitive wind direction DD is calculated as sum of the two ARMA(0,1) processes:

$$DD(t) = DD''(t) + DD'(t)$$

(7.2.32)

The resulting wind roses look reasonable. Of course they can only be approximations. Two examples from the Atlantic Ocean are shown below (Sable Island / NS Canada and Izana Mountain Top / Canaries E). Both the west and the trade wind system are reproduced (Fig. 7.2.12 – 13).
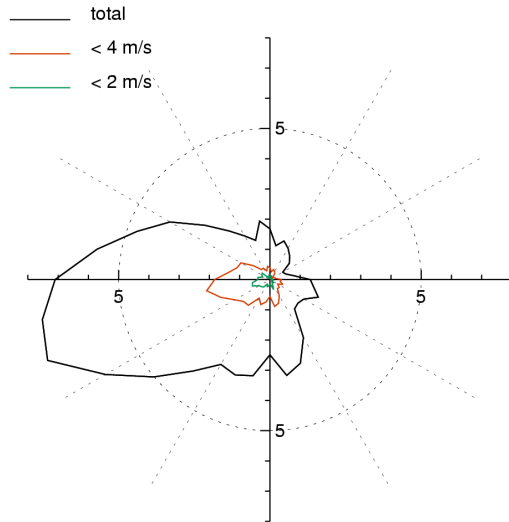

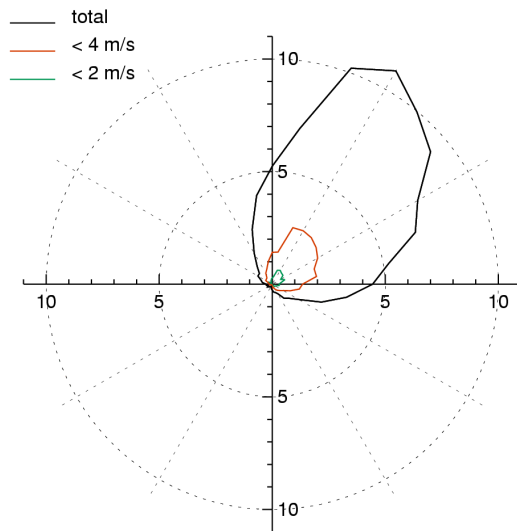Fig. 7.2.12: Wind rose of Sable Island (west wind system).

Fig. 7.2.13: Wind rose of Izana Mountain Top (trade wind system).

7.2.7   Atmospheric pressure

The atmospheric pressure at a particular station is set to the same value the whole year round. The model used for average air pressure assumes a polytropic atmosphere with constant temperature decrement (-6.5 °C/km) and constant temperature at sea level (15 °C) (7.2.33).

$$p_d = 1013 \cdot \left[1 - \frac{0.0065 \cdot z}{288.15} \right]^{5.264} + \left(Kt_d - KT_m \right) \cdot 20 \qquad (7.2.33)$$

p_d: Daily mean of atmosphere pressure [hPa] z: Height above sea level [m]

As an additional feature in version 6.0 the pressure is varied from day to day to give a certain (when not truly realistic) variation. The pressure variations enhance the variations of the mixing ratio and give a more realistic distribution of this.

7.2.8   Heating degree days

The heating degree days (HDD) represent a simple and commonly used method for calculating the energy consumption of heated buildings. In Version 5.0 (as in the previous version), heating degree days are estimated using generated hourly temperature series. They can be calculated with the output formats LESOSAI or sia 380/1. The generated values have an accuracy of about 1% compared to the listed values in Switzerland (sia 381/2).

7.2.9   Precipitation

In former versions of *METEONORM,* precipitation was only available as monthly sums. A new generation process is introduced for version 5. It is based on the broad knowledge available from many publications of weather generation, which are mostly related with the WGEN generator (Richardson and Wright, 1984).

The reason for choosing new algorithm was that time series of precipitation are also needed in building simulation and that no existing method was based on solar radiation, which is available in this case. Generally the generation of the dry or wet days' time series is the first step. Additionally the existing generators are fitted to agricultural simulations, mostly provide only daily time series and are site dependent. The proposed method produces first daily precipitation series and then hourly values for every site worldwide.

7.2.9.1 Daily precipitation values

At the beginning of the generation process the worldwide, monthly values of precipitation and the number of days with precipitation above 1 mm are known. Additionally clear and all sky radiation, cloud amounts and temperature (ambient, dewpoint) time series are available. The produced time series correspond to mean monthly means.

Before the generation starts the number of days with precipitation above 0.1 mm (Rd_0) is calculated with the following Equation:

$$Rd_0 = INT \left[0.971 + 3.445 \cdot \frac{Rd_1}{RR_m} \right], \quad 0 < Rd_0 < Rd_1 \qquad (7.2.34)$$

The Equation has been adapted to data of 25 European stations with measurements from 1901–99 (r^2 = 0.726).

A second value for the generation process is calculated: the mean amount of dry spells (Ds) per month:

$$Ds = INT[22.041 - 6.507 \cdot \ln(Rd_1)] \ , \quad 0 < Ds < ndays - Rd_0 \tag{7.2.35}$$

The Equation has been adapted to data of the same 25 European stations (r^2= 0. 773).

The generation process starts with finding the n = Rd_0 days with the lowest clearness indexes of the month. These days are assumed as days with precipitation. The days are sorted according the clearness indexes. The lower the clearness index, the higher the precipitation is set.

The amount of precipitation per day is calculated with a Weibull distribution (Selker and Haith, 1990) also used in the ClimGen generator (http://www.bsyse.wsu.edu/climgen/).

$$RR_d(P) = 0.84 \cdot \frac{RR_m}{Rd_0} (-\ln(1 - P_n))^{1.333} \tag{7.2.36}$$

where

$$P_n = \frac{Rd_0 - n - 0.75}{Rd_0 - 0.5} \ , \quad 0 \le n \le Rd_0 - 1 \tag{7.2.37}$$

The cumulated probabilities P_n are stretched slightly. First tests have shown that the distribution are better reproduced this way.

The precipitation amount is summed for each month. If the sum differs from the interpolated mean the daily values are corrected by a factor.

If the generated dry spells are lower than the modelled ones (Eqn 7.2.35), the rainy days are moved by one day if possible in order to achieve the correct days with dry spells.

7.2.9.2 Hourly values

First the number of hours with precipitation (for days with precipitation) is calculated with the following Equation:

$$n_{rh} = INT\left[1.5 \cdot \left(\frac{4.096 \cdot RR_d}{\dfrac{RR_m}{Rd_0}} + 0.365 \cdot \frac{RR_m}{Rd_0} - 0.029 \cdot RR_d\right)\right] \tag{7.2.38}$$

The number of hours of precipitation is mainly dependent on the amount of precipitation per day (RR_d) and the mean intensity of the precipitation per day of the month (RR_m/Rd_0). The Equation was adapted to hourly precipitation data of Bern-Liebefeld, Neuchatel, Davos, Luzern and Locarno-Magadino with data of 2000 and 2001 (r^2=0.815). The numbers of hours are set between 1 and 24. This set of stations includes regions both south and north of the Alps with different kinds of precipitation regimes (advective and convective). The factor 1.5 was introduced due to lowering of the precipitation hours by other parts of the chain of algorithms. Mainly the time series of cloud cover limits the hours of precipitation.

Hours with precipitation have to fulfil a second condition: the mean cloud cover has to be at least 6 octas. If less hours with 6 octas are available per day, the number of hours are set to this lower value.

In a second step, the possibility of precipitation per hour is simulated with an autoregressive process and a mean daily profile. This is done because the possibility of precipitation is generally higher in the evening and the night than in the morning hours.

$$P_m(h) = 1 + 0.15 \cdot \sin\left(\frac{\pi}{2} + (h+1) \cdot \frac{2\pi}{24}\right) \tag{7.2.39}$$

$$P_s(h) = 0.7 \cdot P_s(h-1) + 0.2 \cdot N(0,1) \tag{7.2.40}$$

$$P_{RR_h}(h) = P_m(h) + P_s(h) \tag{7.2.41}$$

The hours with precipitation is moved to hours with 7 or 8 octas of cloud cover by enhancing the possibility at hours with 8 octas by 0.5 and at hours with 7 octas by 0.25. The possibility of precipitation is used to sort the hours with precipitation. If e.g. the day has 5 hours with precipitation the hours with the 5 highest values of P_{RRh} are chosen and sorted.

The amount of precipitation per hour is defined with a Weibull distribution:

$$RR_h = 0.647 \cdot \frac{RR_d}{n_{rh}} \cdot \left[-\log(1-P_n)\right]^{1.7} \tag{7.2.42}$$

where

$$P_n = \frac{n_{rh} - n - 0.25}{n_{rh} - 0.5} \quad , \quad 0 \le n \le n_{rh} - 1 \tag{7.2.43}$$

The cumulated probabilities Pn are stretched slightly. First tests have shown that the distributions are better reproduced this way. n corresponds to the sorted number of hours with precipitation according to the possibility (P_{RRh}).

The generated hourly values are corrected in order to match the daily sums.

7.2.9.3 Validation

A short validation at 6 stations in Europe was performed (Tab. 7.2.7).

Tab. 7.2.7:   Test sites for precipitation model.

Site	Source	Latitude [°,']	Longitude [°,']	Altitude [m]	Period	Time resolution
Bern-Liebefeld	Meteoswiss	46.56	7.25	565	2000–2001*	Hour
Locarno-Magadino	Meteoswiss	46.10	8.53	197	2000–2001*	Hour
Davos	Meteoswiss	46.49	9.51	1590	2000–2001*	Hour
Vaexjoe/Kronoberg	KNMI	56.87	14.80	166	1901–99	Day
Frankfurt	KNMI	50.12	8.67	103	1901–99	Day
Marseille	KNMI	43.31	5.40	75	1901–99	Day

* Figures in Tab. 7.2.8 have beenwere adapted to mean values 1961–90.

The following points were investigated: Days with precipitation over a certain amount, maximum daily and hourly sums (mean values per year), mean maximum duration of dry and wet spells per year and hours of precipitation (Tab. 7.2.8).

Tab. 7.2.8:   Comparison between measured and generated time series of precipitation.

Site	Type	RR>0 mm [days]	RR>1.0 mm [days]	RR>12.5 mm [days]	Max. daily sum [mm]	Max. hour. sum [mm]	Dry spell [days]	Wet spell [days]	RR [mm]	Prec. Hour [h]
Bern	Measured	170	126	24	47.2	19.0	13	17	1029	1107
Bern	Generated	167	126	23	40.5	13.5	9	9	1025	1034
Locarno	Measured	138	105	47	113.0	36.8	33	10	1773	1149
Locarno	Generated	118	101	42	87.5	29.1	18	5	1772	1084
Davos	Measured	181	129	26	70.1	10.6	14	11	1084	1371
Davos	Generated	165	129	26	44.3	15.2	13	8	1081	1053
Vaexjoe	Measured	186	117	14	32.3	-	16	14	652	-
Vaexjoe	Generated	181	113	12	23.4	8	10	10	610	893
Frankfurt	Measured	172	110	14	35.3		17	12	650	
Frankfurt	Generated	155	106	14	30.4	10.4	18	6	685	845
Marseille	Measured	83	56	20	65.2		33	7	596	
Marseille	Generated	80	60	13	36.1	12.2	28	9	545	523
Mean difference	%	-7 %	-1 %	-10 %	-27.8 %	-12.8 %	-24 %	-33 %	-1 %	-25 %

Days with precipitation are reproduced well. Especially the lower thresholds (RR_d>0mm, RR_d>1mm) are given precisely. Monthly and yearly sums correspond to input values. Small differences in the table are induced by different time periods. The maximum daily sum is calculated too low (-28%). The maximum hourly sum is calculated quite precisely. The amount of wet and dry spells are calculated too low. This is mainly induced by the fact that the calculations are fitted to monthly means and not to yearly means. The number of hours with precipitation is also too low. Nevertheless, the deviations the different magnitudes of the precipitation for the different climates are clearly observable.

In the following figures two time series of hourly precipitation for Bern-Liebefeld are shown. Figure 7.2.14 shows a generated time series, 7.2.15 a measured time series (year 2000).
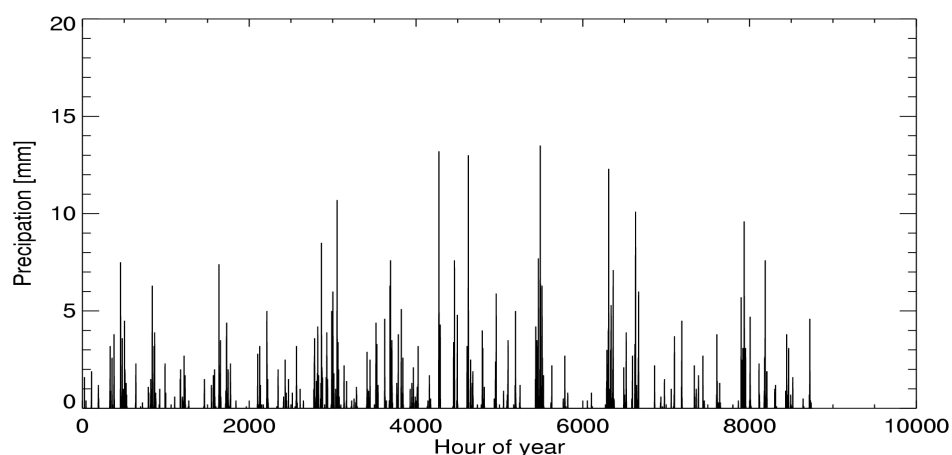

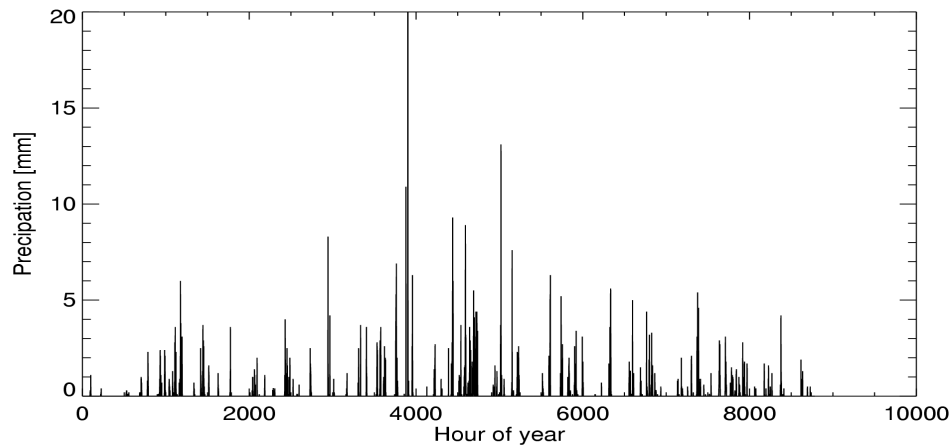Fig. 7.2.14   Generated time series for Bern-Liebefeld.

Fig. 7.2.15   Measured time series for Bern-Liebefeld (year 2000).

7.2.9.4 Driving rain

Driving rain is rain that is carried by the wind and driven onto the building envelope (façades and roofs). It is a complex phenomenon of falling raindrops in a turbulent flow of wind around a building. It is one of the important climatological factors which determine long-term use and durability of building envelopes.

Driving rain is especially important for humidity processes, which are e.g. simulated by WUFI. For this format the output format TRY can be saved (without driving rain, but with precipitation and wind speed).

Straube's method (Straube, 2001) for calculating the amount of wind driven rain impinging on a wall was selected for use. It was chosen because it is one of the most conservative of the methods generally available and was also the method selected for incorporation into current models (Cornick et al., 2002). It is based on Lacy's method (Lacy, 1965).

The top corner of the building was assumed to be the location of interest; this was used in determining the RAF factor.

$$WDR = RAF \cdot DRF(RR_h) \cdot \cos\theta \cdot FF \cdot RR_h \qquad (7.2.44)$$

where: WDR is the wind driven load (mm/h),
RAF is the rain admittance factor. set to 0.9 here,
RR_h is the horizontal rainfall intensity (mm),
FF is the wind speed at 10 m above ground (m/s),
and θ is the angle of the wind to the wall normal.

In *METEONORM* WDR is given without the factor cos θ, if elevation is set to 0.

The driving rain factor DRF can by calculated from:

$$DRF = \frac{1}{V_t} \qquad (7.2.45)$$

where: DRF is the driving rain factor
V_t is the terminal velocity of raindrops (m/s)

The terminal velocity can be calculated from:

$$V_t = -0.16603 + 4.91884 \cdot \Phi - 0.888016 \cdot \Phi^2 + 0.054888 \cdot \Phi^3 \quad , \Phi \leq 9.2 \qquad (7.2.46)$$

While Straube recommended using D_{50} for the raindrop diameter, the predominant raindrop diameter, D_{pred}, is used here for Φ (like for other current models like MEWS). This is the diameter of drops that accounts for the greatest volume of water in the air.

$$\Phi = D_{pred} = a \cdot \left(\frac{n-1}{n}\right)^{\frac{1}{n}} \approx RR_h^{0.232} \qquad (7.2.47)$$

where:

$$a = 1.3 \cdot RR_h^{0.232} \qquad (7.2.48)$$

n = 2.25

7.2.10 Spectral radiation

For spectral radiation we use the model developed by UMIST in the framework of the EU IST project SoDa. Spectral radiation is used here as an umbrella term for UV bands UVA, UVB and the erythemal radiation (Page and Kift, 2003).

Four UV products are delivered:

- the estimation of UVA radiation between 320 and 400 nm.

- the estimation of UV B irradiation between 290 and 320 nm.

- the estimation of biologically weighted UV radiation, UV erythemal radiation.

- UV Index: clear sky erythemal UV radiation in Wh/m^2 multiplied by a factor 40. This gives a hint on the amount of sun protection needed at clear sky conditions.

A detailed description of the model would exceed the range of this handbook. The model has not yet been validated.

The model consists of 4 main steps:

1. Calculation of the clear sky radiation.
2. Calculation of the overcast radiation.
3. Calculation of mixed situations.
4. Calculation of inclined planes. For this a slightly adopted Perez model is used (chapter 6.7.2).

At each step global and diffuse radiation is calculated. The models were adapted to SMARTS 2 (Gueymard, 1995) output. Linke turbidity, Angström Beta and water vapour are the most important inputs.

7.2.11 Sunshine duration

The simple equation to calculate sunshine duration is based on clearness index:

With chanages included in Version 6 a better adoption to monthly values and to high horizons are possible.

$$Sd = Sd_{max} \cdot \exp\left[c_h \cdot (kt - kt_l)^2\right] \quad \text{where} \tag{7.2.49}$$

Sdmax   =   maximum possible sunshine duration (depending on chosen horizon)
kt_l =   0.75

$$c_h = -10.239 + 0.001368 \cdot z$$

If the sunshine duration differs more than 10% and 10 hours the the values of ch and ktl are variied until the Sunshine duration without horizon equals the monthly sunshine duration:

1. kt_l: variations from 0.62 – 0.92 allowed

2. c_h: -7 to -60 allowed

If within given ktl and ch values the generation differs more than the 10% and 10 hours, the sunshine duration calculation is aborted.

As an additional feature in version 6.0 the monthly sunshine duration data are cleared for horizon effect.

7.2.12 Photosynthetically active radiation (PAR)

In the patch version 6.016 (November 7th 2007) the parameter photosynthetically active radiation (PAR) was introduced. The model of Alados-Arboledas (2000) as stated in the paper of Rubio et al (2005) is used:

$$G_{PAR} = Gh \cdot \frac{\left[1.832 - 0.191 \cdot \ln(kt) + 0.099 \cdot \sin(hs)\right]}{4.6} \tag{7.2.50}$$

The values are given in W/m^2 (the values in µE/m^{2}s are therefore divided with the factor 4.6).

PAR is available in the output format science and user defined (as option).

A short validation at three BSRN/Surfrad sites Desert Rock NV, Boulder CO and Goodwin Creek (MS) with data of 3 years (2004 – 2006) showed an mbe of 2 W/m^2 and a rmse of 4 W/m^2 (5%) for monthly means.

7.3   Summary of results

Tables 7.3.1 and 7.3.2 provide a short summary of the main data used in validating the various models and the combined model in Chap. 7.

Tab. 7.3.1:   Summary of principal data for interpolation validation.

Model	rmse	rmse
	Monthly means/sums	Yearly means/sums
Interpolation of G_h	9%	10%
Interpolation of Ta	1.4 ℃	1.2 ℃
Interpolation of Td	1.5 ℃	1.3 ℃
Interpolation of FF	1.1 m/s	1.1 m/s
Interpolation of RR	40%	31 mm
Interpolation of Rd	2.7 days	2.1 days
Interpolation of Sd	12%	10%

Tab. 7.3.2:   Summary of principal data for generation model validation.

Model	Resolution	Remarks	mbe	rmse
Generation of N	hour		-0.1 octas	1.8 octas
Calculation of D_h:				
- Hourly model	hour	G_h measured, (rmse: $G_h > 0$)	4 W/m^2	39 W/m^2
- Hourly model	month	G_h generated	1 W/m^2	5 W/m^2 (7%)
Calculation of G_k:				
- plane inclination 35°	hour	G_h measured, (rmse: $G_h > 0$)	5 W/m^2	33 W/m^2
- plane inclination 90°	hour	G_h measured, (rmse: $G_h > 0$)	3 W/m^2	51 W/m^2
- all (Perez)	Month	G_h generated	4 W/m^2	10 W/m^2
- all (Hay)	Month	G_h generated	0 W/m^2	9 W/m^2 (6%)
- Perez inclination 0-50°	Year	G_h generated		7 W/m^2
- Perez inclination >50°	Year	G_h generated		7 W/m^2

8 Literature

Aguiar, R. and M. Collares-Pereira (1988): A simple procedure for generating sequences of daily radiation values using a library of markov transition matrices. *Solar Energy*, Vol. 40, No.3, pp. 269-279.

Aguiar, R. and M. Collares-Pereira (1992): TAG: A time-dependent auto-regressive, Gaussian model. *Solar Energy*, Vol. 49, No.3, pp. 167-174.

Alados-Arboledas, L., F.J. Olmo, I. Alados, M. Perez (2000): Parametric models to estimate photosynthetically active radiation in Spain. *Agr. For. Meteor*. 101, 187–201.

Aubinet, M. (1994): Longwave sky radiation parametrizations. *Solar Energy*, Vol. 53, No.2. pp. 174-154.

Box, G. O., G.M. Jenkins and G.C. Reinsel. (1994): Time series analysis: Forecasting and control. 3rd edition. Prentice Hall, Englewood Cliffs, NJ.

Collier L.R. and J.G. Lockwood (1974): The estimation of solar radiation under cloudless skies with atmospheric dust. *Quart. J. Roy. Meteor. Soc.,* pp. 678-681

Commission of the European Communities, Directorate General XII for Science, Research and Development (CEC) (1985): Test Reference Year TRY. Weather Data Sets for Computer Simulations of Solar Energy Systems and Energy Consumption in Buildings. 1985 ECSC, EEC, EAEC Brussels and Luxemburg.

Cornick, S.; Dalgliesh, A.; Said, N.; Djebbar, R., Tariku, F.; Kumaran, M.K. (2002): Report from Task 4 of MEWS Project. Environmental Conditions Final Report. Institute for Research in Construction National Research Council Canada, Ottawa, Canada K1A 0R6

Deutscher Wetterdienst (DWD) (1979): Aspirations- und Psychrometertafeln. 6th edition. Friedrich Vieweg&Sohn. Braunschweig/Wiesbaden.

Dognaux, P. (1975): Variations géographiques et climatiques des expositions énergétiques solaires sur des surfaces réceptrices horizontales et verticales. IRM, Miscsell. B38.

Dumortier, D. (2002): Prediction of air temperatures from solar radiation. SoDa Deliverable D-5-2-4. Internal document.

Eidg. Materialprüfungs Anstalt (EMPA) (1985): Proposal for calculating the thermal irradiance of the environment. Draft.

Erbs D.G (1982): Estimation of the diffuse radiation fraction for hourly, daily and monthly-average global radiation. *Solar Energy* Vol. 28, No. 44, pp. 293-302, 1982.

Gabathuler and Marti (2000): Parametrization of longwave atmospheric radiation at high mountain environments. Draft.

Gansler, R.A., S.A. Klein and W.A. Beckman (1994): Assessment of the accuracy of generated meteorological data for use in solar energy simulation studies. *Solar Energy*, Vol. 53, No.3, pp. 279 - 287.

Gilgen H., M. Wild M., A. Ohmura (1998): *Means and trends of shortwave incoming radiation at the surface estimated from Global Energy Balance Archive data. Journal of Climate*, 11, 2042-2061.

Graham, V. and K. Hollands (1990): A method to generate synthetic hourly solar radiation globally. *Solar Energy*, Vol. 44, No.6, pp. 333-341.

Gueymard CA (1987) An anisotropic solar irradiance model for tilted surfaces and its comparison with selected engineering algorithms. *Solar Energy*, Vol. 38, pp. 367-386. Erratum: *Solar Energy,* Vol. 40, pp. 175, 1998

Gueymard CA (1995) SMARTS2, a simple model of atmospheric radiative transfer of sunshine: algorithms and performance assessment. Document FSEC-PF-270-95 Florida Solar Energy Centre, 1679 Clearlake Road, Cocoa, Florida, 32922-7703.

Hay JE (1979) Calculation of monthly mean solar radiation on horizontal and inclined surfaces. *Solar Energy*, Vol. 23, pp. 301-307.

Holben BN, Tanre D, Smirnov A, Eck TF, Slutsker I, Abuhassan N, Newcomb WW, Schafr J, Chatenet B, Lavenue F, Kaufman YF, Vande Castle J, Setzer A, Markham B, Clark D, Frouin R, Halthore R, Karnieli A, O'Neill NT, Pietras C, Pinker RT, Voss K, Zibordi G (2001) An emerging ground-based aerosol climatology: Aerosol Optical Depth from AERONET, J. Geophys. Res., 106, 12 067-12 097

Houghton, J.T., J. Jenkins and J.J. Ephraums (eds.) (1990): Climate Change. The IPCC scientific assessment. Cambridge University Press, Cambridge.

Ineichen P. and B. Dürr (2007): private communication.

Iribarne ,J.V. and W.L. Godson (1981): Atmospheric Thermodynamics. D. Reidel Publishing Company, p. 259.

Kasten, F. (1980): A Simple Parametrization of the Pyrheliometric Formula for Determining the Linke Turbidity Factor. *Meteorol. Rdsch*. 33. 124-127.

Kasten, F., K. Dehne, H.D. Behr and U. Bergholter (1984): Die räumliche Verteilung der diffusen und direkten Sonnenstrahlung in der Bundesrepublik Deutschland. Federal Ministry of Research and Technology, Research Report No. T 84-125, June 1984.

Kasten, F. (1990): Höhenabhängigkeit der Globalstrahlung bei wolkenlosem Himmel. Private communication from F. Kasten, DWD, to A. Zelenka, SMA.

Krist, T. (1976): Formeln und Tabellen der Internationalen Einheiten mit SI-Einheiten. Technik-Tabellen-Verlag Fikentscher & Co., Darmstadt.

Kunz, S. and R. Volz (1984): Sonnenenergie Nutzungszonen Schweiz (SONUS). Swiss Federal Office of Energy (SFOE), Bern.

Lacy, R. E. (1965): Driving-Rain Maps and the Onslaught of Rain on Buildings, Proceedings of the RILEM/CIB Symposium on Moisture Problems in Buildings, Helsinki Finland, 1965.

Lefèvre, M., M. Albuisson and L. Wald (2002): Joint Report on Interpolation Scheme "Meteosat" and Database "Climatology I (Meteosat). SoDa Deliverable D3-8 and D5-1-4. Internal document.

Lumb, F.E. (1964): The influence of cloud on hourly amounts of total solar radiation at the sea surface. *Quart. J. Roy. Meteor. Soc*. 90, pp. 43-56.

Müller, G. and A. Ohmura (1993): Radiation Annual Report ETH No.2 1990 and 1991. Zürcher Geographische Schriften (ZGS), No. 52. vdf, Zürich. pp. 17-18.

Müller, M.J., K. Baltes, E. Lutz, G. Richter and D. Werle (1985): Handbook of Selected World Weather Stations. Soil Erosion Research Group of the University of Trier, Mertensdorf (Ruwertal). 3rd edition.

Müller-Westermeier, G. (1990): Klimadaten der Bundesrepublik Deutschland, Zeitraum 1951-80. Published by the Deutscher Wetterdienst. Offenbach am Main, 1990.

Molineaux, B, P. Ineichen and Delauney, J.J. (1995): Direct luminous efficacy and atmospheric turbidity – improving model performance. *Solar Energy* Vol. 55, No. 2, pp. 125-137, 1995.

NASA (2007): http://eosweb.larc.nasa.gov/ and http://modis-atmos.gsfc.nasa.gov/index.html

NCDC (1995): International Station Meteorological Climate Summary (ISMCS), Version 3.0, March 1995. Fleet Numerical Meteorology and Oceanography Detachment, National Climatic Data Center and USAFETAC OL-A.

NCDC (2002): Globalsod. Global surface daily data: temperature, precipitation, winds, pressure, snow, etc. (http://ncdc.noaa.gov).

Page, J. K. (1961): The estimation of monthly mean values of daily total short wave radiation on vertical and inclined surfaces from sunshine records for latitudes 40 ° N-40 ° S. Proc. U.N. Conf. on New Sources of Energy, paper No.S 98, 4, 378, (1961).

Page, J., and R. Kift (2003): Advanced Parameters – Spectral Model. SoDA Deliverable D5-2-5 Internal document.

Perez, R., R. Stewart, C. Arbogast, R. Seals and J. Scott (1986): An anisotropic hourly diffuse radiation model for sloping surfaces: Description, performance validation, site dependency evaluation. *Solar Energy*, 36, 6, 481-497.

Perez, R., R. Seals, P. Ineichen, R. Stewart and D. Menicucci (1987): A new simplified version of the Perez Diffuse Irradiance Model for tilted surfaces. *Solar Energy*, Vol. 39,No.3,pp. 221-231.

Perez, R., P. Ineichen, R. Seals, J. Michalsky and R. Stewart (1990): Modeling daylight availability and irradiance components from direct and global irradiance. *Solar Energy*, Vol. 44, No.5, pp. 271-289.

Perez, R., P. Ineichen, E. Maxwell, R. Seals and A. Zelenka (1991): Dynamic Models for hourly global-to-direct irradiance conversion. Edited in: Solar World Congress 1991. Volume 1, Part II. Proceedings of the Biennial Congress of the International Solar Energy Society, Denver, Colorado, USA, 19-23 August 1991.

Perraudeau, M. (1986) : Climat lumineux à Nantes, résultats de 15 mois de mesures. CSTB EN-ECL 86.14L. (1986).

Remund, J. and S. Kunz (1995): METEONORM – a comprehensive meteorological database and planning tool for system design. In Proceedings of 13th Solar Energy Photovoltaic Conference and Exhibition, Nice. Commission of the European Communities (CEC). Volume I.

Remund, J. and S. Kunz (1997): Worldwide interpolation of meteorological data. In Proceedings of 14th Solar Energy Photovoltaic Conference and Exhibition, Volume 1, 1997.

Remund, J., E. Salvisberg and S. Kunz (1998): *Generation of hourly shortwave radiation data on tilted surfaces at any desired location. Solar Energy.* Vol. 62, Nr. 5.

Remund, J. M. Lefevre, T. Ranchin, L. Wald (2002): Constructing maps of the Linke Turbidity Factor. SoDa Deliverable D5-2-1. Internal document.

Remund, J. and J. Page (2002): Chain of algorithms: short- and longwave radiation with associated temperature prediction resources. SoDa Deliverable D5-2-2/3. Internal document.

Richardson, C.W. and D.A. Wright (1984): *WGEN: A model for generating daily weather variables*. U.S. Dept. Agric., Agric. Res. Svc. Pub. No. ARS-8, 83 pp.

Rigollier C, Bauer O, Wald L (2000) On the clear sky model of the ESRA with respect to the heliosat method. Solar Energy 68: 33-48

Risoe National Laboratory (1990): Europäischer Windatlas. Risoe National Laboratory Roskilde, Dänemark.

Robinson, N. (ed.) (1966): Solar Radiation. Elsevier Publishing Company, Amsterdam, London and New York, 1966.

Rubio, M.A., G. Lopez, J. Tovar, D. Pozo, F.J. Batlles (2005): The use of satellite measurements to estimate photosynthetically active radiation. *Physics and Chemistry of the Earth* 30 (2005) 159–164.

sia (1982): sia Recommendation No. 381/3: Heating Degree Days in Switzerland (Heizgradtage der Schweiz). 1982 edition. Swiss Association of Engineers and Architects, PO Box, 8039 Zürich.

sia (1991): sia Recommendation No. 381/2: Klimadaten zu Empfehlung 380/1 "Energie in Hochbau". 1991 edition. Swiss Association of Engineers and Architects, PO Box, 8039 Zürich.

sia (1993): sia Recommendation No. 380/1: Energie im Hochbau. 1993 edition. Swiss Association of Engineers and Architects, PO Box, 8039 Zürich.

Scartezzini, J.-L., M. Nygard Ferguson and F. Bochud (1990): Compression of multi-year meteorological data. Final Report. OFEN Project EF-REN (90)009. Solar Energy and Building Physics Laboratory, Department of Architecture, Swiss Federal Institute of Technology, Lausanne.

Selker, J.S. and Haither, D.A. (1990): Development and Testing of Singe-Parameter Precipitation Distribuations. *Water Resources Research 26(11):2733-2740*.

Sfeir, A.A. and G. Guarracino (1981): Ingénierie des systèmes solaires TEC&DOC.

Skartveit A. and J. A. Olseth (1986): Modelling slope irradiance at high latitudes. *Solar Energy*, Volume 36, Issue 4, 1986, Pages 333-344-

Skartveit, A., H. Lund. and J.A. Olseth (1992): The Design Reference Year. Recent Advancements in Solar Radiation Resource Assessment. Seminar, Denver, Colorado, November 16-19,1992.

Straube, J. (2001): Driving Rain Measurement Contract - Final Report, MEWS, Institute for Research in Construction, National Research Council Canada, Ottawa, Canada K1A 0R6

Swiss Federal Office of Energy (SFOE) (1985): **METEONORM'85.** Infoenergie, Postfach 311, 5200 Brugg, Switzerland.

Swiss Federal Office of Energy (SFOE) (publ.) (1995): **METEONORM** 1995 edition. Technical Documentation.

Troll, C. and K. Paffen (1980): Jahreszeitenklimate der Erde. (Reduced scale reproduction of wall chart 1:16'000'000), Berlin 1969.

Unsworth, M.H. et al. (1975): Longwave radiation at the ground*. Quarterly Journal of the Royal Meteorological Society*.

UK Met. Office (2007): http://www.metoffice.gov.uk/research/hadleycentre/models/modeldata.html

Vose, R.S., R.L. Schmoyer, P.M. Steurer, T.C. Peterson, R. Heim, T.R. Karl and J.K. Eischeid (1992): The Global Historical Climatology Network: long-Term Monthly Temperature, Precipitation, Sea Level Pressure and Station Pressure Data (NDP-041)*.* Downloadable from Carbon dioxide information analysis center (http://cdiac.ornl.gov).

Wald, L. and M. Lefèvre (2001): Interpolation schemes - Profile Method (a process-based distance for interpolation schemes). SoDa Deliverable D5-1-1. Internal document.

World Meteorological Organisation (WMO) (1971): Climatological Normals (Clino) for climate and climate ship stations for the period 1931-60. WMO/OMM - No.117.TP.52.

World Meteorological Organisation (WMO) (1998): 1961 – 90 Climatological Normals (Clino). Version 1.0 – November 1998.CD-ROM.

Wright, J., R. Perez and J.J. Michalsky (1989): Luminous Efficacy of Direct Irradiance: Variation with Moisture Conditions. *Solar Energy*, Vol. 42,pp. 387-394.

Zentralanstalt für Meteorologie und Geodynamik (ZAMG) (1994): Wetter- und Klimaübersicht Januar - Dezember 1994.

Zelenka, A., G. Czeplak.,V. D'Agostino, J. Weine., E. Maxwell., R. Perez, M. Noia, C. Ratto and R. Festa (1992): Techniques for supplementing solar radiation network data, Volume 1-3. IEA Report No.IEA-SHCP-9D-1.